

**PLA-based bionanocomposites with  
modulated degradation rate:  
preparation and processing by  
microinjection molding**

**Valentina Iozzino**



# UNIVERSITY OF SALERNO



***DEPARTMENT OF INDUSTRIAL ENGINEERING***

*Ph.D. Course in Industrial Engineering*

*Curriculum in Chemical Engineering - XXX Cycle*

**PLA-based bionanocomposites with modulated degradation rate: preparation and processing by microinjection molding**

**Supervisor**

*Prof. Roberto Pantani*

**Ph.D. student**

*Valentina Iozzino*

**Scientific Referee**

*Prof. Vincent Verney*

**Ph.D. Course Coordinator**

*Prof. Ernesto Reverchon*



*A papà Mario;  
ne sarai felice ed un giorno, ridendo, mi risponderai:  
"aie fatto o' quarto ra' metà ro' dovere tuoje" ...*



# Ringraziamenti

L’Il, quanta vita è passata qui dentro: ci ha visti da matricole alle prime armi fino a vederci ingegneri, dottorandi, assegnisti, accasati, genitori...e finanche Direttori di dipartimento. È un posto molto particolare: è caratterizzato da un proprio microclima (gelido in inverno e tropicale in estate) ed è dotato di una propria fauna tutta da studiare. Le persone che lo popolano sono singolari: hanno come “wall of fame” un albero di Natale e possono elencare i successi conseguiti contando i tappi di sughero finiti sulla Pressa. Queste persone arrivano addirittura a parlare direttamente ai campioni analizzati: ad un certo punto poi i campioni ti rispondono pure, è in quel momento che capisci che il lavoro fatto si trasformerà in pubblicazione. Non tutti i campioni sono diligenti: come quando, per opera di mani sapienti, decisero di socializzare selvaggiamente tra loro mentre si stavano essiccando in stufa.

Il mio percorso di dottorato sarebbe stato molto più difficile senza il supporto delle eccezionali persone che costituiscono il gruppo dell’Il. Ringrazio infinitamente il prof. Roberto Pantani, le cui capacità scientifiche mi lasciano ancora senza parole dopo tanti anni, grazie per avermi guidato con tanta disponibilità ed immensa pazienza; ora so che la sua “imposizione delle mani” funziona per davvero. Ringrazio tanto Valentina Volpe (il mio costante punto di riferimento, non la ringrazierò mai abbastanza...), Annarita De Meo (la “madre” dei miei campioncini stampati), Felice De Santis, Sara Liparoti e Vito Speranza; grazie a tutti loro per il costante supporto.

Ringrazio tutti gli studenti che ho avuto il piacere di seguire nel loro percorso di tesi: Ottavio Novello, Pasquale Napoli, Federico Immediata ed Anna Guariniello, grazie per il vostro prezioso contributo al mio lavoro di dottorato.

Un ringraziamento dal profondo del cuore va alla mia formidabile famiglia, soprattutto ai miei straordinari genitori che, solo per Amore, hanno avuto il coraggio e la pazienza di ripartire ancora una volta da zero con pappe e pannolini. Nella nostra famiglia non esistono nipoti, ci sono solo fortunatissimi figli.

Infine ringrazio gli uomini della mia vita, mio figlio Emanuele e mio marito Claudio: loro sono il mio sogno realizzato, l’ Amore che si tocca con le mani... ora siamo in tre a “contare”...

# Publications list

- “Poly(Lactic Acid)-Based Nanobiocomposites with Modulated Degradation Rates”  
Iozzino, Valentina; Askanian, Haroutioun; Leroux, Fabrice; Verney, Vincent; Pantani, Roberto  
October 2018, Materials 2018, 11, 1943;  
DOI: 10.3390/ma11101943
- “Polylactide melt stabilization by high-surface-area graphite and carbon black”  
Luciana D'Urso, Maria Rosaria Acocella, Gaetano Guerra, Valentina Iozzino, Felice De Santis, Roberto Pantani  
February 2018 Polymers 10(2):139  
DOI: 10.3390/polym10020139
- “Tuning the hydrolytic degradation rate of poly-lactic acid (PLA) to more durable applications”.  
Valentina, Iozzino; Haroutioun, Askanian; Fabrice, Leroux; Vincent, Verney; Roberto, Pantani(2017).  
In Maazouz A. AIP Conference Proceedings Pag.1-4 , American Institute of Physics Inc..  
ID:130601 book chapter (268)  
DOI: 10.1063/1.4937341
- “Tuning the Hydrolytic Degradation Rate of Poly-Lactic Acid (PLA) to more Durable Applications”.  
Iozzino, Valentina; Novello, Ottavio; Askanian, Haroutioun; Leroux, Fabrice; Verney, Vincent; Pantani, Roberto(2016).  
32nd International Conference of the Polymer Processing  
Lione Luglio 2016  
In: Atti del 32nd International Conference of the Polymer Processing Society  
Pag.1-5  
ID:103804 conference paper (273)
- “PLA-based nanobiocomposites with modulated biodegradation rate”.  
Iozzino, V; De Santis, F; Volpe, V; Pantani, R(2016).  
Wivace/Bionam International Conference 2016  
Salerno Ottobre 2016  
In: Atti del Wivace/Bionam International Conference 2016 Pag.1-3  
ID:103807 conference paper (273)  
Book chapter in:

Advances in Bionanomaterials, pp.51-60

DOI: 10.1007/978-3-319-62027-5\_5

- “Effect of an acid filler on hydrolysis and biodegradation of poly-lactic acid (PLA)”.

Iozzino, Valentina; Speranza, Vito; Pantani, Roberto.(2015).

Polimer processing with resulting morphology and properties: feet in the present and eyes at future. Pag.020063/1-020063/5 , AIP.

ID:87098 book chapter (268)

- “Effect of basic and acid fillers on hydrolysis and biodegradation rate of poly-lactic acid (PLA)”

Iozzino, Valentina; Speranza, Vito; Pantani, Roberto(2015).

Atti del Convegno “Polymer processing with resulting morphology and properties: feet in the present and eyes at the future” Pag.53-53

Salerno Ottobre 2015

ID:103798 conference paper (273)

- “Modulation of biodegradation rate of Poly(Lactic Acid)”

Iozzino, Valentina; Novello, Ottavio; Askanian, Haroutioun; Leroux, Fabbriche; Verney, Vincent; Pantani, Roberto(2015).

Proceedings of the Polymer Processing Society Regional Conference Graz 2015 Pag.238-238

Graz (Austria) 21-25 Settembre 2015

ID:86925 conference paper(273)

- “Biphasic PLA products by micro-injection molding samples presenting a selective degradation rate”

*In preparation*



# Table of Contents

Table of Contents.....	I
List of Tables.....	VII
Abstract.....	IX
Chapter 1.....	1
The state of the art.....	1
1.1. Poly(lactic acid).....	1
1.2. Hydrolysis of PLA.....	3
1.3. Modulation of biodegradation rate of Poly(Lactic Acid).....	5
1.4. Additives.....	6
1.5. The aim of this work.....	11
Chapter 2.....	13
Materials and methods.....	13
2.1. Materials.....	13
2.2. Methods.....	14
2.2.1. Synthesis of layered double hydroxide.....	14
2.2.2. Production of the samples.....	15
Extrusion process.....	15
Compression molding.....	17
Micro-injection molding.....	17
2.2.3. Hydrolysis tests.....	20
2.2.3. Characterization of the samples.....	21
Gel Permeation Chromatography (GPC).....	21
Differential Scanning Calorimetry (DSC).....	21
Rheological tests (hydrolysis at high temperature analysis).....	22
Mechanical tests.....	22
Chapter 3.....	25
Selection of the Materials.....	25
3.1. Selection of the Benchmark LDHs.....	25
3.1.1. Hydrolysis tests: experimental results.....	26
Hydrolysis at high temperature (Rheological analysis).....	26
Weight loss.....	26
Calorimetric analysis (DSC).....	27
Gel Permeation Chromatography (GPC).....	29
3.2. Optimization of the percentage of (LDHs + organic).....	33
3.2.1. Hydrolysis tests: experimental results.....	33
Weight loss.....	34
Calorimetric analysis (DSC).....	35
3.3. LDH-organic acid selection.....	36
3.3.1. Hydrolysis tests: experimental results.....	37
Hydrolysis at high temperature (Rheological analysis).....	37
Weight loss.....	38
Calorimetric analysis (DSC).....	38

Gel Permeation Chromatography (GPC) .....	40
Mechanical tests .....	50
Visual analysis of hydrolyzed samples .....	52
Evolution of the pH .....	54
3.4. PLA loaded with pure organic acids: a faster degradation.....	55
3.4.1. Hydrolysis tests: experimental results .....	55
Weight loss.....	55
Calorimetric analysis (DSC) .....	56
Gel Permeation Chromatography (GPC) .....	58
Mechanical tests .....	63
Images of hydrolyzed samples .....	64
3.5. Effect of LDH-organic acids against hydrolysis on an amorphous grade of PLA (4060D) .....	66
Weight loss.....	66
Calorimetric analysis (DSC) .....	67
Gel Permeation Chromatography (GPC) .....	69
Mechanical tests .....	74
Images of hydrolyzed samples .....	75
Chapter 4.....	79
Micro-injection molding.....	79
4.1. Biphasic samples from micro-injection molding .....	79
4.1.1. Hydrolysis tests, experimental results: micro-injected biphasic PLA samples .....	85
Calorimetric analysis (DSC) .....	86
Gel Permeation Chromatography (GPC) .....	86
Mechanical tests .....	87
Images of hydrolyzed samples .....	90
4.1.2. Hydrolysis tests, experimental results: micro-injected biphasic PLA and PLA + LDH samples .....	91
Calorimetric analysis (DSC) .....	92
Gel Permeation Chromatography (GPC) .....	93
Mechanical tests .....	96
Conclusions.....	99
Bibliography .....	105
Appendix .....	111

# List of Figures

<b>Figure 1.</b> Structure of poly-lactic acid.....	2
<b>Figure 2.</b> Hydrolysis mechanism of PLA .....	3
<b>Figure 3.</b> SEM of Hydrotalcite .....	8
<b>Figure 4.</b> General structure of LDH .....	8
<b>Figure 5.</b> Chemical Structure of succinic acid .....	9
<b>Figure 6.</b> Chemical Structure of fumaric acid.....	10
<b>Figure 7.</b> Chemical Structure of ascorbic acid.....	11
<b>Figure 8.</b> Reaction system for LDH synthesis .....	15
<b>Figure 9.</b> Minilab Thermo Scientific Extruder and its counter-rotating screws.....	16
<b>Figure 10.</b> Haake miniJet.....	17
<b>Figure 11.</b> Exploded view of the elements composing the mold. ....	19
<b>Figure 12.</b> Slab, cavity dimension and heated zone .....	19
<b>Figure 13.</b> Schematic view of the assembled mold .....	20
<b>Figure 14.</b> (a) Assembly for penetration test; (b) Scheme of the test. ....	22
<b>Figure 15.</b> Time evolution of the complex viscosity during rheological tests (unhydrolyzed PLA and PLA + LDH/nitrate ) .....	26
<b>Figure 16.</b> Weight loss during hydrolysis (PLA and PLA + LDH/nitrate or carbonate).....	27
<b>Figure 17.</b> Evolution of degree of crystallinity during hydrolysis (PLA and PLA + LDH/nitrate or carbonate).....	28
<b>Figure 18.</b> Evolution of molecular weight distribution during hydrolysis (PLA and PLA + 3% LDH-NO <sub>3</sub> ) for different hydrolysis times: a) 0 days; b) 5 days; c) 14 days; d) 21 days.....	31
<b>Figure 19.</b> Evolution of weight average molecular weight (M <sub>w</sub> ) during hydrolysis (PLA and PLA + 3% LDH-NO <sub>3</sub> ).....	32
<b>Figure 20.</b> Evolution of number average molecular weight (M <sub>n</sub> ) during hydrolysis (PLA and PLA + 3% LDH-NO <sub>3</sub> ).....	32
<b>Figure 21.</b> Weight loss during hydrolysis (PLA and PLA + LDH-succinic acid for different percentages wt/wt) .....	34
<b>Figure 22.</b> Weight loss during hydrolysis (PLA and PLA + LDH-fumaric acid for different percentages wt/wt) .....	34
<b>Figure 23.</b> Evolution of degree of crystallinity during hydrolysis (PLA and PLA + LDH-succinic acid for different percentages wt/wt) .....	35
<b>Figure 24.</b> Evolution of degree of crystallinity during hydrolysis (PLA and PLA + LDH-fumaric acid for different percentages wt/wt) .....	36
<b>Figure 25.</b> Time evolution of the complex viscosity during rheological tests of unhydrolyzed samples (PLA and PLA + 3% LDH-organic acids).....	37
<b>Figure 26.</b> Weight loss during hydrolysis (PLA and PLA + 3% LDH-organic acid).....	38

<b>Figure 27.</b> Evolution of degree of crystallinity during hydrolysis (PLA and PLA + 3% LDH-organic acid).....	39
<b>Figure 28.</b> Evolution of molecular weight distribution during hydrolysis (PLA and PLA + 3% LDH-organic acid) at different hydrolysis times: a) 0 days; b) 5 days; c) 14 days; d) 21 days; e) 35 days. ....	41
<b>Figure 29.</b> Evolution of weight average molecular weight (Mw) during hydrolysis (PLA and PLA + 3% LDH-organic acids).....	42
<b>Figure 30.</b> Evolution of number average molecular weight (Mn) during hydrolysis (PLA and PLA + 3% LDH-organic acids).....	43
<b>Figure 31.</b> Evolution of $\ln(Mn-M)$ during hydrolysis (PLA and PLA + 3% LDH-organic acids).....	45
<b>Figure 32.</b> Deconvolution of the MWD of 4032D at 0 and 41 days.....	47
<b>Figure 33.</b> Time evolution of Mn calculated from the overall curve (no deconvolution) and from the peaks resulting from deconvolution. A circle identifies the peak with the largest area among those which describe the curve at each time of hydrolysis.....	48
<b>Figure 34.</b> 4032D + 3% (LDH-succinic acid). Time evolution of Mn calculated from the overall curve (no deconvolution) and from the peaks resulting from deconvolution. A circle identifies the peak with the largest area among those which describe the curve at each time of hydrolysis. ....	49
<b>Figure 35.</b> Time evolution of Mn calculated using only the peak with the largest area among those which describe the curve at each time of hydrolysis.....	50
<b>Figure 36.</b> Evolution of force at break during hydrolysis (PLA and PLA + 3% LDH-organic acids).....	51
<b>Figure 37.</b> Evolution of modulus during hydrolysis (PLA and PLA + 3% LDH-organic acids).....	51
<b>Figure 38.</b> Images of hydrolyzed samples (PLA and PLA + 3% LDH-organic acids); a) hydrolyzed for 42 days; b) hydrolyzed for 56 days. ....	53
<b>Figure 39.</b> Evolution of $H^+$ released during hydrolysis (PLA and PLA + 3% LDH-succinic acids).....	54
<b>Figure 40.</b> Weight loss during hydrolysis (PLA and PLA + 1% organic acid) .....	56
<b>Figure 41.</b> Evolution of degree of crystallinity during hydrolysis (PLA and PLA + 1% organic acid) .....	57
<b>Figure 42.</b> Evolution of molecular weight distribution during hydrolysis (PLA and PLA + 1% organic acid) at different hydrolysis times: a) 0 days; b) 5 days; c) 14 days; d) 21 days; e) 35 days .....	60
<b>Figure 43.</b> Evolution of weight average molecular weight (Mw) during hydrolysis (PLA and PLA + 1% organic acids).....	61
<b>Figure 44.</b> Evolution of number average molecular weight (Mn) during hydrolysis (PLA and PLA + 1% organic acids).....	61
<b>Figure 45.</b> Evolution of $\ln(Mn-M)$ during hydrolysis (PLA and PLA + 1% organic acids).....	62

<b>Figure 46.</b> Evolution of force at break during hydrolysis (PLA and PLA + 1% organic acids) .....	63
<b>Figure 47.</b> Evolution of modulus during hydrolysis (PLA and PLA + 1% organic acids).....	64
<b>Figure 48.</b> Images of hydrolyzed samples (PLA and PLA + 1% organic acids); a) hydrolyzed for 42 days; b) hydrolyzed for 56 days. ....	65
<b>Figure 49.</b> Weight loss during hydrolysis (4060D and 4060D + 3% LDH-organic acid) .....	67
<b>Figure 50.</b> Evolution of degree of crystallinity during hydrolysis (4060D and 4060D + 3% LDH-organic acid).....	68
<b>Figure 51.</b> Evolution of molecular weight distribution during hydrolysis (4060D and 4060D + 3% LDH-organic acid) at different hydrolysis times: a) 0 days; b) 5 days; c) 14 days; d) 21 days.....	71
<b>Figure 52.</b> Evolution of weight average molecular weight (Mw) during hydrolysis (4060D and 4060D + 3% LDH-organic acids).....	72
<b>Figure 53.</b> Evolution of number average molecular weight (Mn) during hydrolysis (4060D and 4060D + 3% LDH-organic acids).....	72
<b>Figure 54.</b> Evolution of $\ln(Mn-M)$ during hydrolysis (4060D and 4060D + 3% LDH-organic acids) .....	73
<b>Figure 55.</b> Evolution of force at break during hydrolysis (4060D and 4060D + 3% LDH-organic acids) .....	74
<b>Figure 56.</b> Evolution of modulus during hydrolysis (4060D and 4060D + 3% LDH-organic acids) .....	75
<b>Figure 57.</b> Images of hydrolyzed samples (4060D and 4060D + 3% LDH-organic acids); hydrolyzed for: a) 14 days; b) 21 days; c) 28 days; d) 42 days. ....	76
<b>Figure 58.</b> Example of local heating speed of the mold .....	80
<b>Figure 59.</b> Length of the injected sample as a function of cavity temperature .....	80
<b>Figure 60.</b> Injected samples produced at different cavity temperatures .....	81
<b>Figure 61.</b> Schematization of the production of injected biphasic samples (amorphous in the tip and crystalline in the gate).....	81
<b>Figure 62.</b> Temperatures during filling and post filling steps.....	82
<b>Figure 63.</b> Micro-injected biphasic PLA sample (amorphous tip, crystalline gate) .....	82
<b>Figure 64.</b> DSC analysis of micro-injected biphasic PLA sample (amorphous tip, crystalline gate), first scan.....	83
<b>Figure 65.</b> Schematization of the production of injected biphasic samples (amorphous in the gate and crystalline in the tip).....	84
<b>Figure 66.</b> Micro-injected biphasic PLA sample (crystalline tip, amorphous gate) .....	84
<b>Figure 67.</b> DSC analysis of micro-injected biphasic PLA sample (amorphous gate, crystalline tip), first scan.....	85

<b>Figure 68.</b> Evolution of degree of crystallinity during hydrolysis of micro-injected biphasic PLA sample (amorphous gate, crystalline tip) .....	86
<b>Figure 69.</b> Evolution of number average molecular weight (Mn) during hydrolysis of micro-injected biphasic PLA sample (amorphous gate, crystalline tip) .....	87
<b>Figure 70.</b> Evolution of force at break during hydrolysis of micro-injected biphasic PLA sample (amorphous gate, crystalline tip) .....	88
<b>Figure 71.</b> Evolution of modulus during hydrolysis of micro-injected biphasic PLA sample (amorphous gate, crystalline tip) .....	88
<b>Figure 72.</b> Evolution of force at break during hydrolysis of micro-injected biphasic PLA sample (amorphous gate, crystalline tip) .....	89
<b>Figure 73.</b> Evolution of modulus during hydrolysis of micro-injected biphasic PLA sample (amorphous gate, crystalline tip) .....	90
<b>Figure 74.</b> Images of hydrolyzed samples of micro-injected biphasic PLA sample (amorphous gate, crystalline tip) .....	91
<b>Figure 75.</b> Evolution of degree of crystallinity during hydrolysis of micro-injected biphasic PLA and PLA + LDH samples (amorphous gate, crystalline tip) .....	92
<b>Figure 76.</b> Evolution of number average molecular weight (Mn) during hydrolysis of micro-injected biphasic PLA and PLA + LDH samples (amorphous gate, crystalline tip) .....	93
<b>Figure 77.</b> Evolution of molecular weight distribution during hydrolysis of micro-injected biphasic PLA and PLA + LDH samples (crystalline tip) .....	94
<b>Figure 78.</b> Evolution of $\ln(M_n - M)$ during hydrolysis of micro-injected biphasic PLA and PLA + LDH samples (amorphous gate, crystalline tip) ..	95
<b>Figure 79.</b> Evolution of force at break during hydrolysis of micro-injected biphasic PLA and PLA + LDH sample (amorphous gate, crystalline tip) .....	96
<b>Figure 80.</b> Evolution of modulus during hydrolysis of micro-injected biphasic PLA and PLA + LDH sample (amorphous gate, crystalline tip) ..	97
<b>Figure 81.</b> Images of hydrolyzed samples of micro-injected biphasic PLA and PLA + LDH samples at 50 days (amorphous gate, crystalline tip; a) PLA; b) PLA + LDH .....	98

# List of Tables

<b>Table 1.</b> Extruded materials .....	16
<b>Table 2.</b> Summary of DSC results: $T_g$ was measured during 2 <sup>nd</sup> heating scan, the reported $T_m$ refers to the highest-temperature peak of the melting endotherm during 1 <sup>st</sup> heating ramp (PLA and PLA + LDH) .....	29
<b>Table 3.</b> Summary of DSC results: $T_g$ was measured during 2 <sup>nd</sup> heating scan, the reported $T_m$ refers to the highest-temperature peak of the melting endotherm during 1 <sup>st</sup> heating ramp (PLA and PLA + 3% LDH-organic acid). .....	39
<b>Table 4:</b> Kinetic constant of hydrolysis (PLA and PLA + 3% LDH-organic acids) .....	45
<b>Table 5.</b> Summary of DSC results: $T_g$ was measured during 2 <sup>nd</sup> heating scan, the reported $T_m$ refers to the highest-temperature peak of the melting endotherm during 1 <sup>st</sup> heating ramp (PLA and PLA + 1% organic acid). .....	58
<b>Table 6.</b> Kinetic constant of hydrolysis (PLA and PLA + 1% organic acids) .....	62
<b>Table 7.</b> Summary of DSC results: $T_g$ was measured during 2 <sup>nd</sup> heating scan, the reported $T_m$ refers to the highest-temperature peak of the melting endotherm during 1 <sup>st</sup> heating ramp (4060D and 4060D + 3% LDH-organic acid). .....	68
<b>Table 8.</b> Kinetic constant of hydrolysis (4060D and 4060 + 3% LDH-organic acids).....	74
<b>Table 9.</b> Kinetic constant of hydrolysis of micro-injected biphasic PLA and PLA + LDH samples (amorphous gate, crystalline tip) .....	95



# Abstract

Biodegradable polymers can be decomposed by micro-organisms with almost no impact on the environment, and are a promising alternative to conventional polymers for some specific applications.

Among the biodegradable polymers, PLA is one of the most attractive due to its good processability, biocompatibility, interesting physical properties and the possibility of being obtained from renewable sources. Hydrolysis is the major depolymerization mechanism and the rate-controlling step of PLA biodegradation in compost.

The characteristic of being degradable is not *per se* an advantage: the propensity to degrade in the presence of water significantly limits specific industrial applications, particularly for durable products with long-term performance such as in the automotive, electronic, and agricultural industries, as well as in medical applications.

In general, being able to control the degradation rate would be a real advantage: a product should preserve its characteristics during processing and for a time comparable to its application, but should be nevertheless fully biodegradable at longer times. The degradation rate of PLA can be modified using several techniques, such as blending, copolymerization and surface modification. However, these change the physical properties of the material. The use of additives that can change the rate of hydrolysis preserves the nature of PLA. This field of research is just starting and is extremely promising.

Any factor affecting the rate of hydrolysis could either accelerate or retard the whole biodegradation process. It is quite well known that the kinetics of hydrolysis strongly depend on the pH of the hydrolyzing medium.

The idea explored during this study is the use of additives able to control the pH of water when it diffuses inside the polymer. For instance, some acids (e.g. succinic acid, also used as a food additive) are bio- and eco-friendly additives which are able to play this role.

However, in order to control the release of these molecules and their dispersion inside the polymer, intercalation in biocompatible nanofillers like LDH has been considered.

The aim of this work has been to obtain bionanocomposites with a degradation rate which can be modulated in time, so that it can be possible to decide *a priori* the time after which the material will disappear in a given environment. At the same time, the material should preserve its properties during processing.

Several mixtures of PLA (4032D, 4060D) and LDH of cation composition  $Mg_2Al$  organo-modified with organic acids (succinic, fumaric and ascorbic acid) have been obtained by extrusion. From the extruded materials there were obtained films by compression molding; these films were then subjected to hydrolysis tests. The experimental results show that for samples loaded with LDH-organic acid (in particular LDH-succinic acid), there is an increase in the time needed for degradation, and a decrease in this time for samples loaded with organic acid alone.

From the selected material (PLA + LDH-succinic acid) and from pure PLA, biphasic samples (half amorphous and the other half crystalline) have been obtained by micro-injection molding. Also in this case, the experimental results show an increase for the loaded samples in the time needed for degradation compared to pure PLA both for the crystal phase and for the amorphous one, and in particular the presence of a degradation profile within the same sample is observed.

# Chapter 1

## The state of the art

### 1.1. Poly(lactic acid)

The disposal of polymeric waste is increasingly becoming an issue of international concern. The issue of the reduction of waste has forced companies to start researching the use of biomaterials. The use of biodegradable polymers is a possible strategy to face most of the problems related to the disposal of the durable (non-biodegradable) polymers.

The growing attention to biopolymers is due to several factors:

- rising environmental concerns on the part of consumers, who are increasingly willing to pay higher prices for green products (Pantani and Turng, 2015)
- compostability as an alternative end-of-life option, with legislative drivers and with the specific functionality of certain bioplastics contributing to the increasing interest (Soroudi and Jakubowicz, 2013)
- the transition from a fossil-based economy to a bio-based economy is an important EU 2020 Strategy target.

Biodegradable polyesters are among the most important components of the category of biodegradable polymers. The ester bonds present in this kind of polymer are highly hydrolysable, which makes this category of polymers highly prone to degradation in humid environments.

Poly lactic acid, PLA (Garlotta, 2001), an aliphatic thermoplastic polyester produced from renewable sources, is one of the most interesting biodegradable polymers. PLA is a rigid thermoplastic polymer, versatile, recyclable and compostable, with high transparency, high molecular weight, and relatively good processability. Commercial PLA is a copolymer between poly (L-lactic acid) and poly (D-lactic acid). It can be semi-crystalline or totally amorphous, depending on the stereoregularity of the polymer. PLA is obtained from the fermentation of sugar or feedstock or corn, and by the ring-opening polymerization of the cyclic lactide dimer.

## Chapter 1

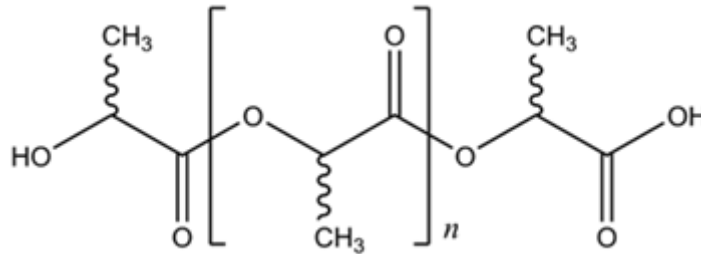


**Figure 1.** Structure of poly-lactic acid

The recent development of a continuous process of production of this PLA has lowered its price to be competitive with other degradable polymers and potentially competitive with petroleum-derived plastics (Soroudi and Jakubowicz, 2013).

The final properties of the polymer are determined by its stereochemical composition, since lactic acid exists as two optical isomers, l- and d-lactic acid. Poly(l-lactide) (PLLA) and poly(d-lactide) (PDLA) are (semi)crystalline polymers which are hard, while poly(d,l-lactide) (PDLLA) is an amorphous polymer which is brittle. Only when the d- and l-unit sequence are completely alternating with each other can the PDLLA be crystalline.

As with other bioplastic materials, PLA shows:

- a slow crystallization kinetics (Pantani et al., 2010),
- a limited processing window due to thermomechanical degradation (Benali et al., 2015, De Santis and Pantani, 2015, Speranza et al., 2014)
- a loss of thermo-mechanical properties when heated or exposed to humidity (Hglund et al., 2012, Harris and Lee, 2010).

PLA is used in a lot of areas, such as biomedical, packaging, and tissue engineering, and there are many companies interested in its properties, mainly in its biodegradability. It is very important to understand the degradation characteristics of PLA, for both consumer and biomedical applications (due to its biocompatibility and bioresorbability).

Propensity to degradation in the presence of water along with thermomechanical resistance, as well as restricted gas barrier properties, significantly limits specific industrial applications, particularly for durable products with long-term performance, such as in the automotive, electronics, biomedical and agricultural fields (Stloukal et al., 2015, Notta-Cuvier et al., 2014, Harris and Lee, 2013). Knowledge of the hydrolytic degradation of poly(lactic acid) (PLA) is essential for the plastics industry to meet current environmental regulations. Furthermore, control of its hydrolytic degradation

and biodegradation is fundamental for medical applications. There are cases where the acceleration of degradation is desirable, while in other cases what is required is to extend the service life of the PLA, depending on the field of application (Auras, 2010). The possibility of controlling the rate of biodegradation is strategic for the application of biodegradable polymers in many sectors.

## 1.2. Hydrolysis of PLA

In the natural environment, the degradation of PLA proceeds either through hydrolytic or enzymatic chain scission of the ester bonds to produce low molecular weight oligomers and monomers, thus enabling assimilation by microorganisms. Biodegradation of PLA proceeds readily in a compost environment. In particular, abiotic hydrolysis, Figure 2, which induces compositional and morphological changes, was suggested as a major depolymerization mechanism and the rate-controlling step of PLA biodegradation in compost (Pantani and Sorrentino, 2013).

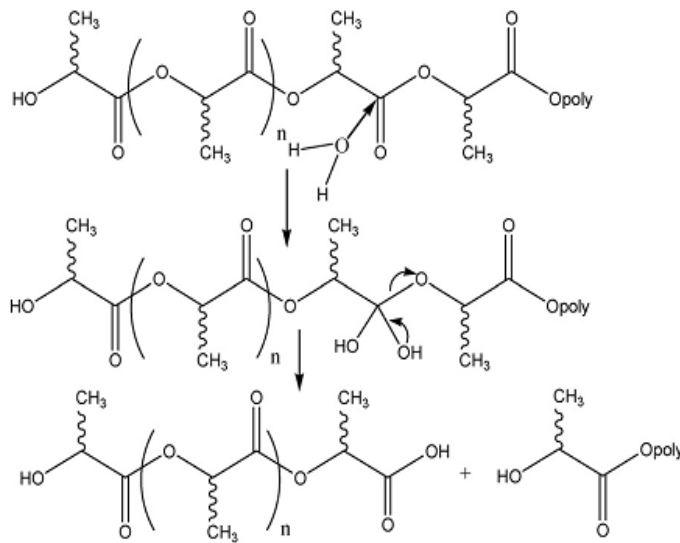


**Figure 2.** Hydrolysis mechanism of PLA

Hydrolysis of PLA has been reported to proceed either at the surface or within the bulk, and is determined by several variables, including chemical composition, stereochemistry, sequence distribution, molecular weight and

## *Chapter 1*

molecular weight distribution, sample morphology, chain orientation, the presence of residual monomers, and environmental degradation conditions (temperature and pH). Therefore, any factor affecting the rate of hydrolysis could either accelerate or delay the whole biodegradation process.

Many studies have been made of the hydrolytic degradation of PLA, analysing the factors that can influence this phenomenon (Lostocco and Huang, 1998, Henton et al., 2005). It has been recognized that hydrolysis is auto-catalytic as a result of acceleration by their carboxyl end groups (Hocking et al., 1995, Li et al., 1990) and that the pH of the degrading medium determines the kinetics (De Jong et al., 2001). The formation of lactic acid oligomers following chain scission increases the concentration of carboxylic acid end groups in the degradation medium, making the hydrolytic degradation of PLA a self-catalyzed and self-maintaining process due to the catalytic action of these end groups. At the same time, the structural and morphological organization of PLA strongly affects its hydrolytic degradation mechanism. It has been found that hydrolytic chain cleavage proceeds preferentially in the amorphous regions, leading to an increase in polymer crystallinity (Jimenez et al., 2015). The rate of the degradation reaction is also affected by the structure of the macromolecules and the shape of the specimen. Chemical hydrolysis reduces the molecular weight of the PLA, and only then can the microorganisms use lactic acid oligomers as an energy source (Itavaara et al., 2002).

As is widely reported, the hydrolytic degradation of PLA typically occurs in stages:

1. Diffusion of water into the material;
2. Hydrolysis of chains in the amorphous region, because of the lower resistance to water attack;
3. Diminution of molecular weight as a result of hydrolytic cleavage of ester bonds and the formation of water-soluble compounds
4. Hydrolysis of the lamellae of the crystalline phase, which can occur through an autocatalytic mechanism by the acidic degradation products as well as by the increasing concentration of carboxylic acid at the ends of the chain (Metters et al., 2000, Piemonte and Gironi, 2013, Tokiwa and Calabia, 2006, Vert et al., 1991).

However, the mechanism of hydrolysis is still not clear: it is reported that random chain scission takes place in acidic conditions (Shih, 1995) and in basic conditions (Belbella et al., 1996). Chain scission can induce a much faster reduction of physical properties (Gleadall et al., 2014) than end scission. Also the effect of the stereochemical composition is not well understood (Hglund et al., 2012, Gorrasi and Pantani, 2013b).

### **1.3. Modulation of biodegradation rate of Poly(Lactic Acid)**

The possibility of controlling the rate of biodegradation is strategic for the application of biodegradable polymers in many sectors (Ha and Xanthos, 2010). The degradation rate of PLA has been modified using several techniques: blending, copolymerization, surface modification, and many others. Blending polymers is a simple way to modify the physical and mechanical properties of polymers and so their degradability. Arias et al. (Arias et al., 2014) have controlled and predetermined degradation profiles through the miscibility of PLA-based materials during hydrolytic degradation and through the miscibility of PLLA melt-blended with different polyesters. However, this method changes the physical properties of the material, including the desired ones.

The use of additives which can change the rate of hydrolysis is a method that preserves the intrinsic properties of PLA. Recently, Stloukal et al. (Stloukal et al., 2015) investigated the stabilization effect of a commercially available aromatic carbodiimide-based anti-hydrolysis agent (which can modify the diffusion of water into the polymer matrix), intended to improve the hydrolysis resistance of PLA based materials and prevent their degradation during processing. Even more recently, Benali et al. (Benali et al., 2015) used silanized zinc oxide nanofiller (ZnOs) to tune the hydrolytic degradation of PLA. Other fillers, such as clays (Balaguer et al., 2016, Ha and Xanthos, 2010), silver (Gorrasi et al., 2015), SiO<sub>2</sub> (Hernández, 2014) and graphene (Bayer, 2017) have been evaluated. Apart from the results reported by Stloukal et al., which show a quite significant delay in hydrolysis, the use of other additives appears to be marginal, if not negative toward the stabilization of PLA.

The aim of this work is to control the degradation rate of PLA so as to obtain plastic products which degrade in a time compatible with the application for which they are used. The route adopted is the combination of two-dimensional layered material and intercalation, which offers a new route for developing nanohybrids with desired functionalities. In particular, layered double hydroxides (LDHs), also called anionic clays, were adopted. This class of fillers is extremely interesting since negatively charged molecules can be incorporated between hydroxide layers as charge compensating anions through ion exchange techniques (Nalawade et al., 2009). These molecules can impart particular properties to the polymer matrix. A review of the state of the art concerning PLA-LDH bionanocomposites can be found in (Sisti et al., 2013). Despite the huge amount of studies on PLA-LDH systems, only a few papers deal with the effect of the presence of LDH on the degradation of PLA. Zhou and Xanthos (Zhou and Xanthos, 2008) found a reduction of the degradation rate in PLA containing 5% calcinated LDH, which was ascribed to the reduction of the

## *Chapter 1*

catalytic effect of the carboxylic end groups induced by the filler. Eili et al. (Eili et al., 2012) observed an increasing biodegradation rate of nanocomposites of PLA and stearate-Zn-Al-LDH on increasing the filler content, possibly due to an increased water sorption. Oyarzabal et al. (Oyarzabal et al., 2016) studied the hydrolytic degradation of a nanocomposite of PLA and LDH modified with 4-biphenyl acetic acid (Bph) and observed that the filler inhibited the degradation rate at the early stages, due to the reduction of the diffusion of the oligomers resulting from hydrolysis, but then promoted a faster weight loss.

Clearly, as expected, the degradation rates of PLA-LDH bionanocomposites depend strongly on the incorporated molecule.

### **1.4. Additives**

Use of polymeric material is growing each day, involving all the aspects of common life as well as very specific sectors. For this reason, each application needs material with suitable features. Although the polymers sector includes today over thousands of different possibilities, these might not be enough to satisfy the market.

Some industries are trying to replace oil-made polymers with biodegradables. However, biodegradable polymers show sometimes a lack of properties, such as low barrier properties against gas or lower mechanical properties than common polymers. The use of additives loaded in the polymeric mold allows improving some specific properties, and nowadays this is becoming more and more widespread. The additives allow the application of the biodegradable polymers in critical sectors, such as electronics, or in disposable applications such as glasses and dishes. In the first case, to produce durable goods, interest is growing in materials derived from fibers of natural origin. In the second case, great importance is given to degradation speed at the end of product life, so there is great interest in additives to be loaded into the polymer in order to speed the process. To develop a formulation suitable for a specific application, without damaging polymer biocompatibility, some regulations about biodegradability must be followed:

- No toxic by-products: the additive must not release toxic waste into the environment;
- Concentrations of heavy metals must not exceed maximum levels permitted by law;

- Evaluation of biodegradability: metal or non-biodegradable constituents are permissible if the percentage is lower than 1% for each constituent and 5% for all the components;
- Determine the final quality of the compost.

Good results in adding filler are not always ensured. Blends are defined as heterogeneous if the components are present in separate phases. Usually the minor component is dispersed in a matrix of the dominant component. Compatibility could depend on the temperature; in this case the blend is considered partially miscible and coalescence could occur, which implies a lower dispersion.

Practically, every aspect (almost) of a polymer can be modified by adding filler, from the mechanical properties to its temperature resistance.

It is of interest for this work to delay the biodegradation time of a polymer, in particular PLA, for applications that require a longer lifetime of the polymer. To reach this goal some additives have been added to PLA.

#### **1.4.1. Layered Double Hydroxides (LDH)**

The possibility of controlling the rate of biodegradation is strategic for the application of biodegradable polymers in many sectors, such as automobile, transport, electronic and electrical appliances, and agriculture. The use of additives which can change the biodegradation rate is therefore extremely interesting.

Some nanoscale materials can be considered as additives: in particular, combining two-dimensional layered materials and the intercalation technique offers a new area for developing nanohybrids with desired functionalities (Nalawade et al., 2009). Layered double hydroxides (LDHs) are also called anionic clays, minerals of this family include hydrotalcite (Mg-Al-CO<sub>3</sub>), Figure 3; negatively charged molecules can be incorporated between hydroxide layers as charge compensating anions through ion exchange.

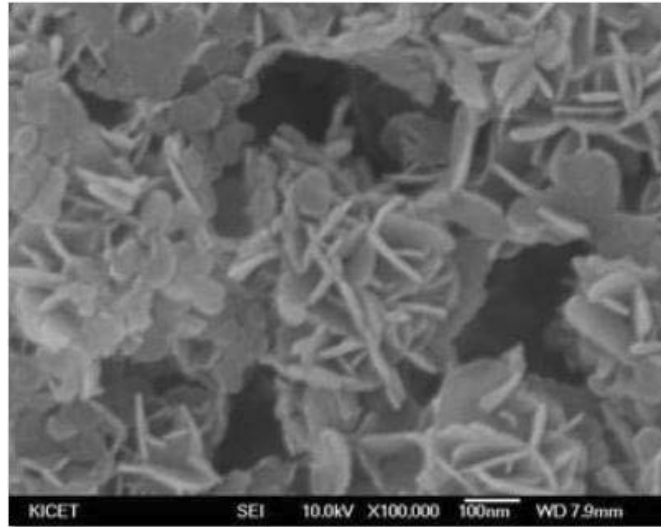
LDHs have technological importance as catalysts, in separation technologies, optics, medicine, and nanocomposite material engineering.

The chemical composition of LDH is generally expressed as

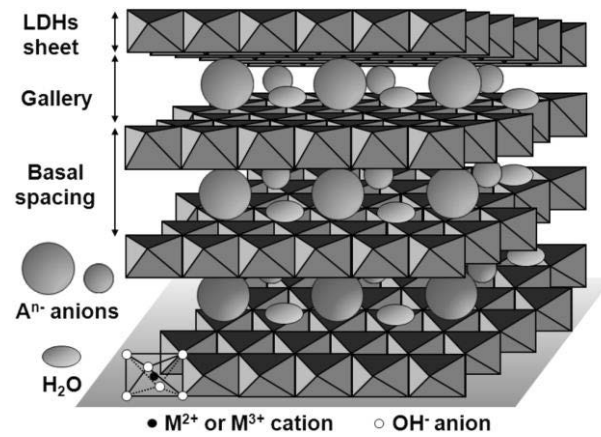


Where

- M<sup>2+</sup> is a divalent cation
- M<sup>3+</sup> is a trivalent cation
- A is an interlayer anion
- n is the charge on interlayer
- x and y are fraction constants



**Figure 3.** SEM of Hydrotalcite



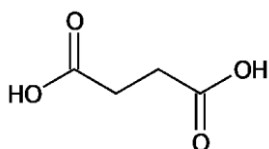
**Figure 4.** General structure of LDH

Figure 3 and Figure 4 show an SEM image and the general structure of LDH.

### 1.4.2. Organic acids

The idea explored during this study is the use of additives to control the pH of water when it diffuses inside the polymer. For instance, acids are bio- and eco-friendly additives which are able to play this role.

In this study three kinds of organic acid have been selected: succinic acid, fumaric acid, and ascorbic acid. These organic acids are from natural sources and biocompatible, they have the common characteristic of remaining in the solid state at the processing temperatures of PLA.



**Figure 5.** Chemical Structure of succinic acid

Succinic acid is a carboxylic acid, in fact it has the carboxylic function -COOH on both terminals of the molecule. It is naturally present in different fruits (in particular in unripe ones) and in different vegetables (as for example in lettuce); for industrial use it is synthesized starting from acetic acid. Succinic acid is an acidity regulator and also a flavouring agent. It can be present in desserts, bakery products, etc.

It can be obtained by the synthesis of nitriles, ethylene chloride and sodium cyanide and subsequent nitrile hydrolysis.

The properties of succinic acid are shown below.

- Molecular formula: C<sub>4</sub>H<sub>6</sub>O<sub>4</sub>
- Molecular mass (u): 118.09 g / mol
- Appearance: white crystalline solid
- CAS number: [110-15-6]
- Density (g / cm<sup>3</sup> in c.s.): 1.55
- Solubility in water at 25°C: 83.3 g / l
- Melting temperature: 183°C (456 K)
- Boiling point: 235°C (508 K)
- Flash point: 206°C (479 K)
- Acidity (pKa): pka<sub>1</sub> = 4.2, pka<sub>2</sub> = 5.6

## Chapter 1

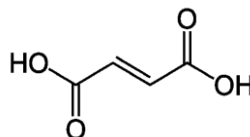


**Figure 6.** Chemical Structure of fumaric acid

Fumaric acid (also trans-butyllic acid) is a naturally occurring acid in fruits and vegetables and is a substance that has been isolated in the roots of the wild herbaceous plant *Fumaria officinalis*, Fumariaceae from which the name derives.

Fumaric acid is an isomer of maleic acid (cisbutendioic acid). The two substances are stable and distinct isomers, since the rotation around a double carbon-carbon bond is prevented. The transition between cis and trans isomers requires significant energy supply.

The characteristics of the two acids are very different: for example, maleic acid is toxic, while fumaric is used as a medicine and in food products. It is produced industrially both by fermentation and synthetically. Fermentation, through the fermentation of sugars by mushrooms, is the way to produce fumaric acid for food use. Fumaric acid is mainly produced by isomerization of maleic acid using urea as a catalyst. It is also obtained as a by-product in the synthesis of malic acid

The properties of fumaric acid are shown below:

- Molecular or molecular formula:  $C_4H_4O_4$
- Molecular mass (u): 116.07
- Appearance: white crystalline solid
- CAS number: [110-17-8]
- Density ( $g / cm^3$  in c.s.): 1,635
- Solubility in water at  $20^\circ C$ : 6.3 g / l
- Melting temperature:  $287^\circ C$  (560 K)
- Boiling point:  $290^\circ C$  (563 K)
- Flash point:  $273^\circ C$  (546 K)
- Acidity (pKa):  $pka_1 = 3.03$ ,  $pka_2 = 4.44$

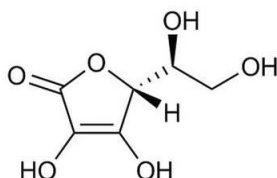


**Figure 7.** Chemical Structure of ascorbic acid

L-ascorbic acid (also known as vitamin C and antiscorbutic principle) is a naturally occurring organic compound with antioxidant properties. It is a white solid that in impure samples, moistened or oxidized by atmospheric oxygen may appear yellowish. It is also a water-soluble vitamin, essential in humans, but not in all mammals, antioxidant, often used in salt form (ascorbate), which performs multiple functions in the body.

Its properties are shown below

- Molecular formula:  $C_6H_8O_6$ ;
- Molecular mass of 176.2 g / mol;
- Appearance: yellow or white solid;
- Density of 1.65 Kg / l;
- Water solubility of 0.33 Kg / l;
- Melting temperature of 190°C–192°C with decomposition
- Acidity (pKa)  $pka_1 = 4.1$   $pka_2 = 11.8$

### 1.5. The aim of this work

The modulation of the degradation rate of a product would be a real advantage: it should preserve its characteristics during processing and for a time comparable to its application, and should be nevertheless fully biodegradable at longer times. The degradation rate of PLA has been modified using several technique: blending, copolymerization, surface modification, and many others, however this changes the physical properties of the material. The use of additives which can change the rate of hydrolysis is a way to preserve the nature of PLA. This field of research is just starting and is extremely promising.

The basic idea of the project is to act on the kinetics and the mechanism of hydrolysis, which is the preparatory step for biodegradation. This has two advantages, giving the chance to control both the degradation in the presence of water (due to hydrolysis) and the biodegradation (when buried in soil or composted).

## Chapter 1

The applicability of PLA will be widened by modulating its durability according to the requirements of the application. This will allow expanding the range of possible applications and open new fields, currently inaccessible due to a too slow or too fast degradation, for example in the automotive and electronics industries. Furthermore, it will be possible to provide PLA new functionalities, such as enhanced barrier properties, anti-oxidant properties, and anti-bacterial properties, thus further enlarging its possible applications and opening new and diversified markets for this biopolymer.

A factor affecting the rate of hydrolysis could either accelerate or retard the whole biodegradation process. It is quite well known that the kinetics of hydrolysis strongly depend on the pH of the hydrolyzing medium.

The idea explored in this study is the use of additives to control the pH of water when it diffuses inside the polymer. In particular, acids will be selected with the following characteristics: a melting temperature higher than the normal processing temperatures of PLA (about 200°C), biocompatibility, and originating from renewable sources. For instance organic acids (e.g. succinic acid, also used as a food additive) are bio- and eco-friendly additives which are able to play this role.

In order to control the release of the acid molecules inside the material in the presence of water, they will be placed as host molecules between the layers of Hydrotalcite-like compounds, also known as layered double hydroxide (LDH), which are known to be excellent reservoirs for drug delivery.

The additives have been dispersed in the polymer by melt compounding, a technique which is readily scalable up to industrial production, being inexpensive, fast, and compatible with current industrial techniques.

The results showed that the mentioned molecules, dispersed in the polymer, are able to control the rate of hydrolysis.

The aim of this work has been to obtain bionanocomposites by micro-injection molding (a technology for high value-added products of increasing application in the areas of medical applications, for example) with a degradation rate which can be modulated in time; so that it can be possible to decide *a priori* the time after which the material will disappear in a given environment. At the same time, the material should preserve its properties during processing.

# Chapter 2

## Materials and methods

### 2.1. Materials

In this work two particular grades of PLA have been used:

- 4032D: This contains about 2% D-lactide with a maximum degree of crystallinity of about 45% and its average molecular weight ( $M_w$ ) is about 106 KDa;
- 4060D: This contains about 15% D-lactide. It is completely amorphous and has average molecular weight ( $M_w$ ) of about 95 KDa.

The values of the  $M_w$  of the two different grades of PLA have been evaluated by GPC. Both kinds of PLA were produced by Natureworks (Minnetonka, MN, USA).

The fillers used were organic acids, all from Sigma Aldrich (St. Louis, MO, USA) (succinic (1,4dioic butane,  $\text{HOOC-CH}_2\text{-COOH}$ , E363), fumaric (trans-butenedioic,  $\text{HOOC-CH=CH-COOH}$ , E297), and ascorbic acids (oxo-3-gulofuranolactone,  $\text{C}_6\text{H}_8\text{O}_6$ , E300)), as well as LDHs of cation composition Mg:Al (2:1) intercalated with the three organic acids just mentioned, used as host molecules.

The selected organic acids were from natural sources and biocompatible. They have the common characteristic of remaining in the solid state at the processing temperatures of PLA. Fumaric, succinic and ascorbic acids were used as received from the supplier.

LDHs intercalated with organic acid have been synthesized through a process that will be explained in the section dedicated to the method. In this process there were used magnesium nitrate, aluminum nitrate and sodium hydroxide, all of them purchased from Sigma Aldrich.

## Chapter 2

### 2.2. Methods

#### 2.2.1. Synthesis of layered double hydroxide

The LDHs were synthesized by co-precipitation. LDHs can be represented by the general chemical formula  $[M^{II}_{1-x}M^{III}_x(OH)_2]^{x+} A^{n-}_{x/n} \cdot mH_2O$ , where  $M^{II}$  and  $M^{III}$  are the divalent and the trivalent cations respectively,  $A^{n-}$  are the exchangeable intralayer anions whose function is to balance any excess positive charge induced by cations. In this work,  $M^{II}$  and  $M^{III}$  were represented by  $Mg^{2+}$  and  $Al^{3+}$  respectively, while  $A^{n-}$  were organic anions deriving from the organic acids mentioned in the previous section.

A metallic solution was prepared using the nitrate of the two cations considered,  $Mg(NO_3)_2$  and  $Al(NO_3)_3$ . The quantities of the salt used were carefully calculated in order to maintain an Mg/Al ratio equal to 2, in particular 28.36 g of  $Mg(NO_3)_2$  and 20.72 g of  $Al(NO_3)_3$  have been used. The salts were inserted in a little vessel and 100 ml of distilled water was added; then the solution was stirred for about two minutes to ensure the complete solubilization of the salts. There was also prepared an alkaline solution, dissolving 8 g of sodium hydroxide (NaOH) in 100 ml of distilled water.

The synthesis reaction of the LDHs was carried out in a one-liter volume reactor. The process was performed under a nitrogen atmosphere, in order to avoid any contamination by carbonation, at 25°C and at atmospheric pressure. During the synthesis reaction of the LDHs, the pH was continuously controlled and kept constant and equal to 9.5, which was found to be the optimal value to yield the present organic-inorganic materials. As an alternative, the same procedure was carried out using the carbonate of the two cations considered to prepare the starting metallic solution.

It is possible to intercalate some molecules inside the LDH. With this aim, organic acid, about 13 g, was directly inserted in the reactor and dissolved in 500 ml of distilled water. The system was covered and continuously stirred. The metallic solution and the alkaline one were slowly pumped into the reactor. The flow rate of the metallic solutions was 0.5 ml/min; a pH-meter and a pump were connected to a computer where a software application analysed the pH and transmitted to the pump the correct flow rate of alkaline solution in order to keep the pH constant.

Once the metal salts were ready, the final solution in the reactor was stirred for three hours. After aging, the material was washed with distilled

### *Materials and methods*

water and centrifuged (4000 rpm) three times, to be sure that all impurities were removed from the reaction products. Lastly, the products were dried in an oven for 24 h at 60°C. After drying, whitish powders were obtained after grinding.

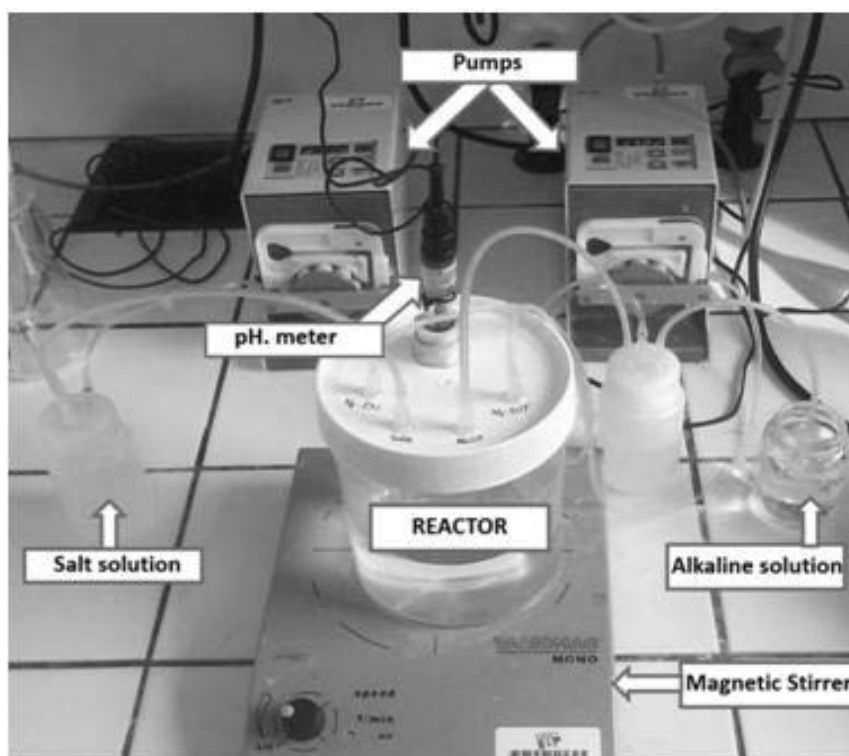


**Figure 8.** Reaction system for LDH synthesis

### *2.2.2. Production of the samples*

#### *Extrusion process*

The pellets of the PLA, organic acids, and the LDHs synthesized were dried under vacuum at 60°C in an oven for 24 h. The dried materials were melt compounded, processed in a twin-screw mini-extruder, Minilab Haake Thermo Fisher Scientific (Waltham, MA, USA), with counter-rotating screws, Figure 9, at a homogeneous temperature of 170°C, at 100 rpm, with a cycle time of 5 min and an average charge time of 4–5 min. The extrusions were carried out using dry nitrogen as the purge gas in the hopper.

## Chapter 2

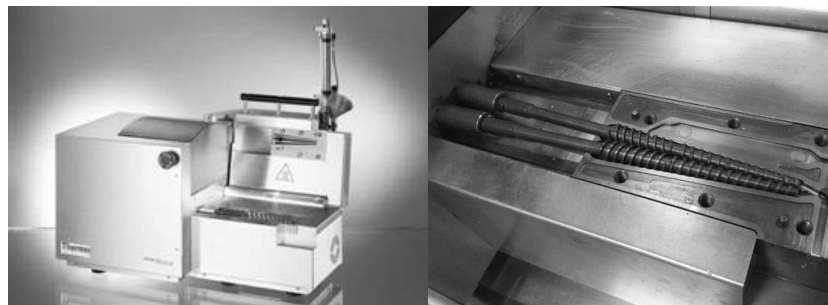


**Figure 9.** Minilab Thermo Scientific Extruder and its counter-rotating screws

Several blends were studied, all reported in Table 1.

**Table 1.** Extruded materials

Groups	Extruded materials
Pure PLA	4060D; 4032D.
4032D + LDH	4032D + (LDH-CO <sub>3</sub> ) (at 3% wt/wt); 4032D + (LDH-NO <sub>3</sub> ) (at 3% wt/wt).
4032D + (LDH-organic acids)	4032D + LDH-succinic acid (at 1%, 3%, 5% wt/wt); 4032D + LDH-fumaric acid (at 1%, 3%, 5% wt/wt); 4032D + LDH-ascorbic acid (at 3% wt/wt).
4032D + organic acids	4032D + succinic acid (at 1% wt/wt); 4032D + fumaric acid (at 1% wt/wt); 4032D + ascorbic acid (at 1% wt/wt).
4060D + (LDH-organic acids)	4060D + LDH-succinic acid (at 3% wt/wt).
4060D + organic acids	4060D + succinic acid (at 1% wt/wt).

No higher percentages of (LDH + organic acids) were considered: this was in order to avoid degradation of the PLA. 1% of organic acids

### *Materials and methods*

corresponds about to the same quantity of organic acid intercalated in 3% (LDH + organic acids).

#### *Compression molding*

Several amorphous films were obtained from the extruded materials by compression molding. A carver laboratory press was used at 170°C for 20 min, with a subsequent fast cooling in air. From these films, whose thickness was about 250 µm, there were obtained samples of dimensions [1 cm × 1 cm], which were then subjected to hydrolysis tests.

#### *Micro-injection molding*

The injection molding machine used was a HAAKE MiniJet II by Thermo Fisher Scientific (Waltham, MA, USA), Figure 10. The HAAKE MiniJet system is a piston injection molding system. Material consumption is reduced dramatically in comparison with conventional injection molding units due to:

- Reduced cylinder volume, resulting in a smaller quantity of required material
- Almost complete transportation of material into the mold, this minimizing any loss of material.



**Figure 10.** Haake miniJet

## *Chapter 2*

Vertical machine design features are:

- Simple loading of powders and pellets within the system cylinder;
- Quick and easy removal of the heated cylinder;
- Simple design for the exchange of molds without tools.

To ensure a high reproducibility of the test specimens, the HAAKE MiniJet is equipped with a microprocessor control. All processing parameters, such as temperature (separately for the injection cylinder and mold), pressure and duration of injection and post pressure phase, are controlled by the PCB. User influences on the quality of the samples can be avoided by the high reproducibility.

In conventional injection molding, the mold temperature is controlled by a continuous cooling method, in which a coolant with constant temperature is circulated in the cooling channels to cool the mold and the polymer melt. During the filling stage, this causes an abrupt polymer solidification close to the mold surface, which reduces the section open to flow and, due to the increase in the viscosity, decreases the ability of the polymer melt to fill the cavity. This issue is particularly significant for micro-injection, in which high aspect ratios are precluded by premature solidification.

In order to overcome the limitations of conventional injection molding of micro-injection molded parts, a new dynamic mold temperature control system for rapid heating and cooling of the mold was employed to produce the micro-injected samples (De Santis and Pantani, 2016). In particular, in two equal regions, one just after the gate and another very close to the first one, the local temperature of the mold surface has been controlled by an ad-hoc software program based on Labview, in order to produce biphasic micro-injected samples. Starting from the standard truncated cone shape of the molds used with HAAKE Minijet II, a novel system comprising a mold with inserts and heating elements was adopted, as shown in the exploded view drawing in Figure 11.

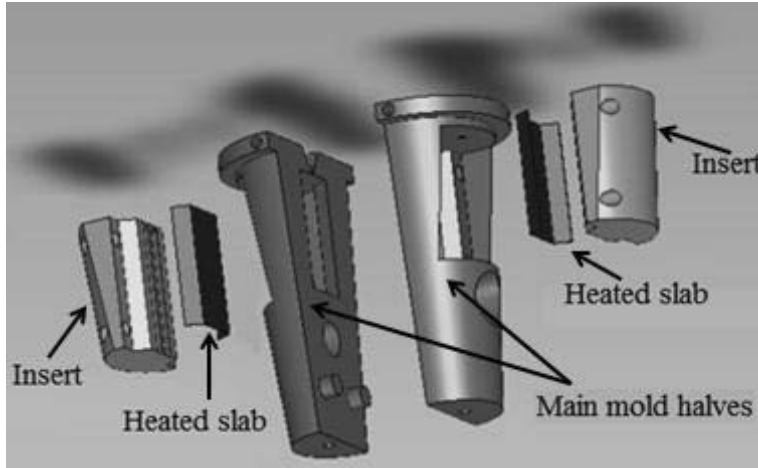


**Figure 11.** Exploded view of the elements composing the mold.

The system consists in an electrical resistive thin component and an insulation layer and can increase the mold surface temperature of some tenths of a degree Celsius in a time of the order of one second. Between the two main mold halves there was inserted a slab that gives a shape to the cavity, see Figure 12.

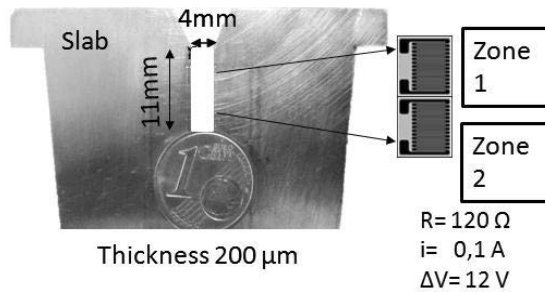


**Figure 12.** Slab, cavity dimension and heated zone

Figure 13 is shows a sectional view of the assembled mold. The two heating elements can work independently: it is therefore possible to selectively heat an area of the cavity.

## Chapter 2

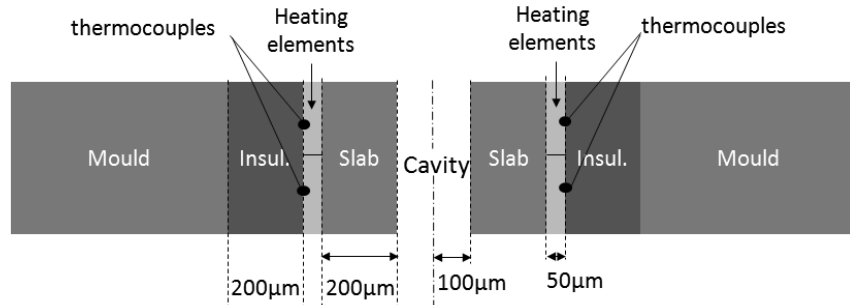


**Figure 13.** Schematic view of the assembled mold

The sample production process consisted of three phases:

- Injection: melted PLA was injected, at 220°C and at 150 bar, into the warm cavity (it was at 160°C), injection time was 20 s;
- Maintenance-cooling: injected PLA was cooled to 60°C at 140 bar, maintenance time was 20 s;
- Crystallization from the glass: half of the sample is heated to 105°C (gate or tip) while the other half remains at 60°C, crystallization time was 1000 s (crystallization half time at 105°C  $\approx$  150 s).

The whole process was carried out under a nitrogen atmosphere.

### 2.2.3. Hydrolysis tests

As mentioned above, for PLA, hydrolysis is the main mechanism of depolymerization and the controlling step of the biodegradation process in compost. Therefore, the rate of hydrolysis gives a direct indication of the rate of degradation during composting. In this work, to carry out hydrolysis tests, distilled water was used, whose pH value was about 6.5. These tests were performed at 58°C, the temperature adopted for biodegradation tests according to ASTM and ISO standards. Several samples of all the blends analysed have been put each one in a glass container filled up with distilled water; the ratio between the amount of water [ml] and the mass of the dried sample [g] was set at 800. In order to keep a constant temperature of 58°C during the hydrolysis test, a thermostatic bath with lid was used. After every 24 h of hydrolysis, the water of each sample was analysed by using a Crison pH-meter at 25°C. After the analysis of pH, the liquid was replaced by the same amount of fresh distilled water as before: the glass vessel was emptied using a

## *Materials and methods*

syringe, equipped with a needle having a diameter of 0.2 mm. At pre-established times, all the samples in their vessels were dried under vacuum at 60°C for about 3 h and weighed. After these operations, one of the samples was kept dry for further analysis. At the end, the several vessels were put again into the thermostatic bath. The samples, for the whole of the hydrolysis test, never left their vessels, in order to avoid undesirable losses of the hydrolyzed material. The hydrolysis of all samples was carried out for about 60 days: after 60 days, some samples were reduced into very small fragments and their mass becomes very small, for this reason it becomes really difficult to carry out the analyses correctly. It is worth mentioning that, according to the literature (Gorrasi and Pantani, 2013a), the rate of hydrolysis at 58°C is about 3–4 orders of magnitude larger than that measured at room temperature. This means that 60 days at 58°C would provide indications concerning the behavior of the samples for several years at lower temperatures.

### **2.2.3. Characterization of the samples**

#### *Gel Permeation Chromatography (GPC)*

GPC analyses were performed in order to evaluate the evolution of molecular weight of the samples as hydrolysis proceeds. The equipment used to carry out the GPC was a high performance liquid chromatography (HPLC) Waters (Milford, MA, USA) equipped with an auto-sampler. The analysed samples, at different hydrolysis times, were dissolved in tetrahydrofuran (THF), with a ratio (sample mass/solvent) equal to about 1/1 [g/mol] at 50°C. The obtained solutions were then filtered by using a filter Chromafil PTFE 0.45 µm.

#### *Differential Scanning Calorimetry (DSC)*

DSC analyses were performed in order to evaluate the Evolution of the degree of crystallinity and of the glass transition temperature of the different samples subjected to hydrolysis. The tests were carried out by means of a DTA Mettler Toledo (DSC 822) (Columbus, OH, USA) under a nitrogen atmosphere. The samples, with a mass of about 5 mg, were subjected to the following thermal program:

- Heating step from -10°C to 200°C at 10°C/min (first heating);
- Isothermal step for 5 min at 200°C;
- Cooling step from 200°C to -10°C at 10°C/min (cooling);
- Heating step from -10°C to 200°C at 10°C/min (second heating).

## Chapter 2

### *Rheological tests (hydrolysis at high temperature analysis)*

In order to assess the significance of hydrolysis in the molten state, time sweep tests at constant frequency were performed. The rheological tests were carried out by a Haake Mars II, Thermo Fisher Scientific (Waltham, MA, USA), rotational rheometer in dynamic mode in parallel plates configuration under a nitrogen atmosphere. The rheological tests were performed at 200°C, with the stress set to 500 Pa and a frequency of 1 rad/s, maintaining all values constant for 3 h. The materials, in order to evaluate the effect of the presence of water, were not dried before the tests. The rheological data will be reported in the plots versus the whole time at test temperature, including the time needed to set the gap. To perform the tests, a plate-plate geometry was used, the diameter of the plate used was 20 mm with a gap of 0.45 mm.

### *Mechanical tests*

Penetration mechanical tests were carried out in order to evaluate the breaking strength of the samples as hydrolysis proceeds. The dynamic mechanical measurements were been carried out using the DMA 8000 Perkin Elmer (Waltham, MA, USA).

A tip with a diameter of 150  $\mu\text{m}$  was used, with a maximum force of 7 N, with a speed of 0.2 N/min. The operating scheme of the apparatus is shown in Figure 14.

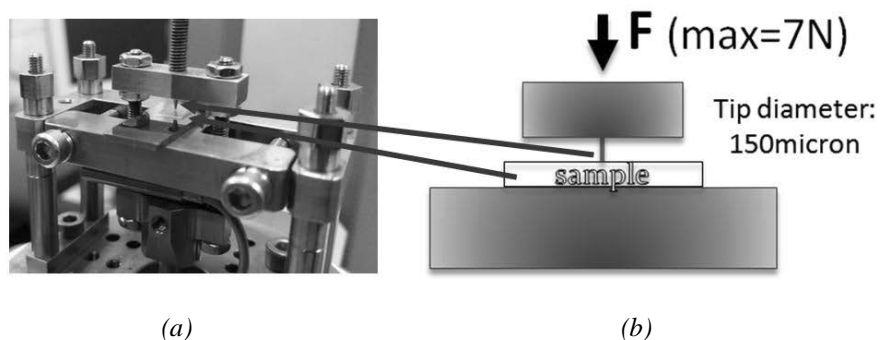


**Figure 14.** (a) Assembly for penetration test; (b) Scheme of the test.

The sample was placed under the tip, the latter moving until contacting the sample, and further provoking deformations and eventually breaking when the sample was more fragile than the maximum allowed value of 7 N (the instrumental limit). DMA processes the data and returns a graph of

### *Materials and methods*

the force according to the displacement of the tip. The data were subsequently processed in order to obtain a stress strain graph. For this purpose, a measurement was carried out in the absence of a sample in order to obtain the maximum displacement that the tip can perform. This value is useful in order to obtain the thickness of the sample, knowing the displacement value when the tip touches the sample.



# Chapter 3

## Selection of the Materials

The experimental procedure can be divided into two steps:

1. The first step is focused on the selection of materials;
2. The second step treats the production and characterization of the samples obtained by micro-injection molding using the materials selected in the previous step.

In this chapter the selection of the materials will be discussed. At first, which kind of pure LDH to use was investigated (with  $\text{NO}_3^-$  or  $\text{CO}_3^{2-}$  as interlayer anion) by studying the effect of adding it to the PLA. After that, the adding of the selected LDH intercalated with organic acid to PLA was studied, choosing at the end: the optimal percentage to add to the PLA and the best LDH-organic acid in order to protect the material from the process of hydrolysis.

From the extruded materials, several films were obtained by compression molding. The samples (1 cm  $\times$  1 cm with a thickness of about 250  $\mu\text{m}$ ), subsequently submitted to the hydrolysis test, were cut from these films. This chapter will present the experimental results for the samples obtained by compression molding submitted to hydrolysis.

### 3.1. Selection of the Benchmark LDHs

In this part of the study, 4032D was used as the PLA matrix. Two different kinds of LDHs were considered:  $\text{NO}_3^-$  and  $\text{CO}_3^{2-}$  as interlayer anion.

PLA was added to the LDHs by melt compounding, as explained in the previous chapter. The amount of LDHs used was 3% wt/wt. In this section, three different samples will be considered:

- 4032D
- 4032D + 3% (LDH- $\text{CO}_3$ )
- 4032D + 3% (LDH- $\text{NO}_3$ )

These samples were subjected to the hydrolysis process. The experimental results are presented below.

## Chapter 3

### 3.1.1. Hydrolysis tests: experimental results

Below are presented the experimental results of the hydrolysis process in the solid state at 58°C under the conditions mentioned in Chapter 2.

#### *Hydrolysis at high temperature (Rheological analysis)*

Figure 15 presents the results of the rheological analyses. The rheological tests were carried out in order to assess the significance of hydrolysis in the molten state. Time sweep tests were performed on 4032D and on 4032D + 3% (LDH-NO<sub>3</sub>).

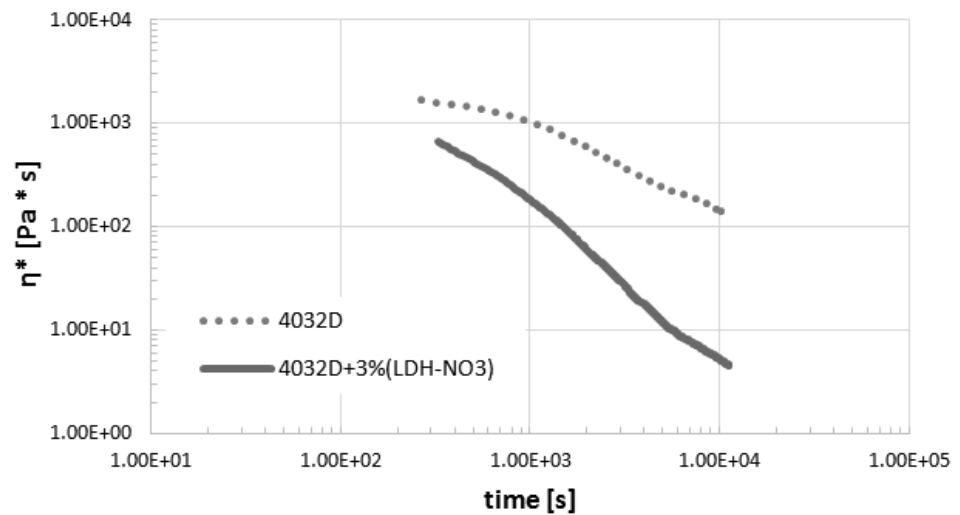


**Figure 15.** Time evolution of the complex viscosity during rheological tests (unhydrolyzed PLA and PLA + LDH/nitrate )

From the data in this figure, we can see that all materials present a decrease in the viscosity over time, due to the hydrolysis and thermal degradation. However, the presence of LDH/nitrate promotes significantly the degradation rate in the molten state. This significantly limits the use of this filler in melt compounding.

#### *Weight loss*

Figure 16 shows the evolution of the sample mass as the hydrolysis proceeds.

### Materials selection

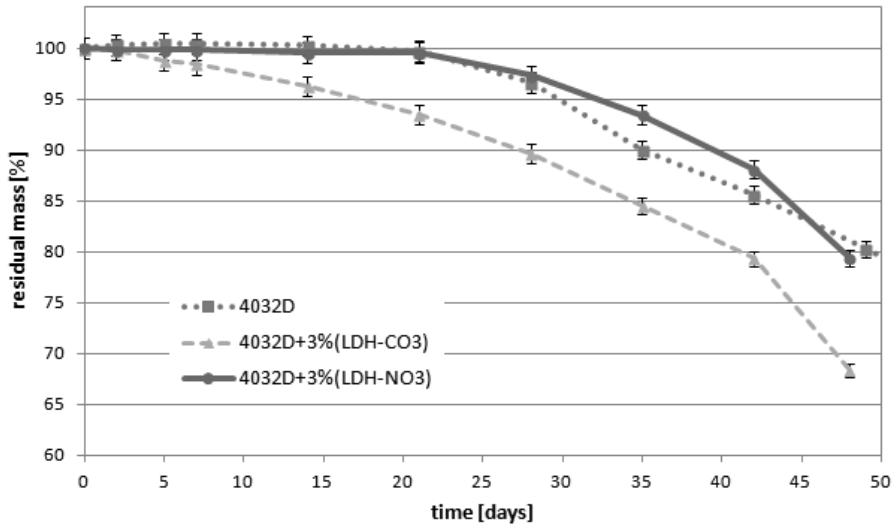


**Figure 16.** Weight loss during hydrolysis (PLA and PLA + LDH/nitrate or carbonate)

When  $H_2O$  penetrates the polymer, hydrolytic degradation starts, converting this very long polymer chain into much shorter water-soluble fragments, a reverse polycondensation process. When these fragments leave the samples, a loss of weight of the samples is easily detected. From Figure 16 we can observe the effect on the resistance to hydrolysis process of adding LDH to pure PLA. The presence in PLA of LDH- $CO_3$  decreases the stability of the material with respect to hydrolysis. Using LDH- $NO_3$  as filler, instead, makes PLA more resistant to hydrolysis process up to 45 days, after that there is no significant difference between the pure PLA and PLA + 3% (LDH- $NO_3$ ).

### Calorimetric analysis (DSC)

In Figure 17 we can see the evolution of the degree of crystallinity as a function of hydrolysis time.

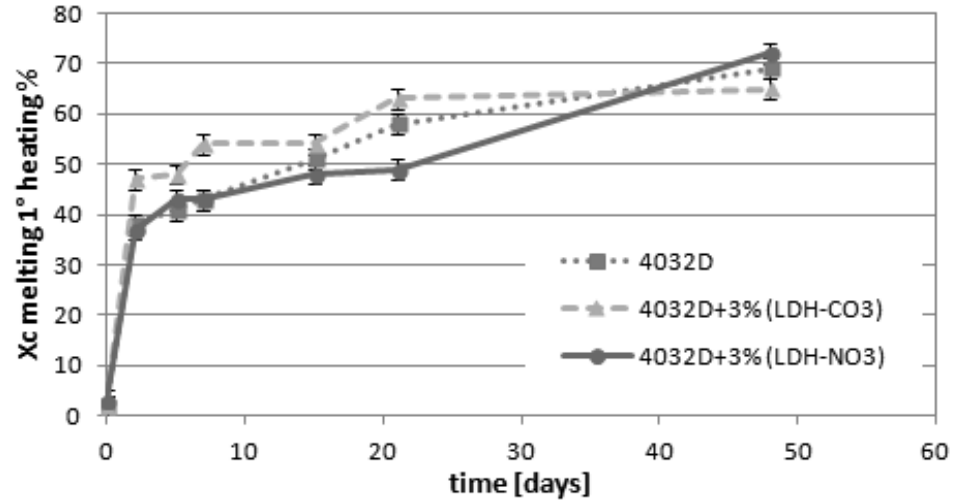


**Figure 17.** Evolution of degree of crystallinity during hydrolysis (PLA and PLA + LDH/nitrate or carbonate)

The degree of crystallinity was calculated from the thermograms obtained during the first heating scan according to the formula

$$X_c(t) = \frac{\int_0^t \frac{\delta Q}{\delta t} dt}{\int_0^{t_\infty} \frac{\delta Q}{\delta t} dt} = \frac{\Delta H(t)}{\Delta H_\infty} \quad (1)$$

in which  $\delta Q/\delta t$  is the heat flow measured by the calorimeter,  $\Delta H$  is the integral of the heat flow after the subtracting the baseline, and  $\Delta H_\infty$  is the latent heat of crystallization of a fully crystalline PLA, which can be found in the literature to be 93 J/g (Fischer et al., 1973).

The degree of crystallinity ( $X_c$ ) increases on increasing the hydrolysis time. These degrees of crystallinity are very high if compared with the maximum value reachable by the same materials as a consequence of thermal treatments (less than 45%). This can be partly due to the erosion of the amorphous segments, but is evidently due to a crystallization of the amorphous phase, since most of the samples were amorphous at the beginning of the test.

As mentioned above,  $X_c$  increases for all the samples. There are however some differences between the samples. Indeed, up to 40 days, 4032D + 3% (LDH-CO<sub>3</sub>) exhibits a higher  $X_c$  than the other two samples, probably indicative of a stronger hydrolysis occurring in that case, and in agreement with its larger weight loss (Figure 16). In contrast, the lowest

### Materials selection

value of  $X_c$  is measured for 4032D + 3% (LDH-NO<sub>3</sub>), which presents a relatively better resistance to hydrolysis. Table 2 presents the evolution of the glass transition temperature ( $T_g$ ) and melting temperature peak ( $T_m$ ) during the hydrolysis.

**Table 2.** Summary of DSC results:  $T_g$  was measured during 2<sup>nd</sup> heating scan, the reported  $T_m$  refers to the highest-temperature peak of the melting endotherm during 1<sup>st</sup> heating ramp (PLA and PLA + LDH)

Sample		Days of Hydrolysis				
		0	5	14	21	48
4032D	$T_g$ [°C]	63.8	63.7	61.4	61.4	51
	$T_m$ [°C]	169.9	168.4	167.8	164.9	154.3
4032D + 3% (LDH-CO <sub>3</sub> )	$T_g$ [°C]	61.8	/	/	/	50.2
	$T_m$ [°C]	166.4	164.8	162.9	158.6	150.3
4032D + 3% (LDH-NO <sub>3</sub> )	$T_g$ [°C]	63.3	62.9	62.2	62.5	56.9
	$T_m$ [°C]	168.2	167.5	166.8	166	155.3

From the temperatures reported in Table 2, we can see that both  $T_g$  and  $T_m$  decrease for all the samples with the progression of the hydrolysis: their values remain higher for 4032D + 3% (LDH-NO<sub>3</sub>).

The DSC results show that the presence of 3% (LDH-NO<sub>3</sub>) as filler of PLA preserves the samples from hydrolysis. The thermograms of all the analysed samples are given in the Appendix.

### Gel Permeation Chromatography (GPC)

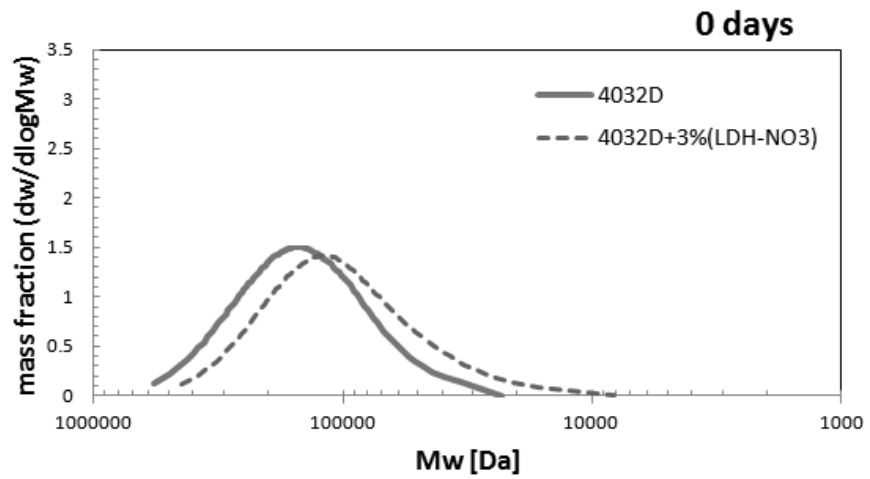
GPC analyses were performed on 4032D and on 4032D + 3% (LDH-NO<sub>3</sub>); we no longer considered 4032D + 3% (LDH-CO<sub>3</sub>): previous analyses have shown how using (LDH-CO<sub>3</sub>) as filler accelerates the hydrolysis of PLA.

In order to evaluate any degradation phenomena of the extrusion process on the PLA, GPC analyses were performed on the unhydrolyzed extruded PLA and PLA pellets. The average molecular weight of pure PLA after extrusion ( $M_n = 70$  KDa;  $M_w = 102$  KDa) is very similar to that of the pellets ( $M_n = 75$  KDa;  $M_w = 106$  KDa), which demonstrates that

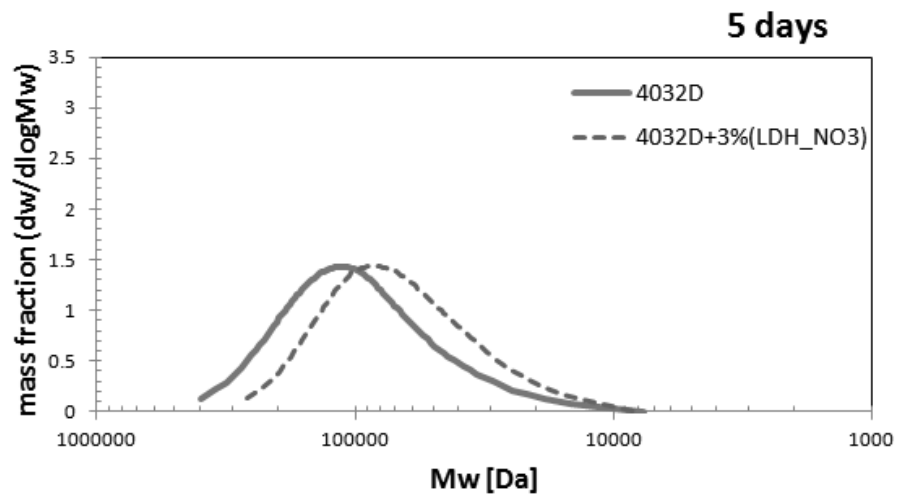
Chapter 3

the extrusion process induces only a negligible degradation of the pure PLA.

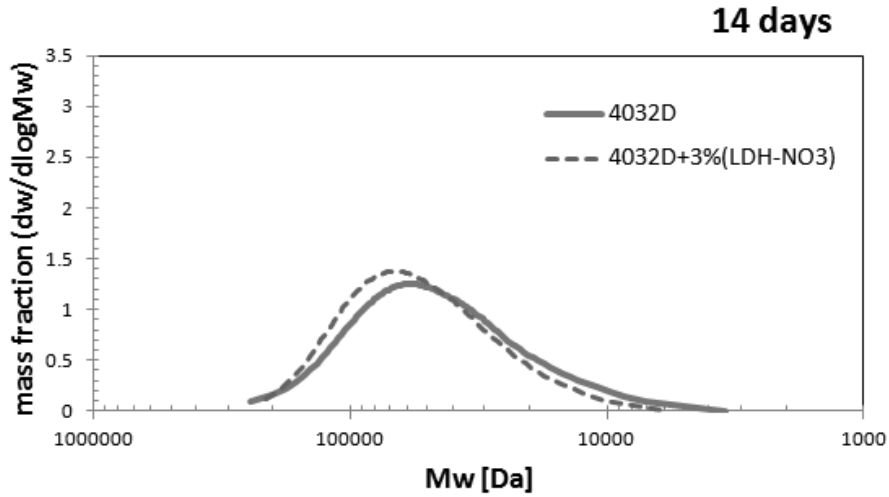
Figure 18 shows the molecular weight distribution curves of the sample analysed by GPC at determined hydrolysis times.



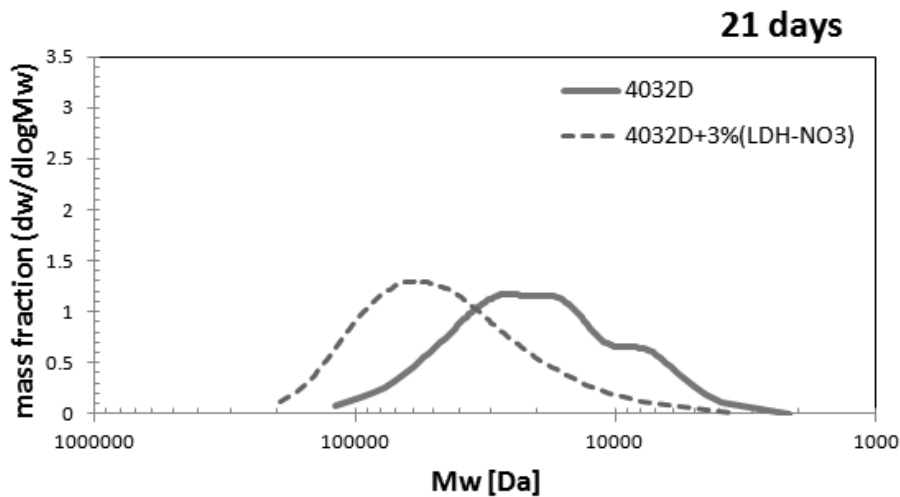
a)



b)



c)



d)

**Figure 18.** Evolution of molecular weight distribution during hydrolysis (PLA and PLA + 3% LDH-NO<sub>3</sub>) for different hydrolysis times: a) 0 days; b) 5 days; c) 14 days; d) 21 days.

From the figure above, it can be seen that the curves for both materials are shifted towards smaller molecular weights with ongoing hydrolysis. In particular, the molecular weight distribution curves for the PLA loaded with LDH are, for the first 5 days, characterized by lower molecular weights than those for the pure PLA; this is probably due to a degradation in the molten state during processing. From day 14 onwards, the distribution of the molecular weight of the PLA with LDH is still being

Chapter 3

shifted toward smaller molecular weights but more slowly than that of pure PLA. In fact, the molecular weight distribution curve of the PLA is located at lower values than that of the PLA with LDH. The data confirm that LDH platelets protect PLA from hydrolysis.

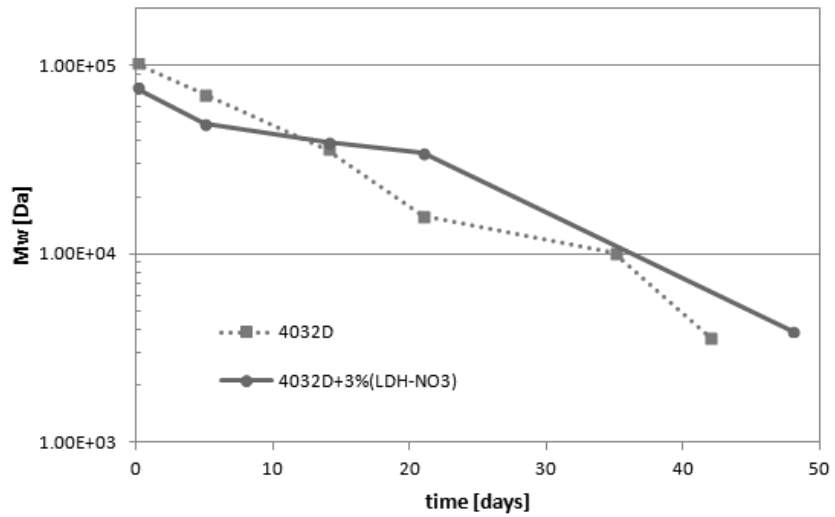


**Figure 19.** Evolution of weight average molecular weight ( $M_w$ ) during hydrolysis (PLA and PLA + 3% LDH-NO<sub>3</sub>)

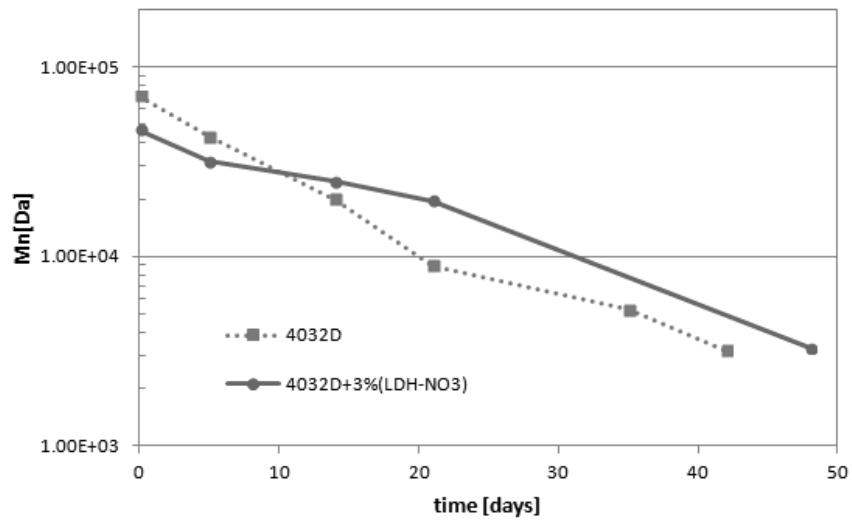


**Figure 20.** Evolution of number average molecular weight ( $M_n$ ) during hydrolysis (PLA and PLA + 3% LDH-NO<sub>3</sub>)

The above figures present the evolution of  $M_w$  [Da] and  $M_n$  [Da] of the two samples as functions of the hydrolysis time (days). As a consequence of the hydrolytic process, the polymeric chains undergo a breakdown, and so the molecular weight decreases. The PDI index shows very little change with hydrolysis time. In fact, the data shown in Figure 19 and Figure 20 are very similar to each other. The values of  $M_n$  and  $M_w$  are higher for 4032D + 3% (LDH-NO<sub>3</sub>) than for pure PLA: therefore, the presence of LDH-NO<sub>3</sub> as filler really protects PLA from hydrolysis.

Observing the results of the different analyses carried out, we can say that LDH-NO<sub>3</sub>, used as a filler in PLA, makes it more resistant to the hydrolysis process in the solid state.

### **3.2. Optimization of the percentage of (LDHs + organic)**

In the previous paragraph we could see how the addition of LDH-NO<sub>3</sub> is able to preserve the PLA from the degradation linked to hydrolysis. Since the kinetics of hydrolysis strongly depend on the pH of the medium in which the process takes place, we can look for a filler able to control the pH of the water when it diffuses inside the PLA. We can consider organic acids as fillers to be bio- and eco-friendly additives. In order to control the release of these molecules in the water diffused in the PLA, they have been intercalated in LDH-NO<sub>3</sub>. At this point of the experimental work, in order to verify the efficacy of using LDH intercalated with organic acid and to optimize its quantity, two organic acids were considered (succinic and fumaric acids) at three different percentages (1%; 3%; 5% wt/wt).

Six new samples were analysed:

- 4032D + 1% (LDH-succ)
- 4032D + 3% (LDH-succ)
- 4032D + 5% (LDH-succ)
- 4032D + 1% (LDH-fum)
- 4032D + 3% (LDH-fum)
- 4032D + 5% (LDH-fum)

#### ***3.2.1. Hydrolysis tests: experimental results***

The experimental results for the hydrolysis process in the solid state at 58°C under the conditions mentioned in Chapter 2 will now be presented.

### Chapter 3

#### Weight loss

Figure 21 and Figure 22 present the evolution of the sample mass as the hydrolysis proceeds.

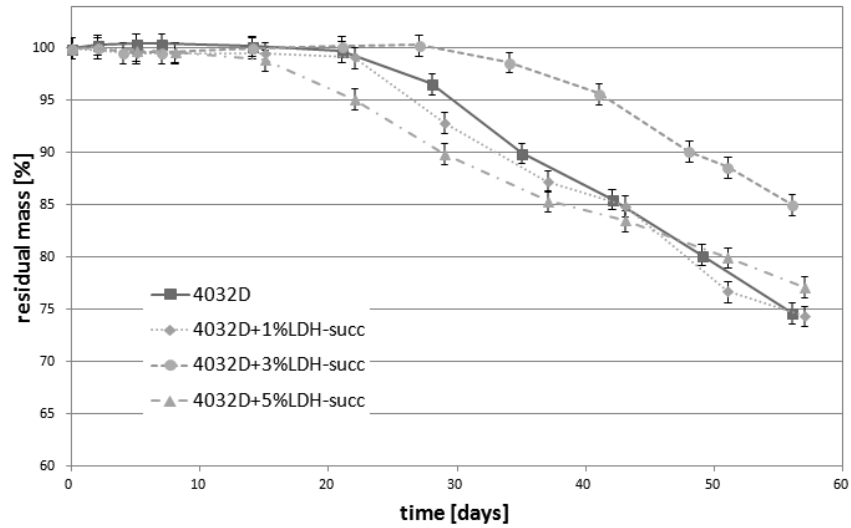


**Figure 21.** Weight loss during hydrolysis (PLA and PLA + LDH-succinic acid for different percentages wt/wt)

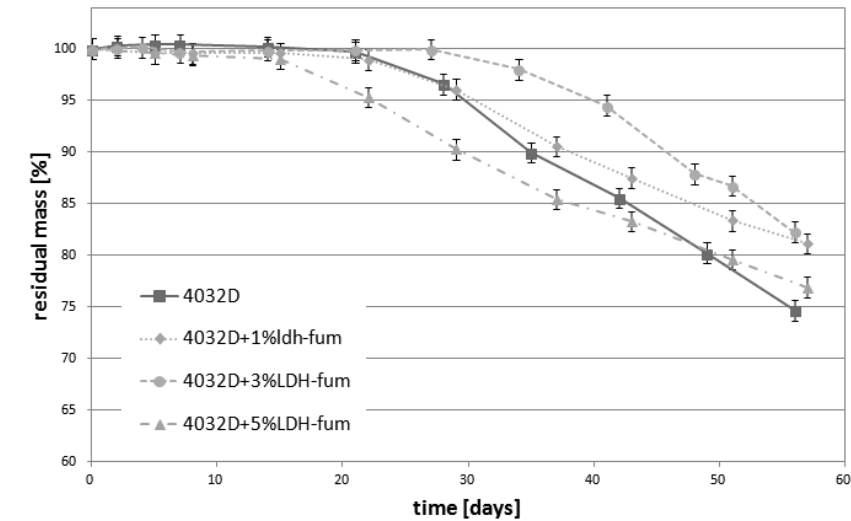


**Figure 22.** Weight loss during hydrolysis (PLA and PLA + LDH-fumaric acid for different percentages wt/wt)

### Materials selection

In the above figures we can see that there is an effect due to the presence of LDH-organic acid, an effect not always protective against hydrolysis. The protective effect against hydrolysis is not proportional to the amount of filler for either acid: 1% LDH-organic acid seems to have a weak effect; 3% LDH-organic acid has a strong protective effect against hydrolysis; 5% LDH-organic acid worsens the resistance of the material, causing it to degrade faster than pure PLA.

### Calorimetric analysis (DSC)

In Figure 23 and in Figure 24 we can see the evolution of the degree of crystallinity as a function of the hydrolysis time.

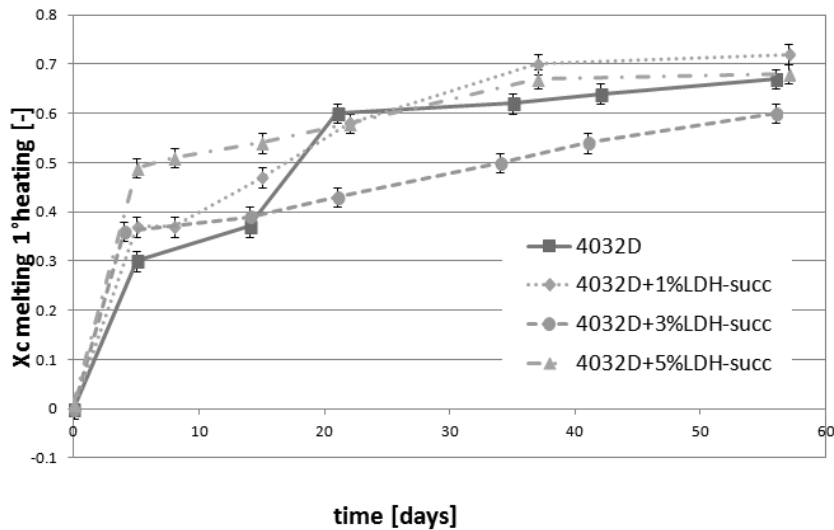


**Figure 23.** Evolution of degree of crystallinity during hydrolysis (PLA and PLA + LDH-succinic acid for different percentages wt/wt)

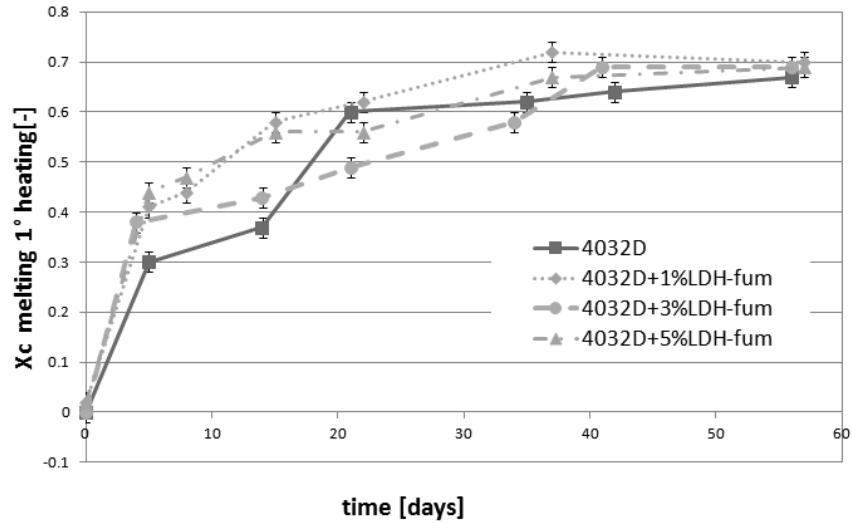


**Figure 24.** Evolution of degree of crystallinity during hydrolysis (PLA and PLA + LDH-fumaric acid for different percentages wt/wt)

The data shown above confirm what we have observed for the weight loss:  $X_c$  increases for all the samples, but for 4032D + 3% LDH-organic acid, the values of  $X_c$  are smaller than its values for the other samples, in particular from 20 days onwards. What we observe can be ascribed to the degradation in the molten state (during the extrusion process): the presence of LDH enhances significantly the degradation.

### 3.3. LDH-organic acid selection

In the previous paragraph the optimal percentage of LDH-organic acid, in order to protect PLA from hydrolysis process, has been chosen: 3% LDH-organic acid wt/wt. In this paragraph, the best LDH-organic acids in order to protect the material from the process of hydrolysis will be researched.

Three different organic acids have been taken into consideration: succinic acid, fumaric acid and ascorbic acid; all of them were intercalated into the LDH. Three different samples were analysed:

- 4032D + 3% LDH-succinic acid (4032D + 3% LDH-succ)
- 4032D + 3% LDH-fumaric acid (4032D + 3% LDH-fum)
- 4032D + 3% LDH-ascorbic acid (4032D + 3% LDH-asc)

### 3.3.1. Hydrolysis tests: experimental results

Below are reported the experimental results of hydrolysis process in the solid state at 58°C under the conditions mentioned in Chapter 2:

#### *Hydrolysis at high temperature (Rheological analysis)*

Figure 25 shows the results of the rheological analyses. The rheological tests were carried out in order to assess the significance of hydrolysis in the molten state. Time sweep tests were performed on 4032D and on 4032D + 3% (LDH-organic acids).

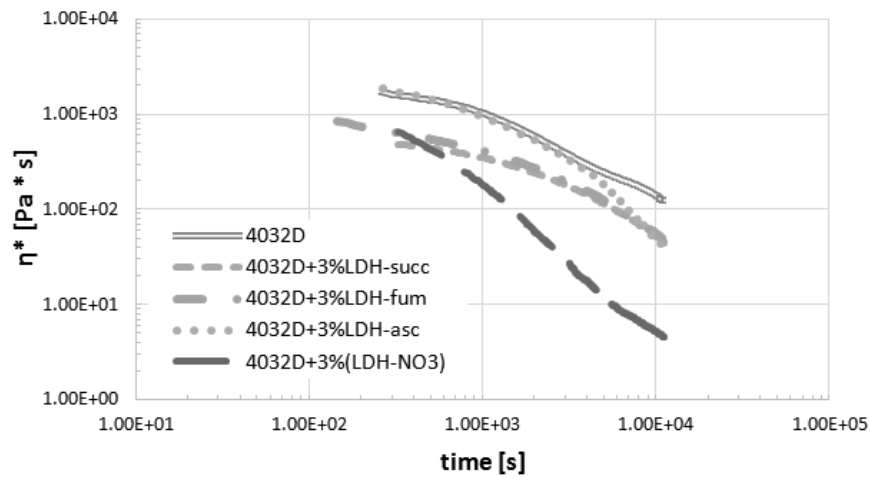


**Figure 25.** Time evolution of the complex viscosity during rheological tests of unhydrolyzed samples (PLA and PLA + 3% LDH-organic acids)

From the data reported above, we can see that all materials present a decrease of viscosity during time, due to the hydrolysis and thermal degradation.

The presence of LDH enhances significantly the degradation. On intercalating the LDH with the acids, however, an increase in viscosity is observed compared to the case of pure LDH used as filler. From the experimental data we can see that, during time sweep tests, the viscosity of PLA + LDH-succinic acid and PLA + LDH-fumaric acid decreases more slowly than the other samples. Using LDH-succinic acid and LDH-fumaric acid as fillers makes PLA more resistant to degradation

### Chapter 3

#### Weight loss

In the figure below, the evolution of the sample mass is reported: for all the samples, a reduction of residual mass is observed, due to hydrolysis.

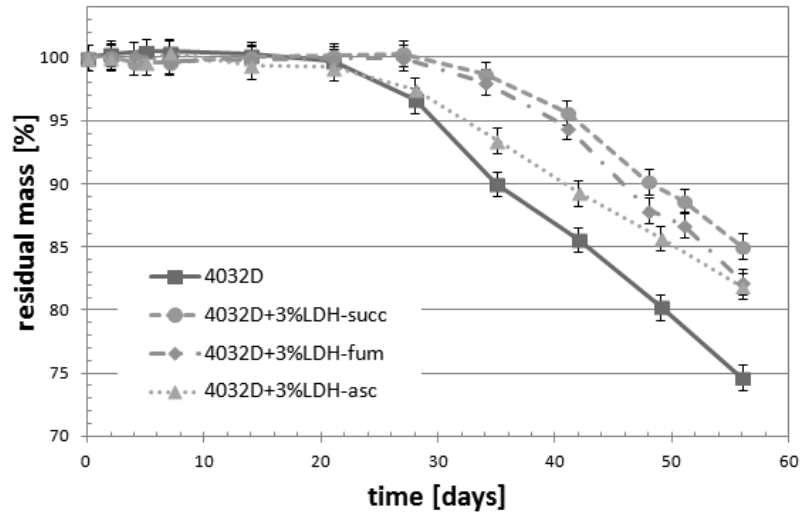


**Figure 26.** Weight loss during hydrolysis (PLA and PLA + 3% LDH-organic acid)

From Figure 26 we can see how the presence of 3% of LDH-organic acid can protect PLA from the hydrolysis process, in particular this is even better exemplified with LDH-succ, which presents the best relative positive effect: the time corresponding to a weight loss of 10%,  $t_{10\%}$ , is about 50 days compared to  $t_{10\%}$  for PLA of 35 days. In summary, for the same residual mass, the time increases by about 40%.

#### Calorimetric analysis (DSC)

Figure 27 shows the evolution of the degree of crystallinity ( $X_c$ ) as a function of the hydrolysis time: for all the samples,  $X_c$  increases as the hydrolysis proceeds.

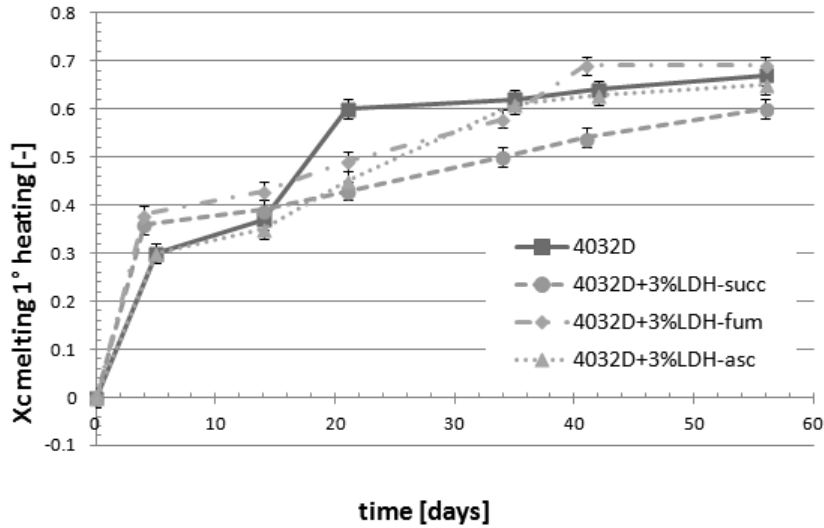


**Figure 27.** Evolution of degree of crystallinity during hydrolysis (PLA and PLA + 3% LDH-organic acid)

In Figure 27 the different curves have a similar trend up to about 15 days, then the Xc of pure PLA increases rapidly while Xc of PLA + 3% LDH-organic filler increases more steadily, with a lower slope in the case of PLA + 3% LDH-succ.

**Table 3.** Summary of DSC results: Tg was measured during 2<sup>nd</sup> heating scan, the reported Tm refers to the highest-temperature peak of the melting endotherm during 1<sup>st</sup> heating ramp (PLA and PLA + 3% LDH-organic acid).

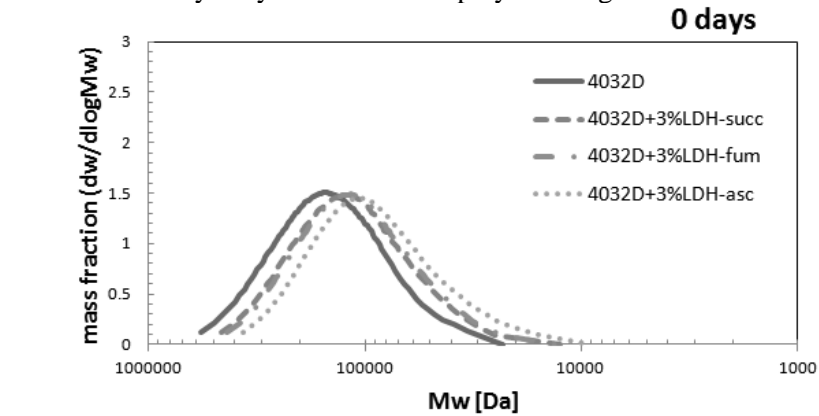
Sample		Days of Hydrolysis				
		0	5	14	21	48
4032D	Tg [°C]	63.8	63.7	61.4	61.4	51
	Tm[°C]	169.9	168.4	167.8	164.9	154.3
4032D + 3% LDH-succ	Tg [°C]	62.8	62.3	61.8	61.7	56.6
	Tm[°C]	169.8	167	166.7	166.5	162.5
4032D + 3% LDH-fum	Tg [°C]	62.2	61.5	61.1	60.9	56.1
	Tm[°C]	169.2	166.9	166.7	166.5	161
4032D + 3% LDH-asc	Tg [°C]	61.2	61.1	59.1	58.6	55.8
	Tm[°C]	169.6	168	167.4	167.3	158.2

### Chapter 3

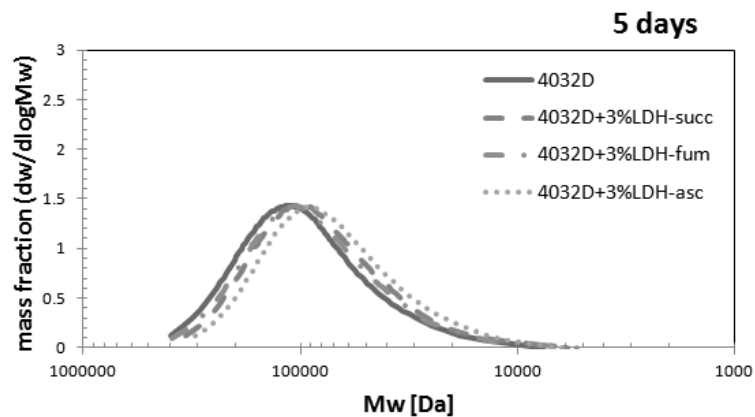
As the hydrolysis proceeds, the polymer chains break down and become shorter. Accordingly, the glass transition temperature ( $T_g$ ) and the highest temperature peak of the melting during the 1<sup>st</sup> heating become smaller and smaller as the hydrolysis proceeds. From the data reported in Table 3, it is clear that  $T_g$  and  $T_m$  decrease for all the samples. However, for the sample with 3% LDH-organic acid, this decrease is less pronounced than for pure PLA, and this happens in particular for PLA + 3% LDH-succ. The results of the DSC analysis confirm what is observed from the weight loss analysis.

### Gel Permeation Chromatography (GPC)

The molecular weight distribution curves of the sample analysed by GPC at determined hydrolysis times are displayed in Figure 28.



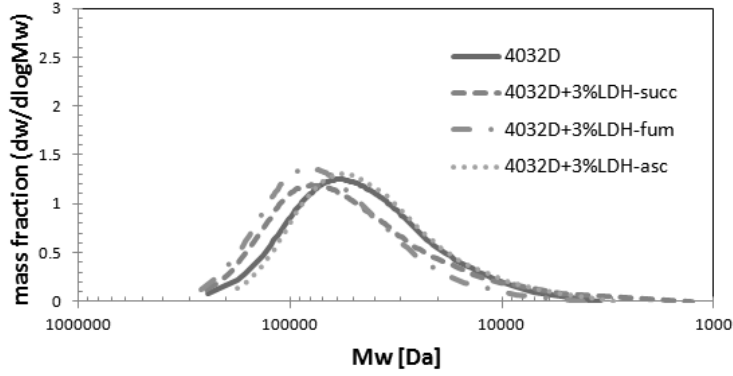
a)



b)

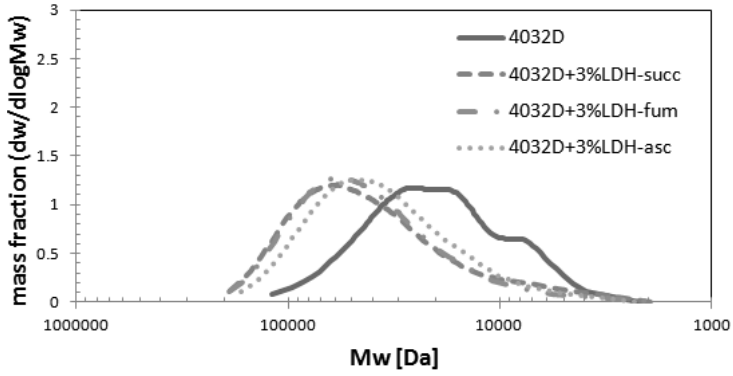
Materials selection

14 days



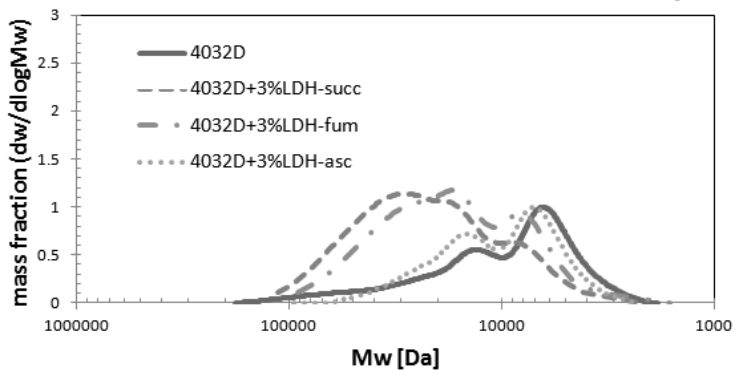
c)

21 days



d)

35 days



e)

**Figure 28.** Evolution of molecular weight distribution during hydrolysis (PLA and PLA + 3% LDH-organic acid) at different hydrolysis times: a) 0 days; b) 5 days; c) 14 days; d) 21 days; e) 35 days.

### Chapter 3

From Figure 28 it is possible to see that the molecular weight distribution curves are shifted towards lower molecular weights as hydrolysis proceeds. In particular a change of shape over time is observed, passing from a unimodal to a multimodal distribution. This is probably due to the fact that the hydrolysis proceeds for all the polymer chains, but the presence of crystals causes a slowing of the hydrolysis with respect to what happens in the amorphous phase, thus leading to the formation of more peaks discriminated by their molecular weight distribution curve. We can observe no differences between the different samples after 14 days, but from 21 days onwards, the molecular weight distribution curves of samples with 3% LDH-organic acid remain at higher molecular weights with respect to pure PLA.

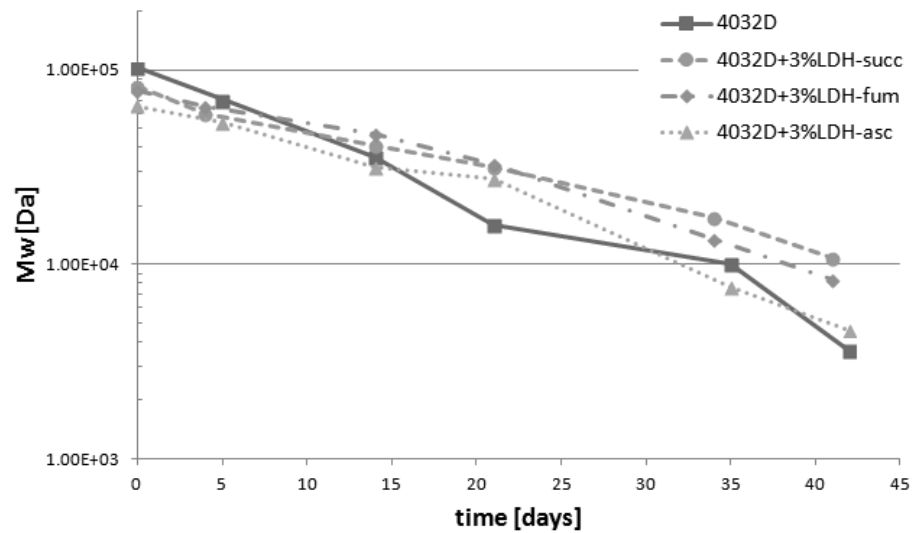


**Figure 29.** Evolution of weight average molecular weight ( $M_w$ ) during hydrolysis (PLA and PLA + 3% LDH-organic acids)

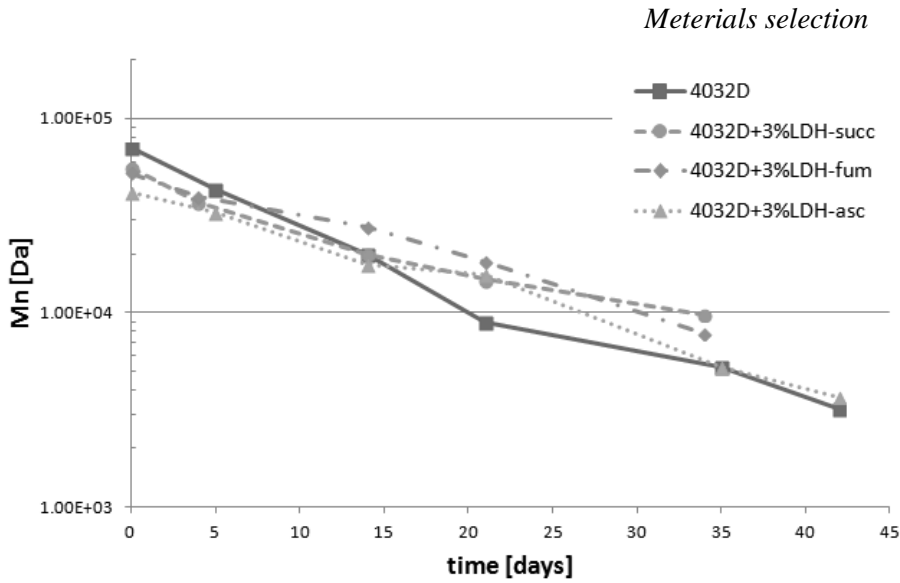
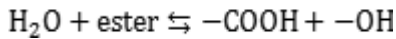


**Figure 30.** Evolution of number average molecular weight ( $M_n$ ) during hydrolysis (PLA and PLA + 3% LDH-organic acids)

In Figure 29 and in Figure 30 the evolution of the weight average molecular weight ( $M_w$ ) and of the number average molecular weight ( $M_n$ ) are reported. As we have observed before, for all samples the molecular weights decrease, but all samples with 3% LDH-organic acids maintain higher molecular weight with respect to neat PLA. Furthermore, we can see that the data for the  $M_n$  and  $M_w$  reported in Figure 29 and in Figure 30 are very similar for both parameters, meaning that the PDI index remains quite unchanged.

We will briefly recall the mechanism of the hydrolysis reaction. The reaction of hydrolysis of PLA can be written as



The kinetics of hydrolysis can be described by an autocatalytic mechanism (Siparsky et al., 1998):

$$\frac{dC_C}{dt} = kC_C C_E C_{\text{H}_2\text{O}} \quad (2)$$

Here,  $C_C$  is the concentration of the carboxylic end-groups and  $C_E$  is the ester concentration.

Both  $C_C$  and  $C_E$  can be related to the molecular weight as follows (Partini et al., 2009):

### Chapter 3

$$C_C = \frac{\rho}{M_n} \quad (3)$$

$$C_E = \frac{\rho}{M_n} (DP - 1) \quad (4)$$

In these equations,  $\rho$  is the density of the polymer sample (about 1210 g/m<sup>3</sup>) and DP is the average degree of polymerization, defined as the ratio  $M_n/M$  ( $M$  is the molecular weight of the repeating unit, equal to 72 g/mol in our case). Equation (3) takes into account the number of ester links in the monomer unit in the case of the polyesters studied in this work. After substituting equation (3) and equation (4) into equation (2) and rearranging, also considering the definition of DP, we obtain

$$\frac{d \ln(M_n - M)}{dt} = -k' \quad (5)$$

where

$$k' = k[H_2O] \frac{\rho}{M} \quad (6)$$

Here,  $k'$  can be considered as the kinetic constant of the hydrolysis process, calculated from the time dependence of the number of average molecular mass of the sample.

In Figure 31,  $\ln(M_n - M)$  is reported as a function of the hydrolysis time.

Materials selection

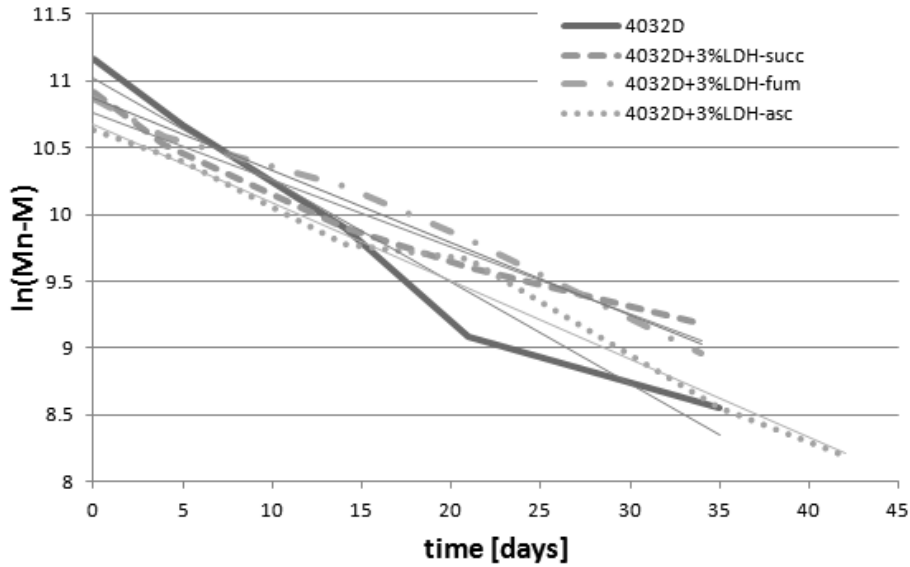


**Figure 31.** Evolution of  $\ln(Mn-M)$  during hydrolysis (PLA and PLA + 3% LDH-organic acids)

The data of each sample in the figure above show an approximately linear trend (the coefficients of reliability reported in Table 4 are quite close to 1). The slope of the lines constitutes the value of the kinetic constant,  $k'$ . A linear dependence on time means that a unique value of  $k'$  is extrapolated for each system. Since the kinetic constant of hydrolysis depends on the pH of the medium, a single  $k'$  value indicates that the pH is mostly constant in time. Correlatively, any irregularity in the slope is indicative of a slight change in  $k'$  and so also of the pH (as observed for PLA after 20 days). Remarkably, a quasi-constant  $k'$  is observed for PLA LDH composites, most probably due to the controlled release of the organic acids intercalated in the LDH. Table 4 shows all the values of  $k'$  and the coefficients of determination.

**Table 4:** Kinetic constant of hydrolysis (PLA and PLA + 3% LDH-organic acids)

	$k'$ [days <sup>-1</sup> ]	$R^2$
4032D	0.0765	0.9628
4032D + 3% LDH-succ	0.0503	0.9591
4032D + 3% LDH-fum	0.0543	0.9871
4032D + 3% LDH-asc	0.0587	0.9868

### Chapter 3

The kinetic constant of PLA + 3% LDH-organic acid is lower than that of the neat PLA, and among the PLA LDH composites, 4032D + 3% LDH-succ has the lowest value, as well as being the sample more resistant to hydrolysis, thus confirming the GPC analysis (Figure 28).

#### *Deconvolution of MWD curves*

It has been reported in the literature that when the MWD (molecular weight distribution) curves present a multimodal behavior, it is appropriate to carry out a deconvolution of the curves in order to perform an analysis of the kinetics.

In this work, the deconvolution was carried out by considering a log-normal function as follows (S. F. Sun, 2004):

$$w_{\log M} = \frac{2.3A}{\sqrt{2\pi \ln \left(\frac{M_w}{M_n}\right)^{\frac{1}{2}}}} \exp \left[ -\frac{\left(\ln(M_w M_n)^{\frac{1}{2}} - \ln(M)\right)^2}{2 \ln \left(\frac{M_w}{M_n}\right)} \right] \quad (7)$$

In which  $A$  is the integral of the curve

$$A = \int_1^{\infty} w_{\log M} d \log(M) \quad (8)$$

and  $M_w$  and  $M_n$  are the weight and number average molecular weight of the curve, respectively.

An example of the deconvolution is shown in Figure 32 with reference to the results of MWD of 4032D at two times of hydrolysis (namely, 0 days and 41 days).

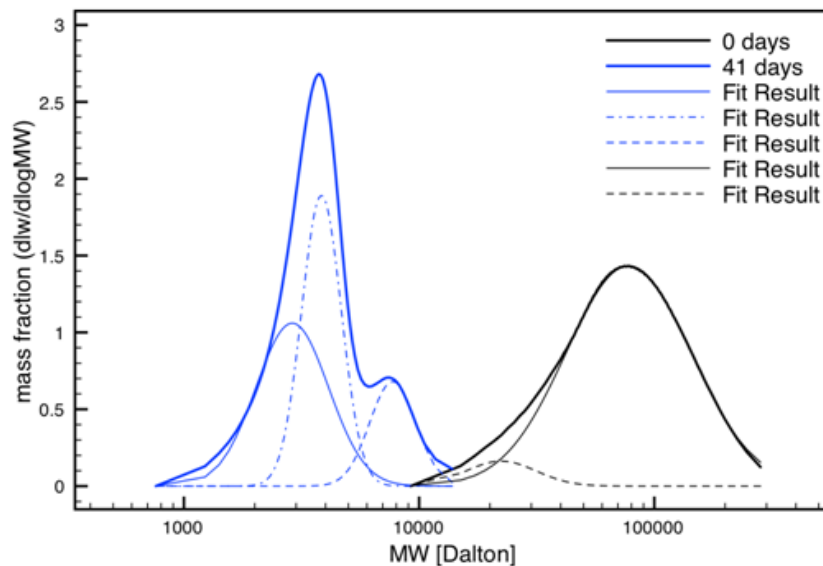


**Figure 32.** Deconvolution of the MWD of 4032D at 0 and 41 days

It can be seen that even at the starting time, the curve needs to be described by two peaks, indicating that a bimodality is present in the sample at the very beginning. After some days, a third peak is needed, which is a clue to the presence of another population of macromolecules. In Figure 33, the result of the deconvolution analysis is reported. In particular, the evolution over time of the number average molecular weight of the several peaks is reported, together with the  $M_n$  calculated from the overall curve (without deconvolution) and used in the previous paragraphs of this thesis.

Chapter 3

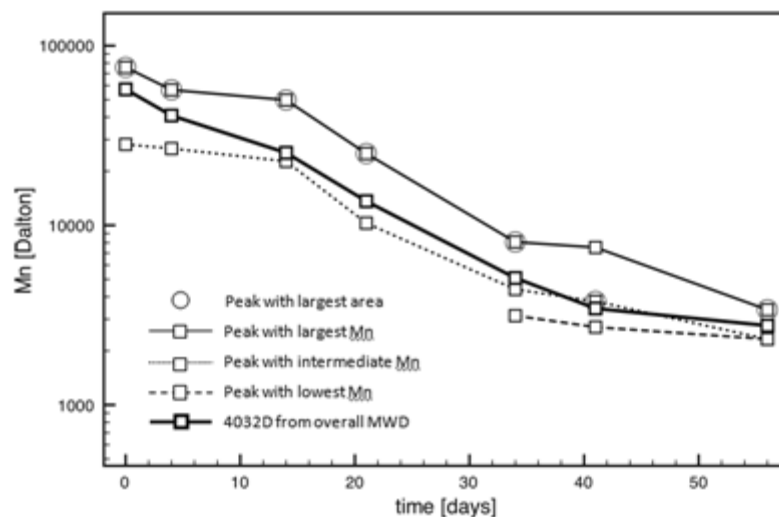


**Figure 33.** Time evolution of Mn calculated from the overall curve (no deconvolution) and from the peaks resulting from deconvolution. A circle identifies the peak with the largest area among those which describe the curve at each time of hydrolysis.

It can be seen that all the lines decrease with time with about the same slope on the semi-log plot. This means that a more accurate analysis of the kinetics of hydrolysis, based on the evolution of each peak rather than the overall curve as done above, would provide about the same results. The same analysis was conducted also for 4032D + 3% (LDH-succinic acid) and is reported in Figure 34.

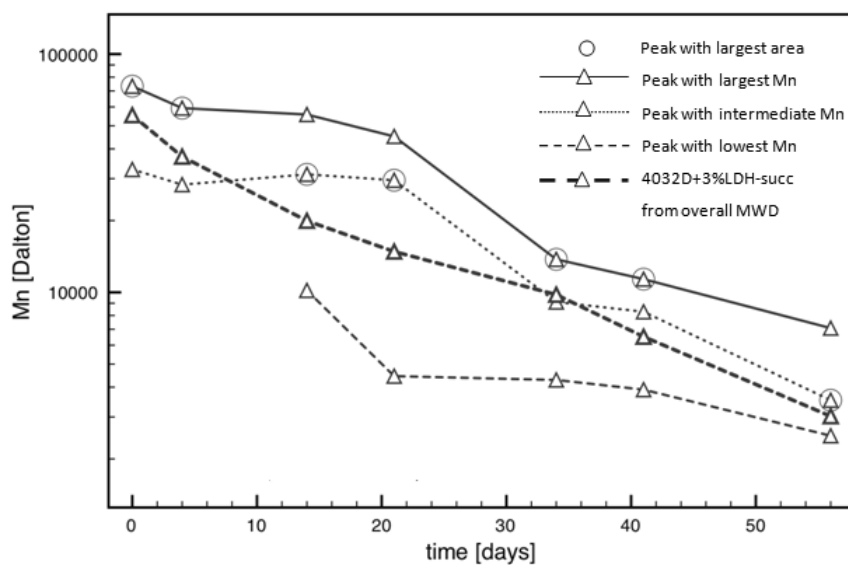


**Figure 34.** 4032D + 3% (LDH-succinic acid). Time evolution of  $M_n$  calculated from the overall curve (no deconvolution) and from the peaks resulting from deconvolution. A circle identifies the peak with the largest area among those which describe the curve at each time of hydrolysis.

In Figure 35, with reference to 4032D and 4032D + 3% (LDH-succinic acid), the time evolution of the  $M_n$  calculated considering only the peak having the largest area is reported.

### Chapter 3

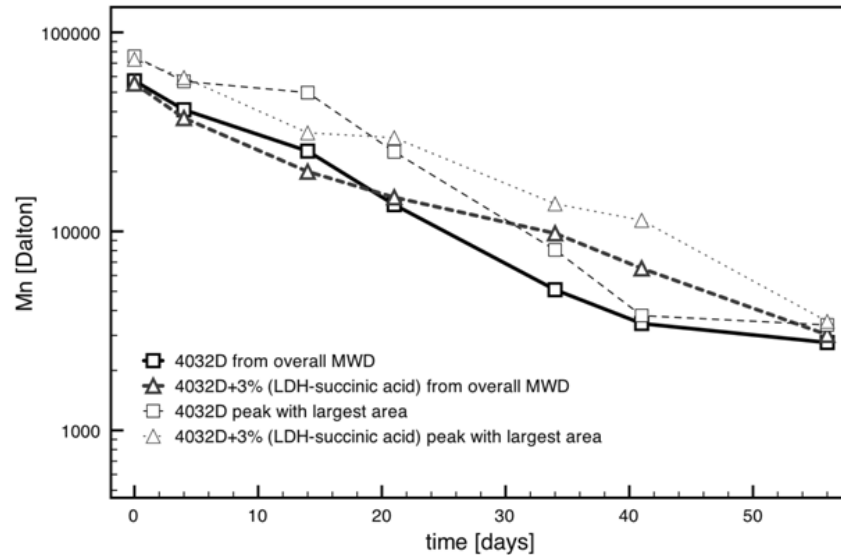


**Figure 35.** Time evolution of  $M_n$  calculated using only the peak with the largest area among those which describe the curve at each time of hydrolysis.

It is evident that for each sample, the slope of the curves on a semi-log plot is about the same, and thus also the kinetic constant would be about the same whether calculated using the deconvolution technique or using the overall curves.

#### *Mechanical tests*

Mechanical test were performed on the hydrolyzed samples: a penetration test, in order to evaluate if the samples more resistant to hydrolysis process were really more mechanically resistant.

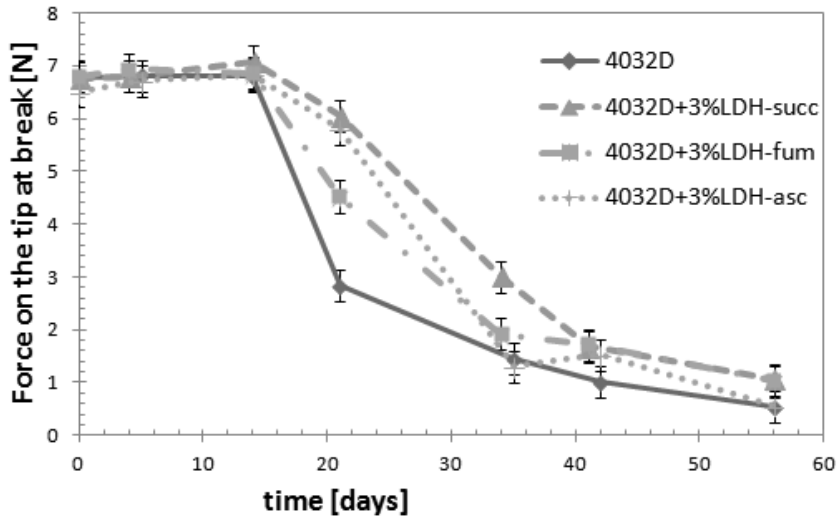


**Figure 36.** Evolution of force at break during hydrolysis (PLA and PLA + 3% LDH-organic acids)

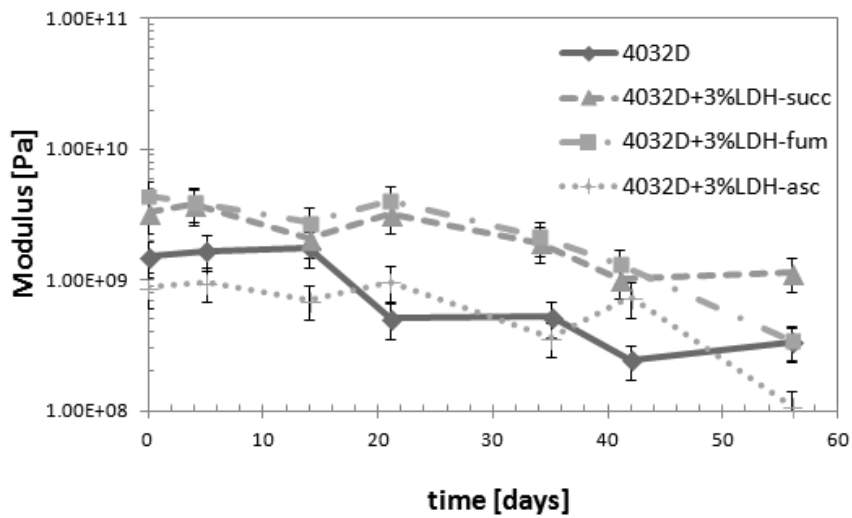


**Figure 37.** Evolution of modulus during hydrolysis (PLA and PLA + 3% LDH-organic acids)

From Figure 36 we can see that up to about 15 days, where the force is near 7 N, there is no fracture for any sample. After 21 days, the samples begin to break at decreasing mechanical stresses as the hydrolysis proceeds. For the 4032D + 3% LDH-organic acid, the force at break is higher than that of neat PLA, in particular for 4032 + 3% LDH-succ. For

### *Chapter 3*

this sample, the same reduction of force at break is found at times more than 30% longer with respect to pure PLA.

As hydrolysis time increases, we can see from Figure 37 a decrease in the modulus of the sample. For the 4032D + 3% LDH-organic acid, the modulus values are higher than that of neat PLA, once again in particular for 4032 + 3% LDH-succ.

This mechanical analysis confirms our previous analysis. Indeed, a dispersion of 3% LDH-organic acid greatly delays the effects of hydrolysis on the PLA; the sample that is the most resistant to hydrolysis is that with the composition filler LDH-succ.

#### *Visual analysis of hydrolyzed samples*

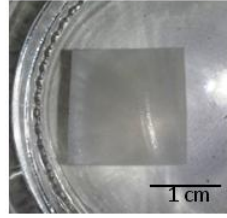
It is interesting to note that all the previous analyses are somehow in agreement from a macroscopic point of view.

Figure 38 displays the photographs of the samples hydrolyzed for different lengths of time.

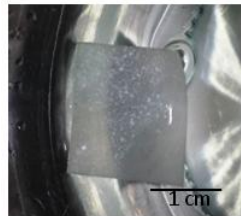
**42days**



PLA



PLA+3%LDH-fumaric



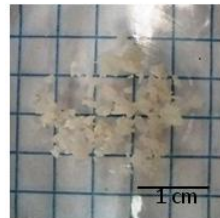
PLA+3%LDH-succinic



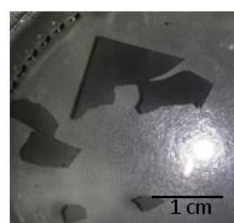
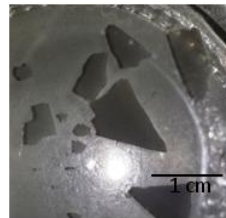
PLA+3%LDH-ascorbic

a)

**56days**



PLA



PLA+3%LDH-succinic



PLA+3%LDH-ascorbic

b)

**Figure 38.** Images of hydrolyzed samples (PLA and PLA + 3% LDH-organic acids); a) hydrolyzed for 42 days; b) hydrolyzed for 56 days.

### Chapter 3

The protective effect of the addition of 3% LDH-organic acids to PLA against hydrolysis is clearly visible. After 42 days, the sample remains intact for PLA composites with LDH-fum and -succ, this is even more pronounced after 56 days, a time when the PLA has entirely broken down.

#### Evolution of the pH

As the hydrolysis proceeded, the pH of the solution in which the PLA samples are hydrolyzed was measured. Here there were considered PLA + 3% LDH-succinic acid (the most resistant sample to the hydrolysis process) and pure PLA. Figure 39 shows the evolution of the quantity of  $H^+$  ions released from the pure PLA as well as from the PLA + 3% LDH-succinic acid samples during the hydrolysis. The experimental data were normalized with respect to the initial mass of the sample (about 0.05 g): pure PLA and the PLA loaded with the selected filler are compared. The quantity of  $H^+$  ions released during the hydrolysis has been calculated from the definition of pH:

$$pH = -\log [H^+]$$

$$[H^+] = 10^{(-pH)}$$

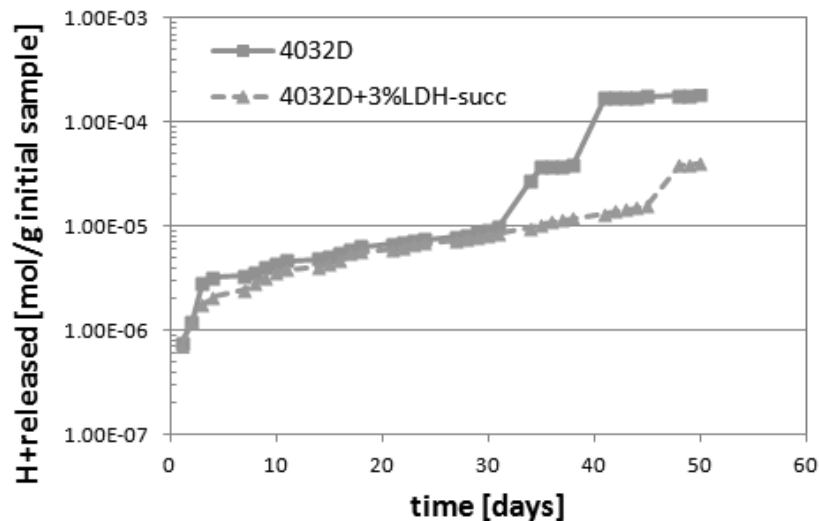


**Figure 39.** Evolution of  $H^+$  released during hydrolysis (PLA and PLA + 3% LDH-succinic acids)

### *Materials selection*

The curves shown in Figure 39 are cumulative curves: at all times taking into account what happened in the previous days. From Figure 39 we can see for the first 15 days that there were more ions released by the pure PLA than released by the loaded PLA. After that, there are no substantial differences between the two samples, up to about 30 days. From that point on, the same trend occurs as in the first 15 days but more accentuated. This further confirms the effectiveness of 3% LDH-succinic acid in protecting PLA from hydrolysis.

### **3.4. PLA loaded with pure organic acids: a faster degradation**

In order to analyse the effect on the hydrolysis process of the organic acids taken into consideration added as filler alone into PLA, new samples have been tested:

- 4032D + 1% succinic acid (4032D + 1% succ)
- 4032D + 1% fumaric acid (4032D + 1% fum)
- 4032D + 1% ascorbic acid (4032D + 1% asc)

The percentages reported above are wt/wt: 1% organic acids corresponds to about the same quantity of organic acid intercalated in 3% (LDH-organic acids).

#### ***3.4.1. Hydrolysis tests: experimental results***

Below are reported the experimental results of hydrolysis process in the solid state at 58°C under the conditions mentioned in Chapter 2:

##### *Weight loss*

In the figure below the evolution of the sample mass is reported: for all the samples we can observe a reduction of residual mass due to hydrolysis.

### Chapter 3

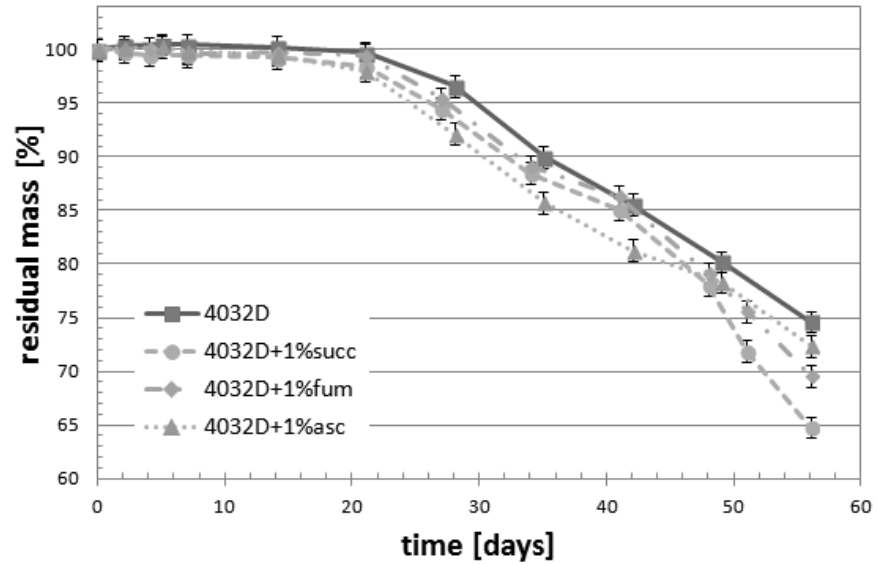


**Figure 40.** Weight loss during hydrolysis (PLA and PLA + 1% organic acid)

In Figure 40 it is evident how the presence of organic acid alone used as fillers makes the PLA less resistant to the hydrolysis process: the weight loss of the PLA + 1% organic acids, at every point of time in the process of the hydrolysis, is higher than that for the neat PLA.

#### Calorimetric analysis (DSC)

Below are reported the results of DSC analysis. As we have seen before, the crystallinity increases with the advance of the hydrolysis.

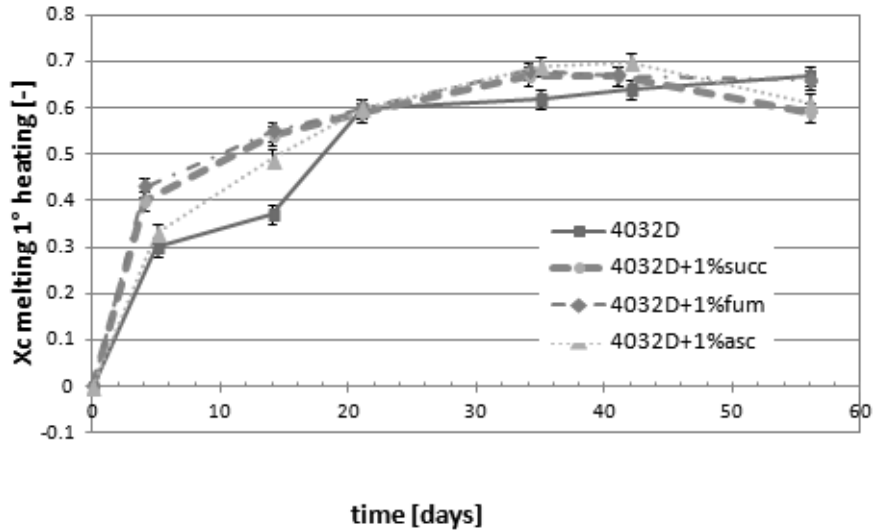


**Figure 41.** Evolution of degree of crystallinity during hydrolysis (PLA and PLA + 1% organic acid)

In Figure 41 the DSC data show that the degree of crystallinity of the samples loaded with only acid increases more rapidly than that of pure PLA. This difference is evident up to about 20 days. After 20 days, there are no evident differences in the degree of crystallinity of the samples. The temperatures of the different samples ( $T_g$  and  $T_m$ ) reported in Table 5 confirm that the presence of organic acids in PLA induces a faster degradation: these temperatures are, in fact, smaller for the samples with acids than the ones for PLA; this difference is particularly evident after 21 days of hydrolysis. At the end of the hydrolysis tests, no difference can be observed in the values of  $T_g$  and  $T_m$  for the different samples.

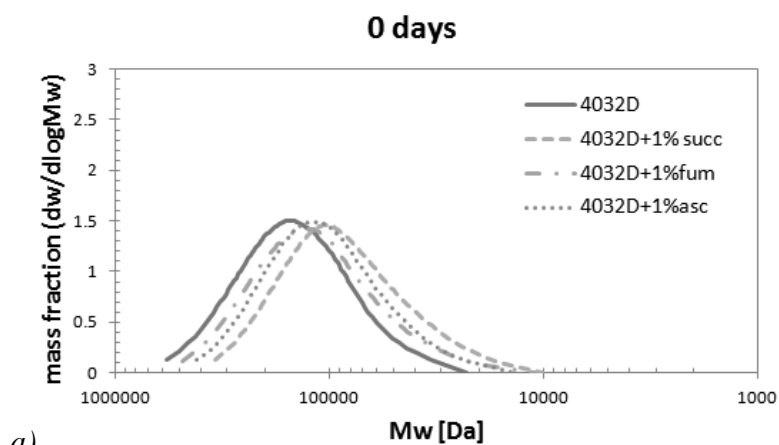
### Chapter 3

**Table 5.** Summary of DSC results:  $T_g$  was measured during 2<sup>nd</sup> heating scan, the reported  $T_m$  refers to the highest-temperature peak of the melting endotherm during 1<sup>st</sup> heating ramp (PLA and PLA + 1% organic acid).

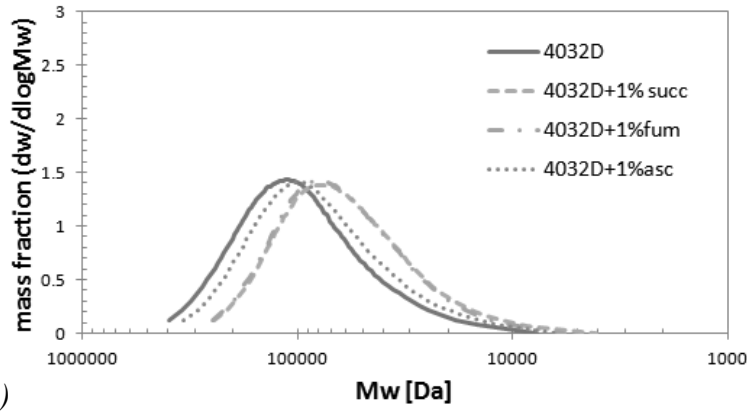
Sample		Days of Hydrolysis				
		0	5	14	21	48
4032D	$T_g$ [°C]	63.8	63.7	61.4	61.4	51
	$T_m$ [°C]	169.9	168.4	167.8	164.9	154.3
4032D + 1% succ	$T_g$ [°C]	60.25	59.8	56.8	55.5	54.9
	$T_m$ [°C]	167.2	166.8	165.4	159.5	154.5
4032D + 1% fum	$T_g$ [°C]	61.7	61.5	58.1	56	55.4
	$T_m$ [°C]	169.5	166.5	165	158	155.9
4032D + 1% asc	$T_g$ [°C]	63.4	63.7	60.9	57.3	52.3
	$T_m$ [°C]	168.7	168.6	166.4	162.8	154.2

### Gel Permeation Chromatography (GPC)

Below are reported the molecular weight distribution curves of the sample analysed by GPC at determined hydrolysis times.

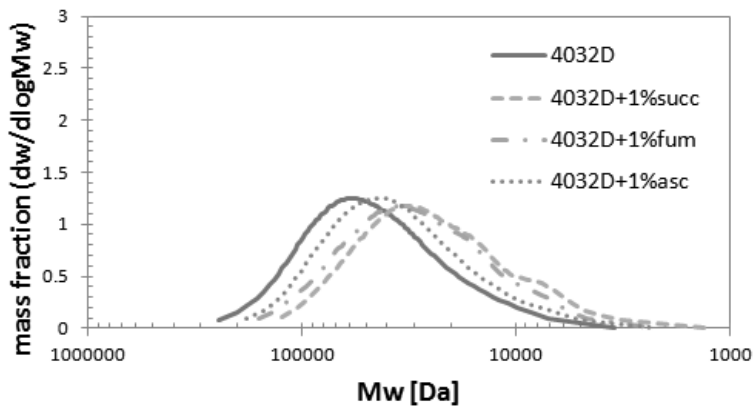


5 days



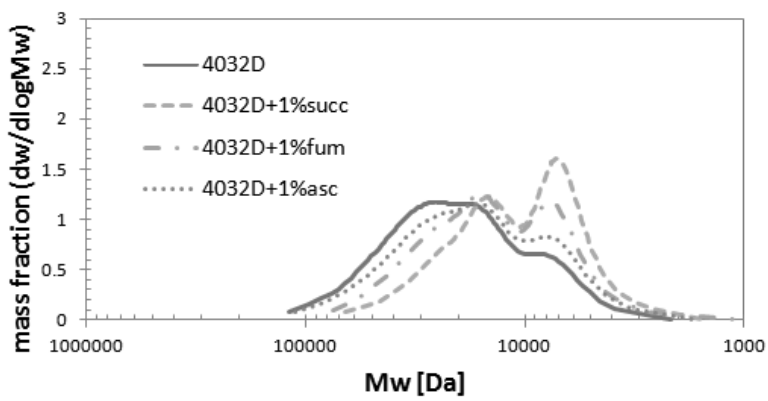
b)

14 days



c)

21 days



d)

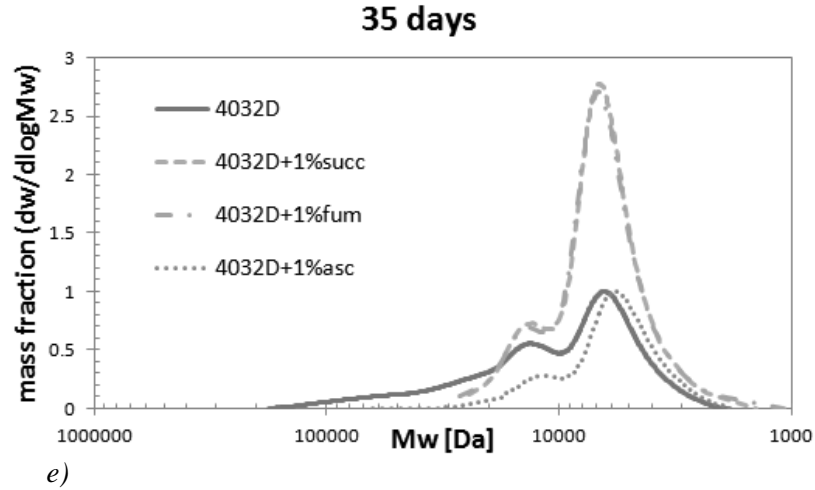


**Figure 42.** Evolution of molecular weight distribution during hydrolysis (PLA and PLA + 1% organic acid) at different hydrolysis times: a) 0 days; b) 5 days; c) 14 days; d) 21 days; e) 35 days

From Figure 42 it is possible to see how the molecular weight distribution curves, of all the samples, move towards lower molecular weights as the hydrolysis proceeds. As we observed in the previous paragraph, their shape changes over time: they become bimodal although previously they were unimodal. We can observe some small differences between the different samples up to 5 days: the curves related to PLA + 1% organic acid are, already at the beginning of the hydrolysis, shifted to lower molecular weights. This particular phenomenon is probably due to the fact that the addition of acids to the PLA induces a partial degradation in the molten state at the stage of the extrusion of the materials, more markedly than for the addition of LDH-organic acids.

Up to 5 days, all the curves have a unimodal distribution. From 14 days onwards, the molecular weight distribution curves of samples with 1% organic acid as filler are at lower molecular weights with respect to pure PLA. At 14 days of hydrolysis, the curves of samples loaded with organic acids have already a bimodal distribution while the curve of neat PLA still has a unimodal distribution: this could indicate that the crystalline fraction present in PLA + organic acid is large enough to slow the hydrolytic process. Up to 21 days of hydrolysis, the curve of neat PLA is at higher values of molecular weight with respect to the samples loaded with acids. This difference is still present at 35 days of hydrolysis.

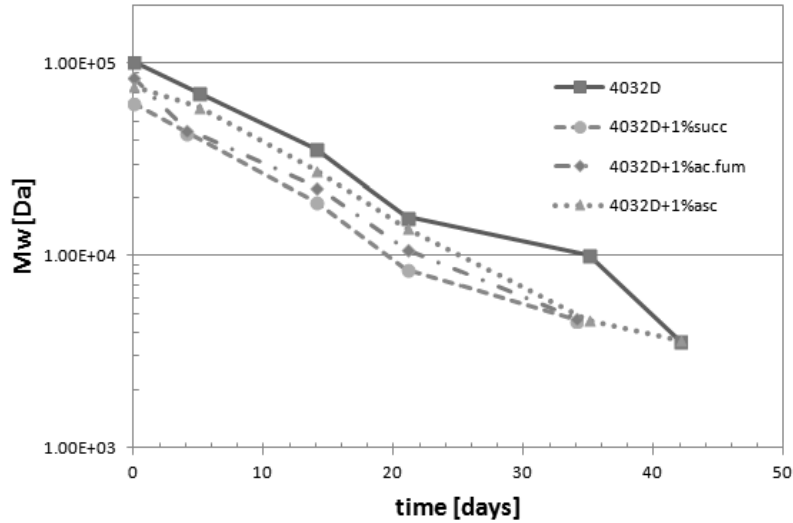


**Figure 43.** Evolution of weight average molecular weight ( $M_w$ ) during hydrolysis (PLA and PLA + 1% organic acids)

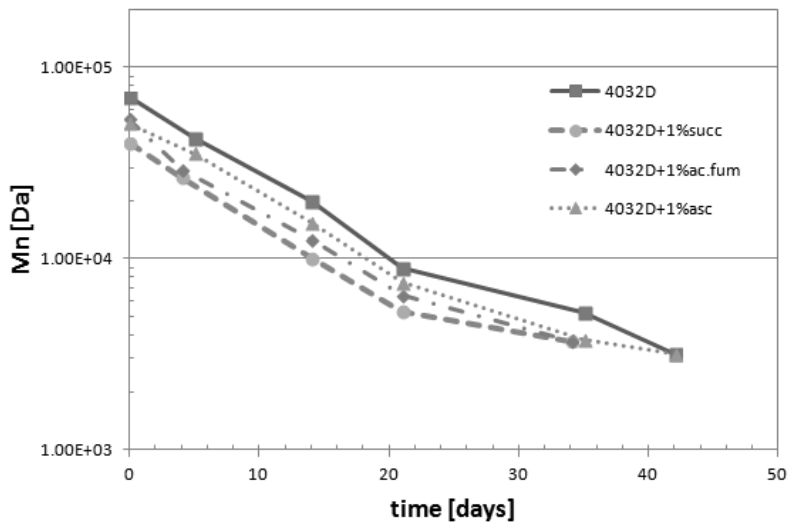


**Figure 44.** Evolution of number average molecular weight ( $M_n$ ) during hydrolysis (PLA and PLA + 1% organic acids)

In Figure 43 and Figure 44 the evolution of the weight average molecular weight ( $M_w$ ) and of the number average molecular weight ( $M_n$ ) are reported. As we have observed before, for all samples the molecular weights decrease, but all samples with 1% organic acids as fillers have a

### Chapter 3

lower molecular weight with respect to neat PLA with increasing hydrolysis. Furthermore we can see that the data are very similar for both parameters, so we can say that the PDI index remain quite unchanged.

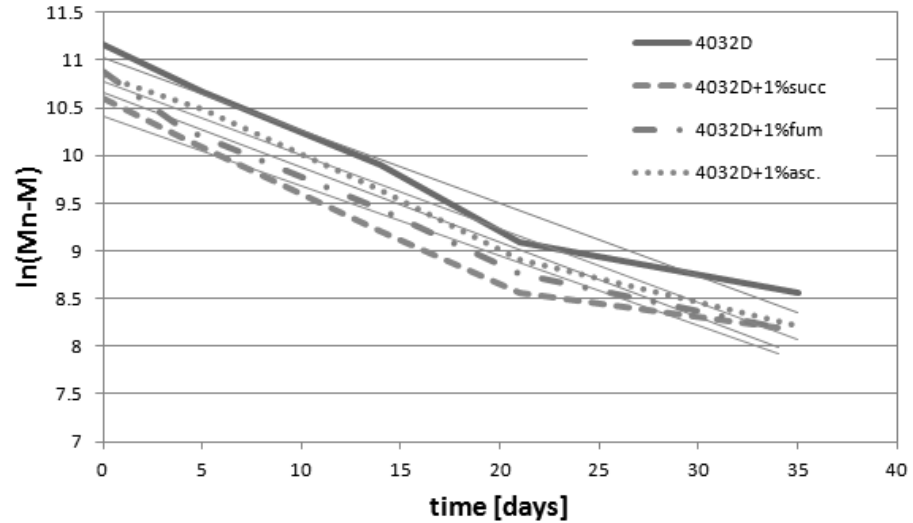


**Figure 45.** Evolution of  $\ln(Mn-M)$  during hydrolysis (PLA and PLA + 1% organic acids)

The data of each sample in the figure above, as we have observed in the previous paragraph, have an approximately linear trend: the slope of the lines represents the value of the kinetic constant.

Table 6 shows all the values of  $k'$  and the coefficients of determination.

**Table 6.** Kinetic constant of hydrolysis (PLA and PLA + 1% organic acids)

	$k'$ [days <sup>-1</sup> ]	$R^2$
4032D	0.0765	0.9628
4032D + 1%-succ	0.0732	0.9425
4032D + 1%-fum	0.0789	0.9624
4032D + 1%-asc	0.0776	0.9796

The kinetic constants of all the samples are quite the same: 4032D + 1%-fum and 4032D + 1%-asc have slightly higher values than that of the neat PLA. The samples loaded with acids alone are less resistant to hydrolysis, so the GPC analysis confirms what we observed in previous analyses.

*Mechanical tests*

Mechanical tests were performed on the hydrolyzed samples: a penetration test, in order to evaluate if the samples more resistant to hydrolysis were really more mechanically resistant.

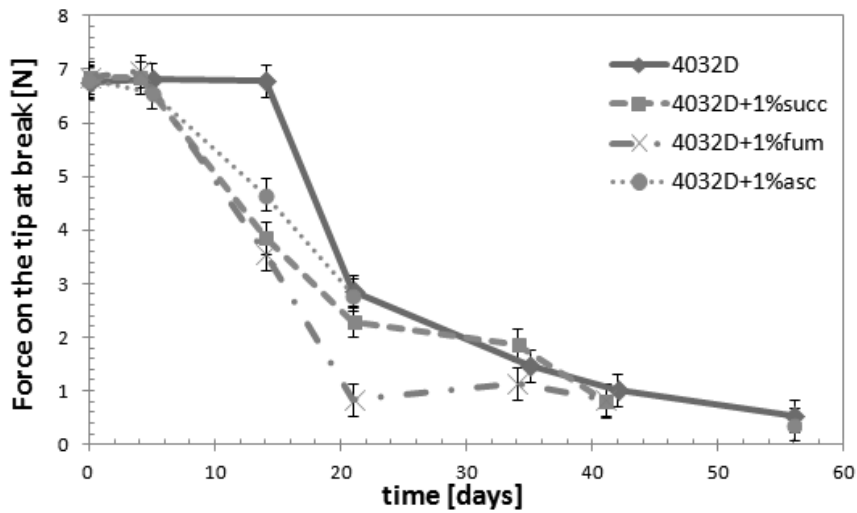


**Figure 46.** Evolution of force at break during hydrolysis (PLA and PLA + 1% organic acids)

From Figure 46 we can observe that up to about 5 days, where the forces are near 7 N, there is no fracture in any sample. After 5 days, the samples loaded with acids begin to break at decreasing mechanical stresses as the hydrolysis proceeds, while the neat PLA still resists the applied force. After 21 days, there is fracture in the pure PLA too.

### Chapter 3

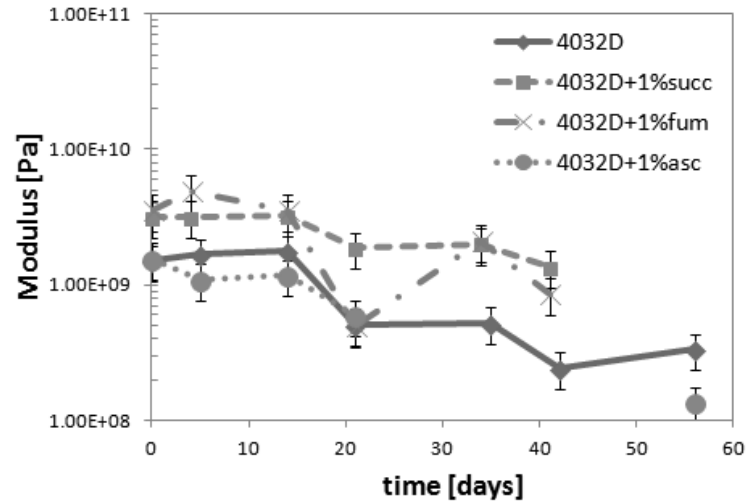


**Figure 47.** Evolution of modulus during hydrolysis (PLA and PLA + 1% organic acids)

As the time of hydrolysis increases, we can see from Figure 47 that there is a decrease in the modulus of the sample. There are no longer any differences between the curves.

This mechanical analysis confirms what we observed in previous analyses: adding 1% organic acid to PLA makes it more sensitive to the hydrolysis: PLA loaded with organic acid has a faster degradation.

#### *Images of hydrolyzed samples*

What has been observed from the analyses carried out is also evident from a macroscopic point of view. Figure 48 presents photos of the samples hydrolyzed for different lengths of time.

**42days**



PLA



PLA+1% succinic



PLA+1% fumaric



PLA+1% ascorbic

**56days**



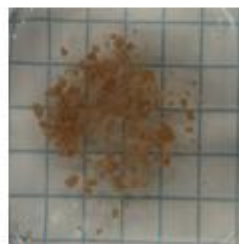
PLA



PLA+1% succinic



PLA+1% fumaric



PLA+1% ascorbic

**Figure 48.** Images of hydrolyzed samples (4032D and 4032D + 1% organic acids); a) hydrolyzed for 42 days; b) hydrolyzed for 56 days.

### *Chapter 3*

These photos show clearly the effect of the addition of 1% organic acids to the PLA: all the samples are broken after 42 days of hydrolysis, but the pure PLA has bigger pieces of the sample than do the samples of PLA + 1% organic acid. This difference is still evident after 56 days, at the end of the hydrolysis tests.

#### **3.5. Effect of LDH-organic acids against hydrolysis on an amorphous grade of PLA (4060D)**

In the previous paragraph, analysing the experimental data, we found that it is possible to protect the PLA from the hydrolysis process using LDH intercalated with organic acids as fillers.

LDH + succinic acid (at 3% wt/wt) was chosen as the best additive for slowing down hydrolysis. In order to test the effectiveness of this filler even with a type of PLA more sensitive to hydrolysis, a different type of PLA was employed: 4060D, completely amorphous after solidification from the molten state. In addition to the LDH + succinic, for comparison, another already tested additive was chosen: LDH + ascorbic acid (3% wt/wt).

In this section, the tested samples are:

- 4060D
- 4060D + 3% LDH-succinic acid (4060D + 3% LDH-succ)
- 4060D + 3% LDH-ascorbic acid (4060D + 3% LDH-asc)

#### *Weight loss*

In the figure below the evolution of the sample mass is reported: for all the samples, we can see a reduction of residual mass due to the hydrolysis process.

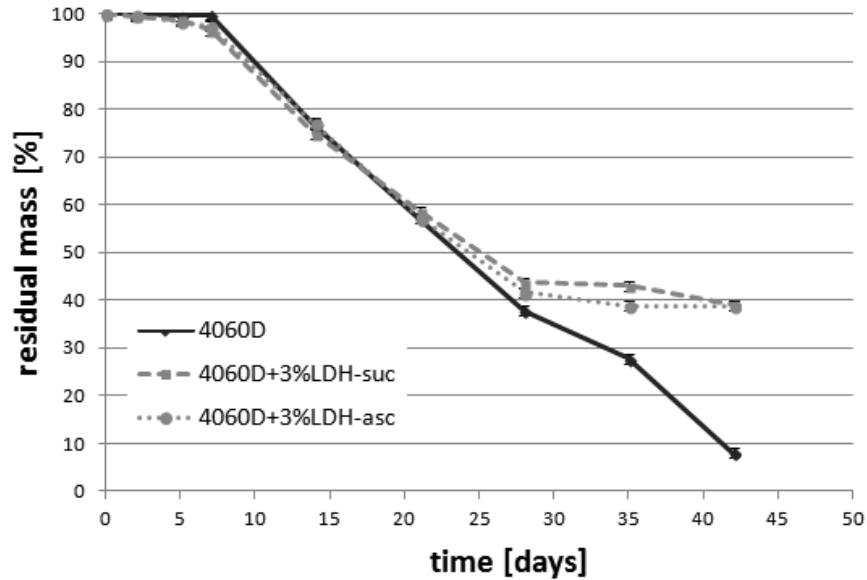


**Figure 49.** Weight loss during hydrolysis (4060D and 4060D + 3% LDH- organic acid)

Comparing Figure 49 and Figure 26 it is possible to see the difference in weight loss between the samples based on 4032D and on 4060D: the same weight loss of about 30% observed for 4060D after 15 days of hydrolysis is observed for 4032D at about 56 days, the end of the hydrolysis tests. It is however important to observe that for both types of PLA the introduction of LDH intercalated with organic acids allows limiting the weight decrease due to degradation: in the case of 4060D, using 3% LDH-organic acids, we have a reduction in weight loss of about 30% at 42 days. In particular, the additive which seems to better preserve 4060D from the phenomenon of hydrolysis is succinic acid intercalated in LDH, as already previously observed for 4032D.

#### *Calorimetric analysis (DSC)*

Below are reported the results of DSC analysis. As we have seen before, the crystallinity increases with the advance of hydrolysis.

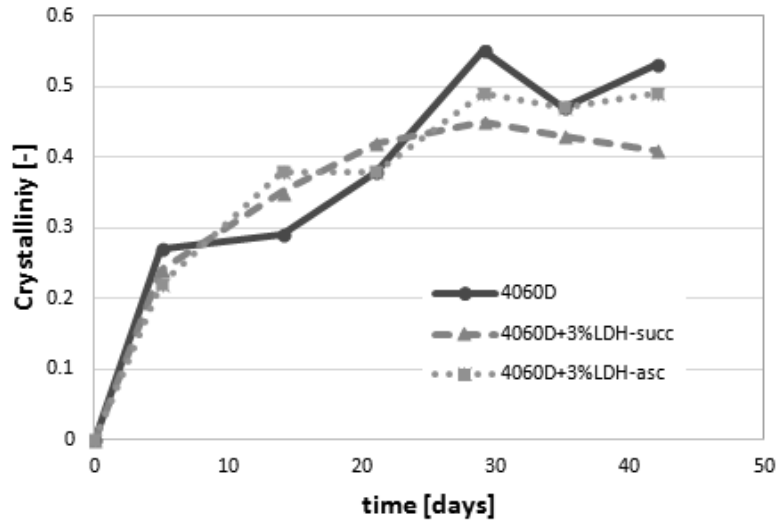


**Figure 50.** Evolution of degree of crystallinity during hydrolysis (4060D and 4060D + 3% LDH-organic acid)

In Figure 50 the DSC data show that the degree of crystallinity of pure 4060D and of 4060D + 3% LDH-organic acid samples has quite the same value up to about 20 days. After 20 days there is a difference in the degree of crystallinity of the samples: 4060D is more crystalline than the 4060D loaded with LDH-organic acid.

The values of  $T_g$  and  $T_m$  of the different samples reported in Table 7.

**Table 7.** Summary of DSC results:  $T_g$  was measured during 2<sup>nd</sup> heating scan, the reported  $T_m$  refers to the highest-temperature peak of the melting endotherm during 1<sup>st</sup> heating ramp (4060D and 4060D + 3% LDH-organic acid).

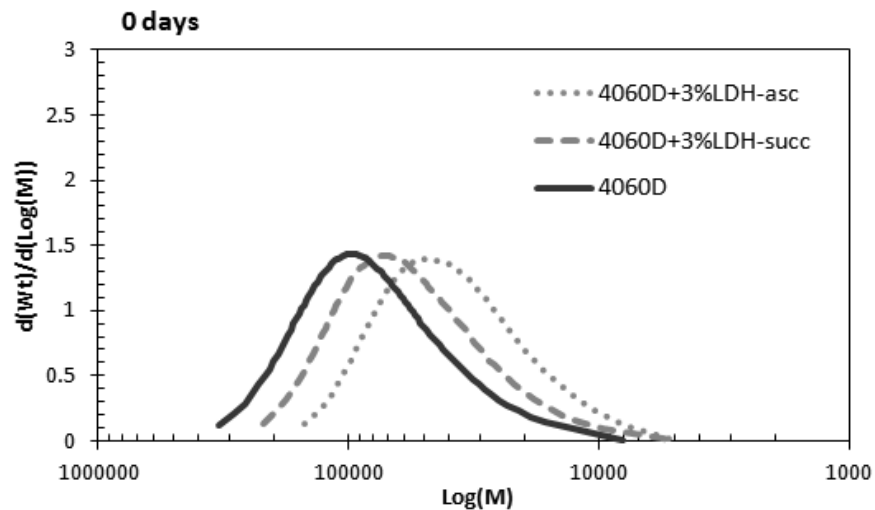
Sample		Days of Hydrolysis				
		0	5	14	21	48
4060D	$T_g$ [°C]	60.1	57.3	56.8	55.3	47
	$T_m$ [°C]	/	123.4	122.8	121.9	109.6
4060D + 3% LDH-succ	$T_g$ [°C]	60.44	56.7	55.4	54.9	45.1
	$T_m$ [°C]	/	123.9	125.7	123.5	108.58
4060D + 3% LDH-asc	$T_g$ [°C]	59.9	56.9	56	55.3	44.9
	$T_m$ [°C]	/	124.6	125.7	121.9	104.7

### Materials selection

Table 7 show that there is a small effect in slowing down hydrolysis: The values of  $T_g$  of the different sample are quite the same as the hydrolysis proceeds, but the values of  $T_m$  of the loaded samples are a little higher than those of the neat 4060D ones, in particular at 5 and 14 days.

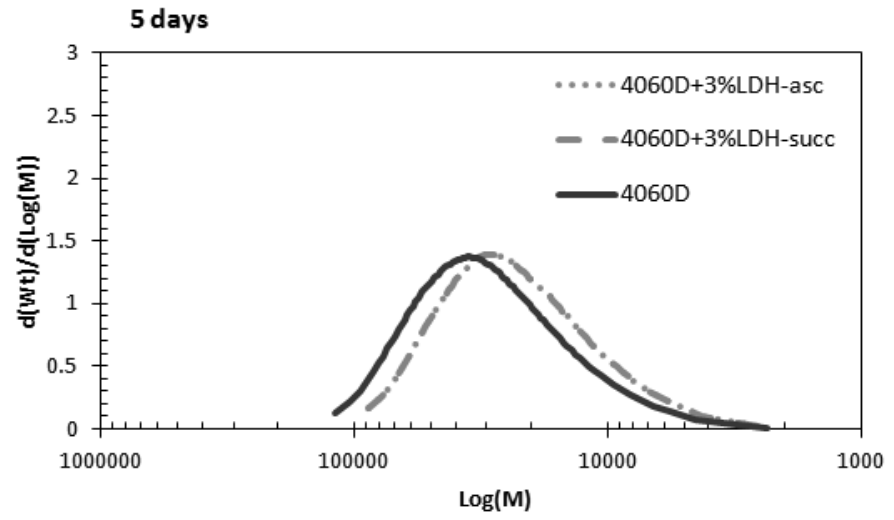
### Gel Permeation Chromatography (GPC)

The GPC analyses reported were carried out for samples hydrolyzed for up to 21 days. The samples hydrolyzed for longer times were not able to be analysed by GPC because, as we will see in the following graphs, the molecular weight became too small to be able to distinguish the GPC curve of the sample from the one of the solvent used to conduct the test. Below are reported the molecular weight distribution curves of the samples analysed by GPC at determined hydrolysis times

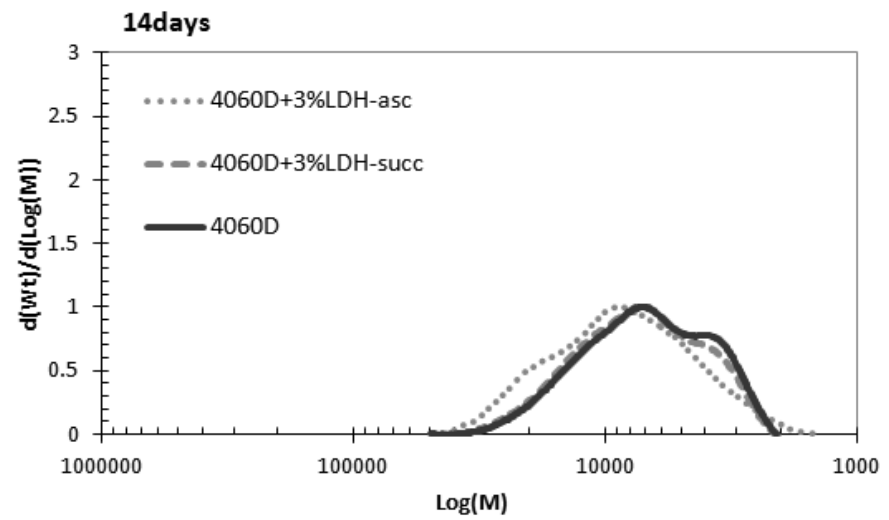


a)

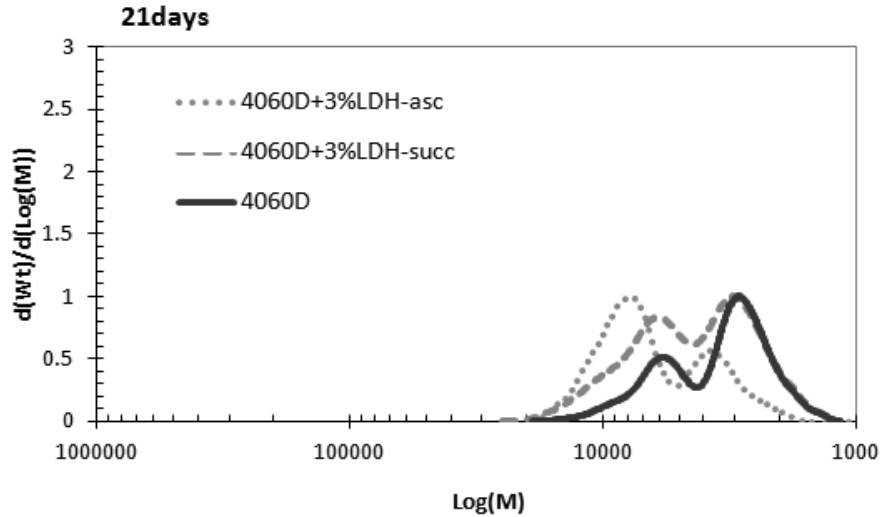
Chapter 3



b)



c)



d)

**Figure 51.** Evolution of molecular weight distribution during hydrolysis (4060D and 4060D + 3% LDH-organic acid) at different hydrolysis times: a) 0 days; b) 5 days; c) 14 days; d) 21 days.

From Figure 51 we can see that the molecular weight distribution curves, of all the samples, move towards lower molecular weights as the hydrolysis proceeds. As we observed in the previous paragraph, their shape changes over time: they change to bimodal from unimodal. We can see only a little difference between the different samples up to 5 days: the curves related to 4060D + 3% LDH-organic acid, already at the beginning of the hydrolysis, are shifted to lower molecular weights. This particular phenomenon is probably due to the fact that the addition of LDH-acids to the PLA induces a partial degradation in the molten state at the stage of the extrusion of the materials that is more marked than occurs with the addition of LDH-organic acid to 4032D.

Up to 5 days all the curves have a unimodal distribution. From 14 days onwards we can observe bimodal curves, the molecular weight distribution curves of 4060D at lower molecular weights with respect to 4060D+LDH-organic acid; in a more evident way, the observed trend is also present at 21 days of hydrolysis.

In Figure 52 and Figure 53 the evolution of the weight average molecular weight ( $M_w$ ) and of the number average molecular weight ( $M_n$ ) are reported.

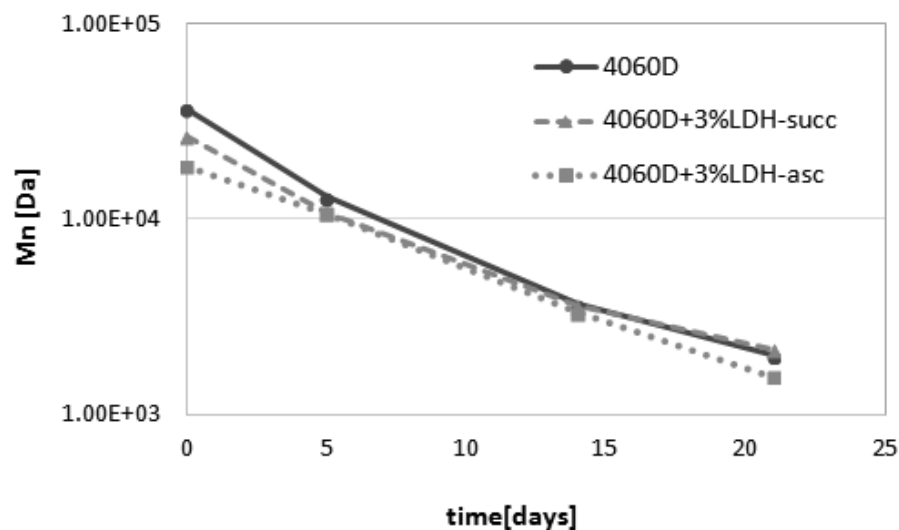


**Figure 52.** Evolution of weight average molecular weight ( $M_w$ ) during hydrolysis (4060D and 4060D + 3% LDH-organic acids)

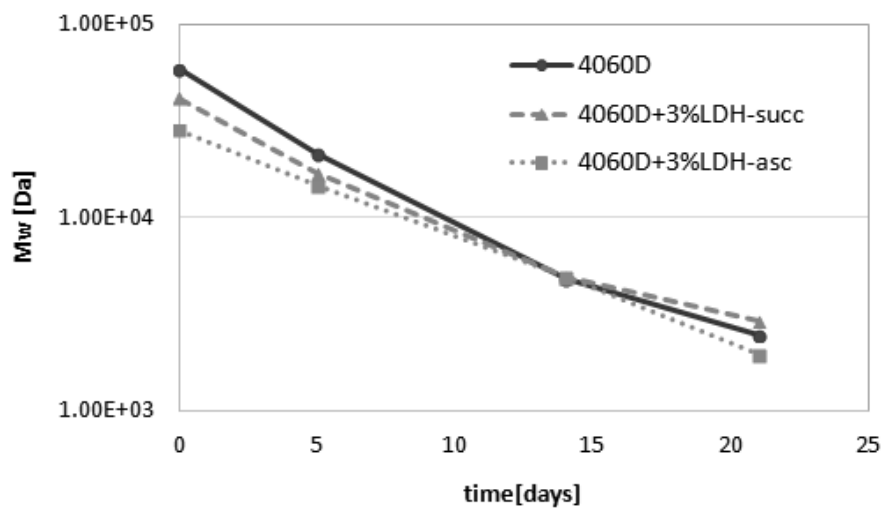


**Figure 53.** Evolution of number average molecular weight ( $M_n$ ) during hydrolysis (4060D and 4060D + 3% LDH-organic acids)

As we have observed before, for all samples the molecular weights decrease. At the beginning of the hydrolysis, we can observe a difference

### Materials selection

between the molecular weights of the samples: the molecular weights of the loaded 4060D are lower than that of the pure 4060D. As said before, this phenomenon is probably due to the fact that the addition of LDH-organic acid to the PLA induces a partial degradation in the molten state at the stage of the extrusion of the materials. The molecular weights of different samples decrease differently: the molecular weight of 4060D decreases more quickly, so we can see a protective effect of LDH-organic acid on 4060D against hydrolysis.

Furthermore we can see that the data reported in Figure 52 and Figure 53 are very similar for both parameters, so we can say that the PDI index remains quite unchanged.

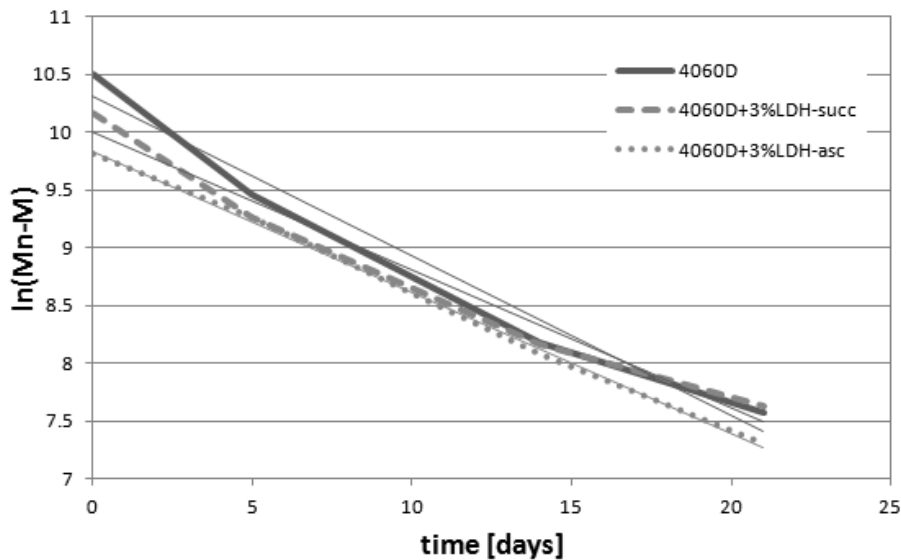


**Figure 54.** Evolution of  $\ln(Mn-M)$  during hydrolysis (4060D and 4060D + 3% LDH-organic acids)

The data of each sample in the figure above, as we have observed in the previous paragraph, have an approximately linear trend: the slope of the lines represents the value of the kinetic constant.

In Table 8 are reported all the values of  $k'$  and the coefficients of determination.

### Chapter 3

**Table 8.** Kinetic constant of hydrolysis (4060D and 4060 + 3% LDH-organic acids)

	$k'$ [days <sup>-1</sup> ]	$R^2$
4060D	0.1386	0.9761
4060D + 3% LDH-succ	0.1199	0.9753
4060D + 3% LDH-asc	0.1217	0.9989

The kinetic constant of 4060D + 3% LDH-organic acid is lower than that of the neat 4060D; 4060D + 3% LDH-succ has the lowest value. The most resistant to hydrolysis is 4060D + 3% LDH-succ, thus the GPC analysis confirms what we observed in previous analyses.

### Mechanical tests

Mechanical test were performed on the hydrolyzed samples: a penetration test, in order to evaluate if the samples more resistant to hydrolysis process were really more mechanically resistant.

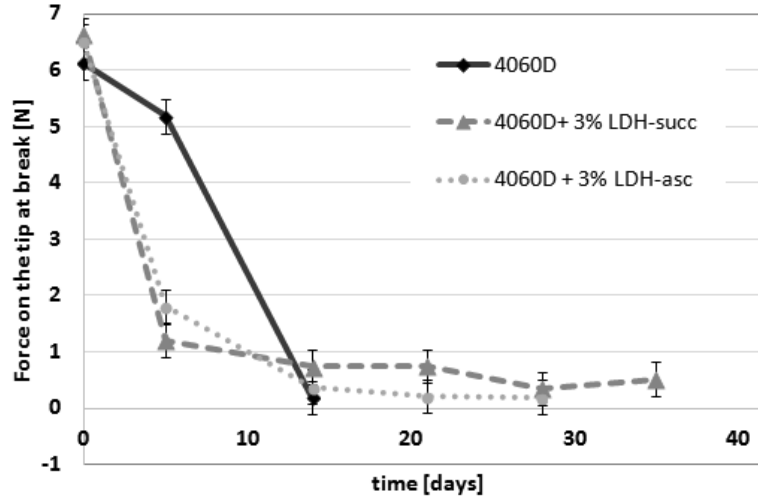


**Figure 55.** Evolution of force at break during hydrolysis (4060D and 4060D + 3% LDH-organic acids)

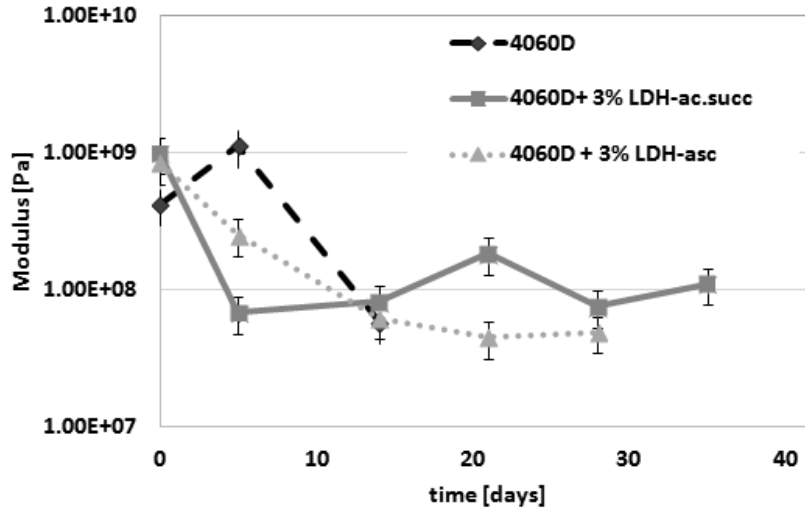


**Figure 56.** Evolution of modulus during hydrolysis (4060D and 4060D + 3% LDH-organic acids)

From Figure 55 we can observe that there is no break only in the unhydrolyzed samples, where the force is near to 7 N. After 5 days, all the samples begin to break at decreasing mechanical stresses as the hydrolysis proceeds. At 5 days, the force at break of pure 4060D is higher than the ones of 4060 + 3% LDH-acids, which we observed could be ascribed to the fact that the addition of LDH-organic acid to the PLA induces a partial degradation in the molten state at the stage of the extrusion of the materials. After 14 days it was no longer possible to carry out mechanical tests on the pure 4060D because the sample was pulverized.

As the hydrolysis progresses, we can see from Figure 56 a decrease in the modulus of the sample. In this figure we can observe the same as in the previous figure: a higher value of the modulus for the pure 4060D. This mechanical analysis confirms what we observed in previous analyses: adding 3% LDH-organic acid to 4060 makes it a little bit more sensitive to the hydrolysis. 4060D, similar to what was observed for 4032D, loaded with 3% LDH-organic acid has a little bit slower degradation than pure 4060D.

### *Images of hydrolyzed samples*

What has been observed from the analyses carried out is also evident from a macroscopic point of view. Figure 57 presents photos of the samples hydrolyzed for different lengths of time.

Chapter 3

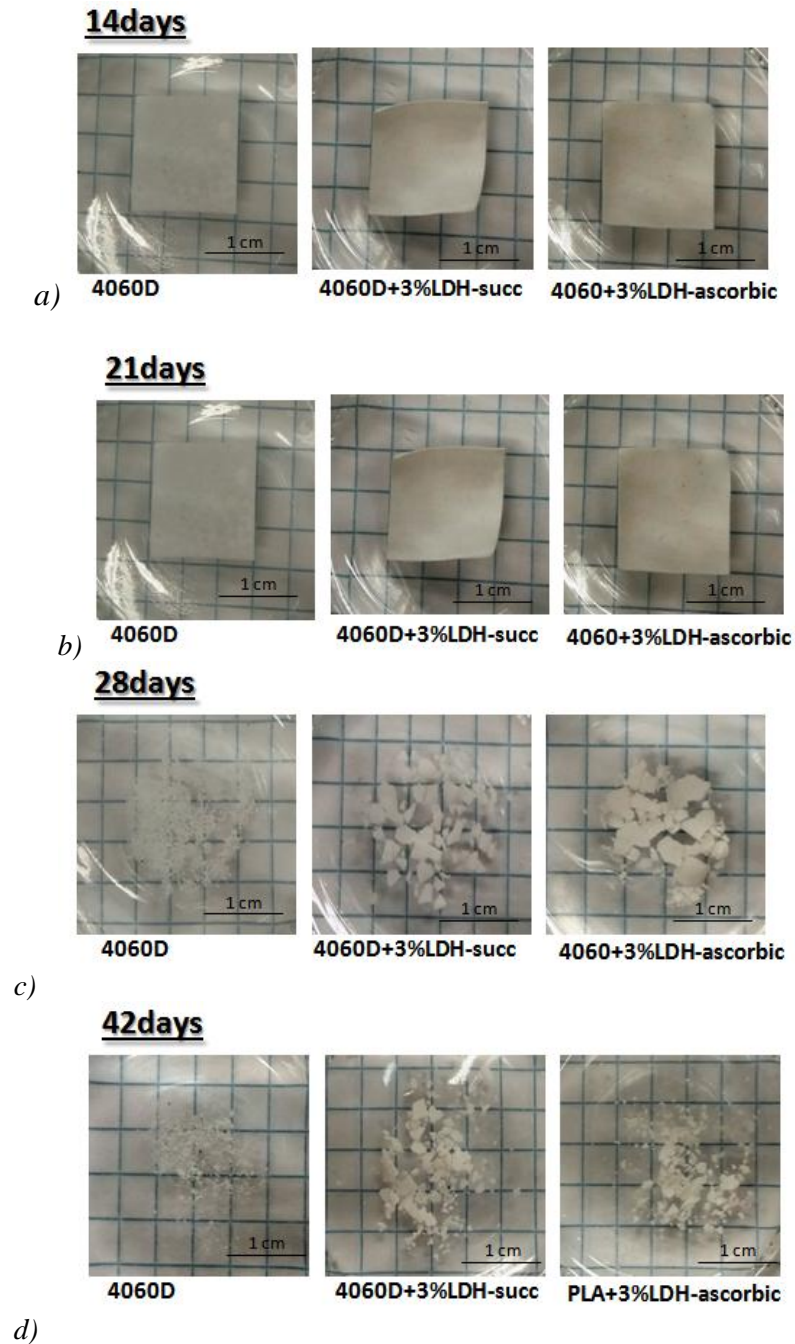


**Figure 57.** Images of hydrolyzed samples (4060D and 4060D + 3% LDH- organic acids); hydrolyzed for: a) 14 days; b) 21 days; c) 28 days; d) 42 days.

### *Materials selection*

From the above photos we can see that there is no difference up to 21 days. At 28 days the effect of the addition of 3% LDH-acids organic to PLA is clear: loaded samples are broken, as is the pure 4060D, but their pieces are bigger than those for the pure 4060D. This difference is still evident after 42 days, at the end of the hydrolysis tests.

The selected filler, the filler that most protects PLA (both 4032D and 4060D) from hydrolysis, is LDH + succinic acid used at 3% wt/wt.



# Chapter 4

## Micro-injection molding

The ultimate aim of this experimental work was to produce samples of PLA by micro-injection molding: samples in which it is possible to realize a degradation profile due to the presence of two different morphologies within the same sample (half amorphous and half crystalline). In order to control this degradation profile, injected samples were obtained from PLA loaded with LDH-succinic.

In this chapter there will be discussed the production and characterization of samples obtained by micro-injection molding using the material selected in the previous chapter: 3% LDH + succinic acid as filler of PLA (4032D).

Several biphasic samples were obtained by micro-injection molding from the extruded materials. The samples (1 cm × 0.4 cm with a thickness of about 250 μm), were subsequently submitted to the hydrolysis test.

This chapter will present the experimental results pertaining to the biphasic samples obtained by micro-injection molding submitted to hydrolysis.

### *4.1. Biphasic samples from micro-injection molding*

In conventional injection molding, the mold is controlled by a continuous cooling method, by which the melt polymer and the mold are cooled. This cooling method causes a sudden polymer solidification near the surface of the mold, leading to a reduction of the section open to flow and so to a decrease of the ability of the polymer melt to fill the cavity. This problem is very significant in micro-injection molding. In order to solve this problem, in this experimental work a new dynamic mold temperature control system for rapid heating and cooling of the mold was used, as explained in Chapter 2.

The local temperature of the surface of the mold has been controlled by an ad-hoc software application based on Labview, in order to produce the biphasic micro-injected samples.

The temperature control developed allows raising the temperature by about 100°C in a few seconds, as shown in Figure 58.

Chapter 4

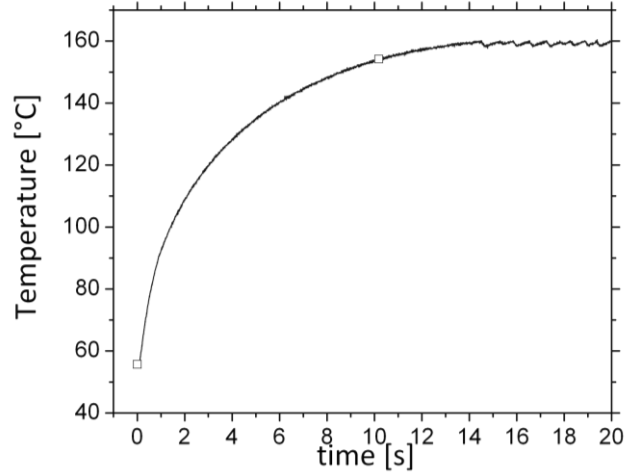


**Figure 58.** Example of local heating speed of the mold

The temperature control developed allows adjusting the temperature at two different points of the mold cavity due to the use of two resistors inserted in correspondence in the two different areas of the cavity. In this way it is possible to produce biphasic micro-injected samples.

The cavity temperature has been optimized: the length of the sample produced changes as the latter changes, as shown in Figure 59 and Figure 60.

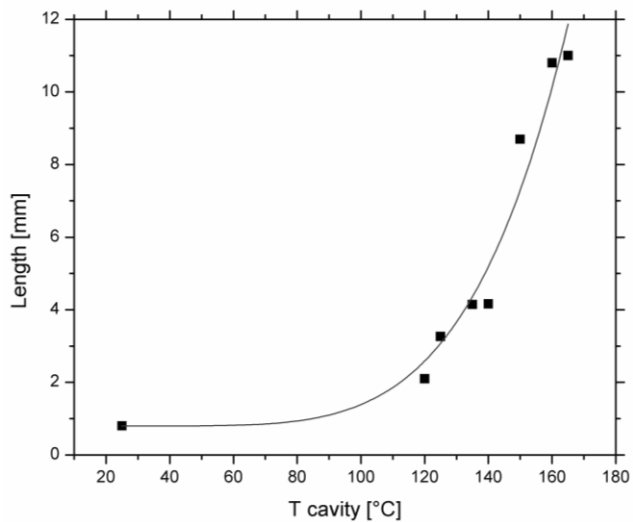


**Figure 59.** Length of the injected sample as a function of cavity temperature

*Micro-injection molding*

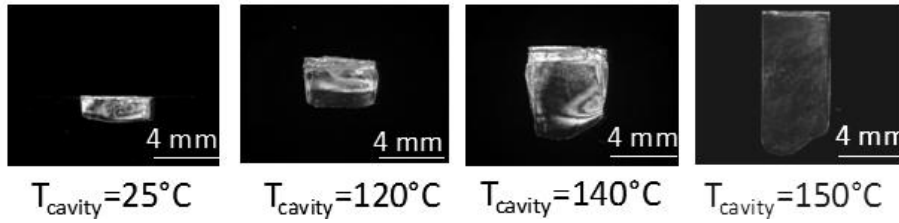


**Figure 60.** *Injected samples produced at different cavity temperatures*

Figure 61 shows a schematization of the production of the injected biphasic samples.

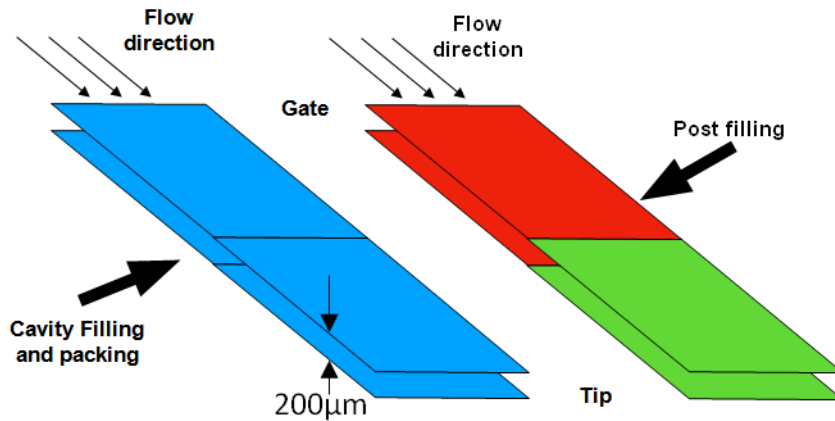


**Figure 61.** *Schematization of the production of injected biphasic samples (amorphous in the tip and crystalline in the gate)*

The parameters used in the production of the injected biphasic samples are:

- Injection pressure = 150 bar
- Injection temperature =  $220^{\circ}\text{C}$
- Post filling pressure = 140 bar
- Cavity temperature =  $160^{\circ}\text{C}$
- T of crystallization from the glass =  $105^{\circ}\text{C}$
- Time of crystallization = 1000 s (crystallization half time at  $105^{\circ}\text{C} \approx 150$  s).

The molten PLA fills the cavity (injection time is about 20 s), the material is then cooled (from about  $160^{\circ}\text{C}$  to about  $50^{\circ}\text{C}$  in 15 s). The solid injected sample is heated again to obtain the crystallization of the

## Chapter 4

chosen zone (tip or gate), in this case the crystalline zone is the gate. Figure 62 shows the temperatures in the different steps and in the different zones of the sample.

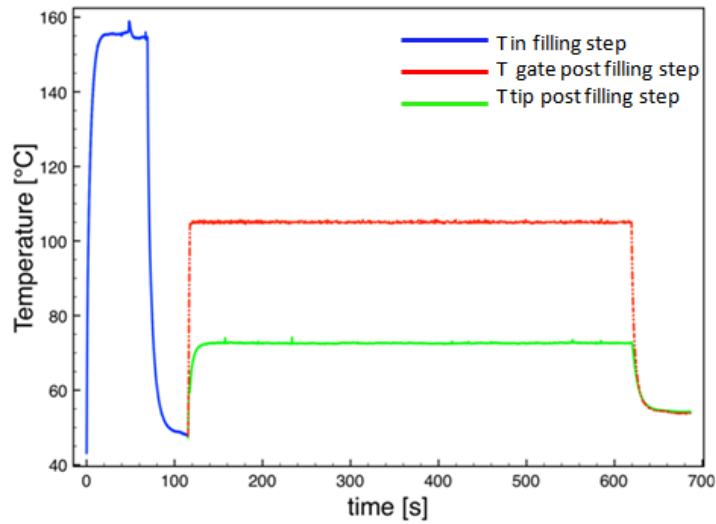


**Figure 62.** Temperatures during filling and post filling steps

In Figure 63 we can observe the micro-injected biphasic sample: the crystalline gate (opaque zone) and the amorphous tip (transparent zone) are evident.

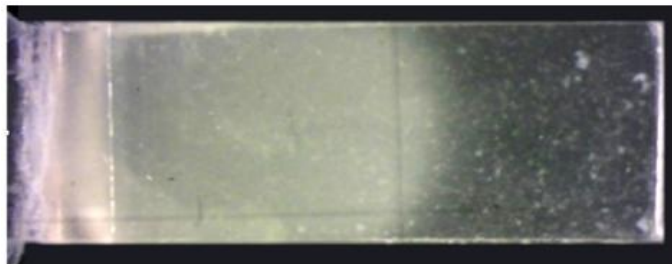


**Figure 63.** Micro-injected biphasic PLA sample (amorphous tip, crystalline gate)

In order to evaluate the morphology of the biphasic PLA sample, DSC analyses were performed.

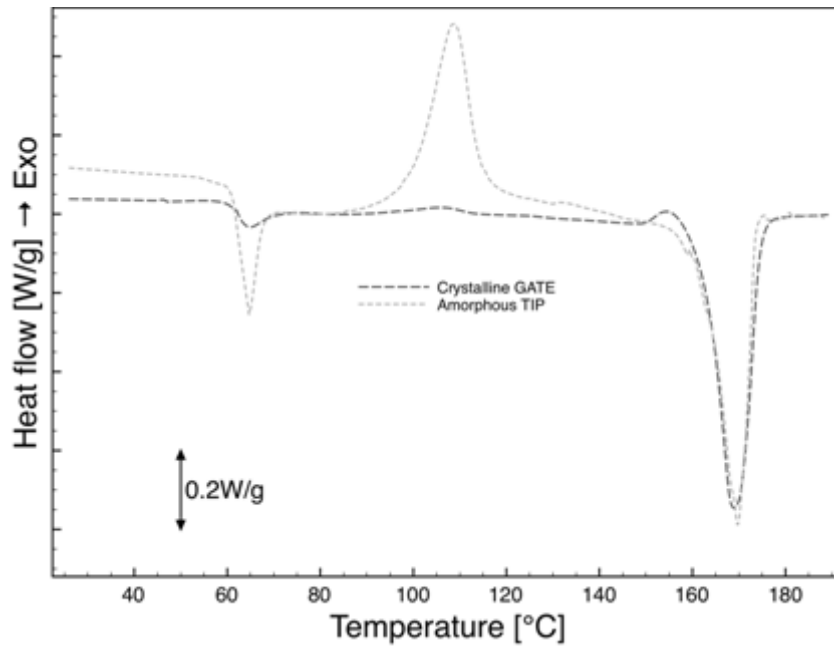


**Figure 64.** DSC analysis of micro-injected biphasic PLA sample (amorphous tip, crystalline gate), first scan

From the results of the DSC analysis, reported in Figure 64, we can see that there is a difference between the phases: there is a crystallization and a fusion for the amorphous phase and there is only fusion for the crystalline phase (the crystallization degree achieved in our process is then maximal).  $T_g$  and  $T_m$  are quite the same for both phases and, in particular, their values are very similar to those observed in the previous chapter: this indicates that no degradation had occurred in the micro-injection process or in the crystallization step. The degree of crystallization has been evaluated from a DSC analysis: for the amorphous phase  $X_c = 0$ , while for the crystalline phase  $X_c = 30\%$ .

The micro-injected biphasic PLA samples were produced by crystallizing the tip area rather than the gate area, to observe hypothetical differences. Figure 65 shows a schematization of the production of the injected biphasic samples.

Chapter 4

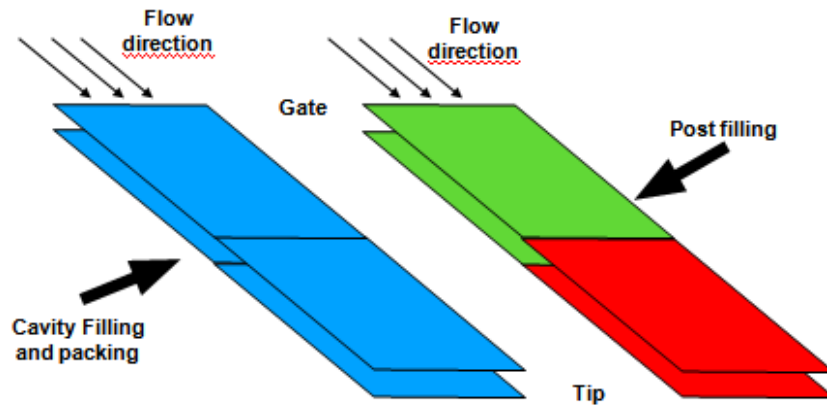


**Figure 65.** Schematization of the production of injected biphasic samples (amorphous in the gate and crystalline in the tip)

The temperature variations in the filling and post filling steps are the same as those reported in Figure 62.

In Figure 66 we can see the micro-injected biphasic sample: the crystalline tip (opaque zone) and the amorphous gate (transparent zone) are evident.

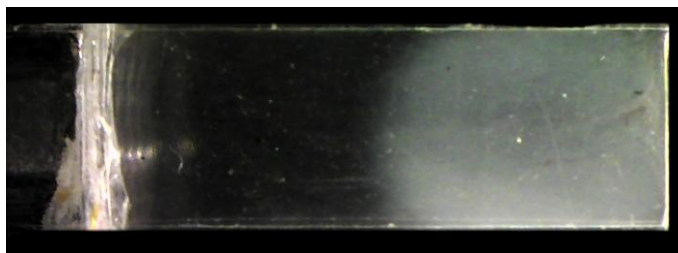


**Figure 66.** Micro-injected biphasic PLA sample (crystalline tip, amorphous gate)

In order to evaluate the morphology of the biphasic PLA sample, DSC analyses were performed.

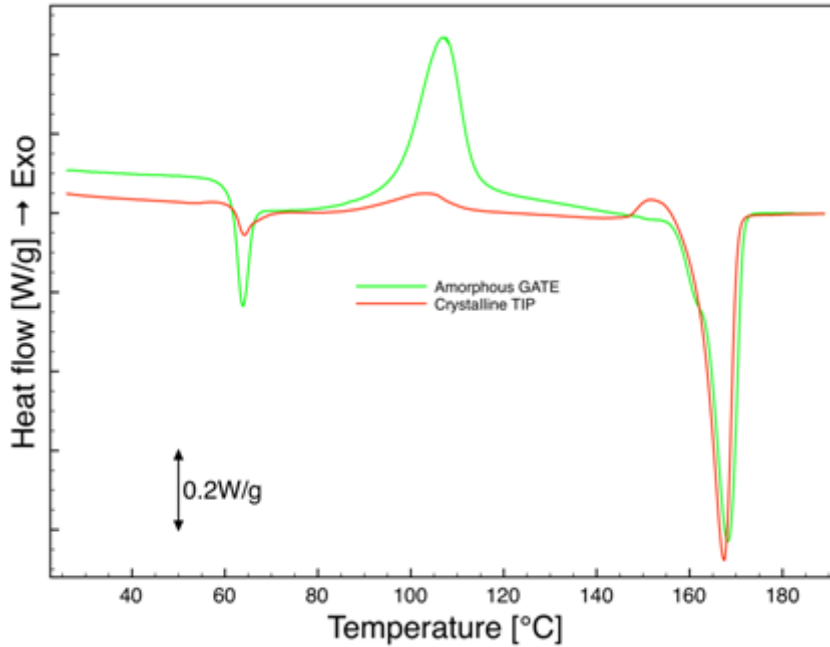


**Figure 67.** DSC analysis of micro-injected biphasic PLA sample (amorphous gate, crystalline tip), first scan

From Figure 67 we can see the same things as in Figure 64: there is a crystallization and a fusion for the amorphous phase and there is only fusion for the crystalline phase and no degradation occurred in either the micro-injection process or in the crystallization step, considering that there is no variation in  $T_g$  and  $T_m$ . The degree of crystallization has been evaluated from the DSC analysis: for the amorphous phase  $X_c = 0$ , while for the crystalline phase  $X_c = 35\%$ .

This type of sample (amorphous gate, crystalline tip) was subsequently submitted to the hydrolysis process.

#### **4.1.1. Hydrolysis tests, experimental results: micro-injected biphasic PLA samples**

Below are reported the experimental results of hydrolysis in the solid state of micro-injected biphasic PLA samples at 58°C under the conditions mentioned in Chapter 2.

From the analyses carried out, we should observe a difference in the degradation rate due to the hydrolysis process in the two parts of the

## Chapter 4

sample: in particular we should see a greater degradation in the amorphous phase compared to what happens in the crystalline zone. The latter should be more resistant to the action of the hydrolysis.

### Calorimetric analysis (DSC)

Figure 68 shows the evolution of the degree of crystallinity ( $X_c$ ) as a function of hydrolysis time: for all the samples,  $X_c$  increases as the hydrolysis proceeds.

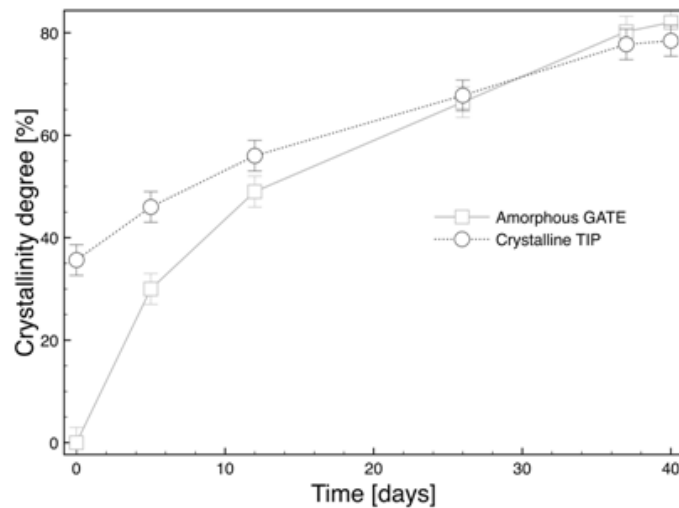


**Figure 68.** Evolution of degree of crystallinity during hydrolysis of micro-injected biphasic PLA sample (amorphous gate, crystalline tip)

In Figure 68 we can see that  $X_c$  of the crystalline phase increases more slowly than the  $X_c$  of the amorphous phase as hydrolysis proceeds: this probably indicates a slower degradation of the crystalline zone with respect to the amorphous one. At about 25 days, no variation can be observed between the values of the  $X_c$  of the two morphologies.

### Gel Permeation Chromatography (GPC)

Figure 69 shows the evolution of the weight average molecular weight ( $M_w$ ) during the hydrolysis of micro-injected biphasic PLA samples.

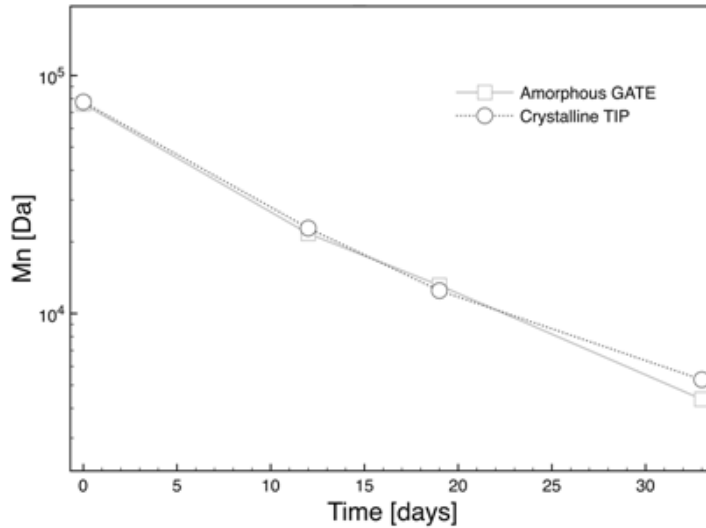


**Figure 69.** Evolution of number average molecular weight ( $M_n$ ) during hydrolysis of micro-injected biphasic PLA sample (amorphous gate, crystalline tip)

As we have observed before, the molecular weights decrease for both zones.

From Figure 69 we can notice no differences in the  $M_n$  of the unhydrolyzed samples: this confirms that no degradation occurred in the crystallization step.

We can observe no differences in the evolution of  $M_n$  as the hydrolysis proceeds: at about 35 days we can see that  $M_n$  for the crystalline zone is a little bit higher than for the amorphous zone.

### *Mechanical tests*

Mechanical tests were performed on the hydrolyzed samples: a penetration test, in order to evaluate if the samples more resistant to hydrolysis process were really more mechanically resistant.

Chapter 4

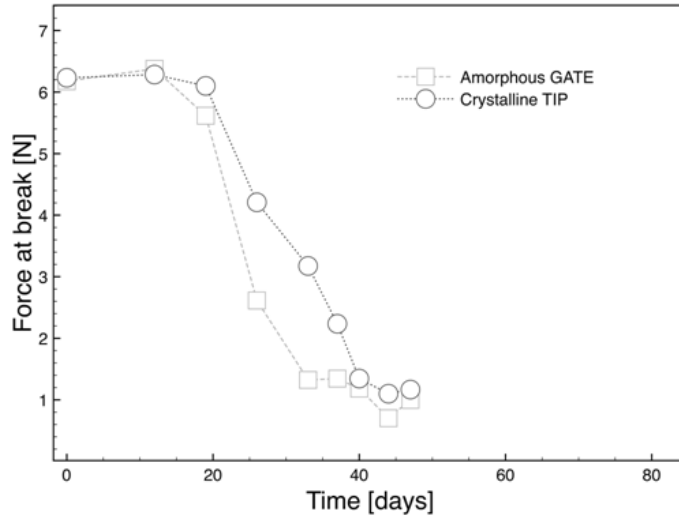


**Figure 70.** Evolution of force at break during hydrolysis of micro-injected biphasic PLA sample (amorphous gate, crystalline tip)

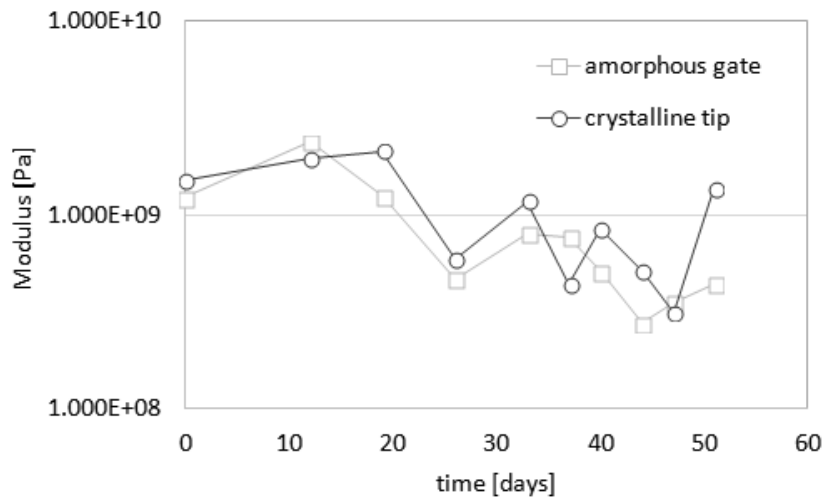


**Figure 71.** Evolution of modulus during hydrolysis of micro-injected biphasic PLA sample (amorphous gate, crystalline tip)

From Figure 70 we can observe that up to 12 days, where the forces are near to 6.5 N, there is no fracture in either phase. After 19 days the sample begin to break at decreasing mechanical stresses as the hydrolysis

### Micro-injection molding

proceeds. For the crystalline phase the force at break is a little bit higher than the amorphous phase. As hydrolysis proceeds, we can notice from Figure 71 a decrease in the modulus of the sample. Up to 19 days we can observe no differences between the moduli of the two different morphologies. After more hydrolysis, the modulus of the crystalline phase is a little bit higher than for the amorphous phase.

Mechanical tests were performed on the other type of biphasic PLA samples with amorphous tip and crystalline gate. The tests, as before, were carried out on hydrolyzed samples.

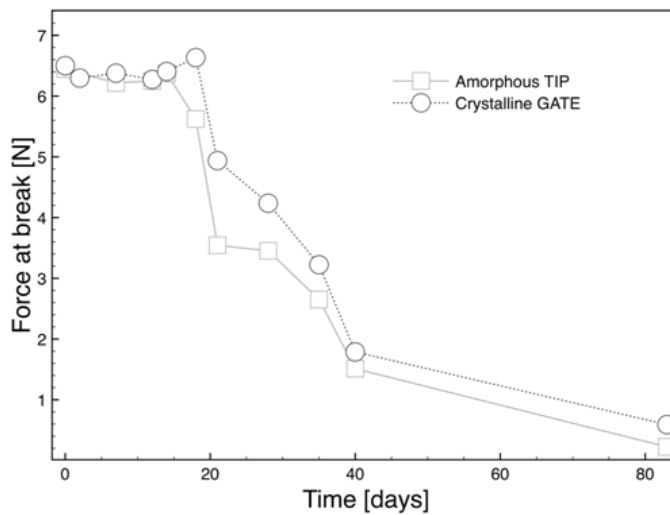


**Figure 72.** Evolution of force at break during hydrolysis of micro-injected biphasic PLA sample (amorphous gate, crystalline tip)

From Figure 72 we can observe that up to 14 days, where the force is near 6.5 N, there is no fracture in either phase. After 18 days the amorphous zone begins to break at decreasing mechanical stresses as the hydrolysis proceeds. Breaks in the crystalline phase can be observed at 21 days. For the crystalline phase the force at break is a little bit higher than for the amorphous phase.

#### Chapter 4

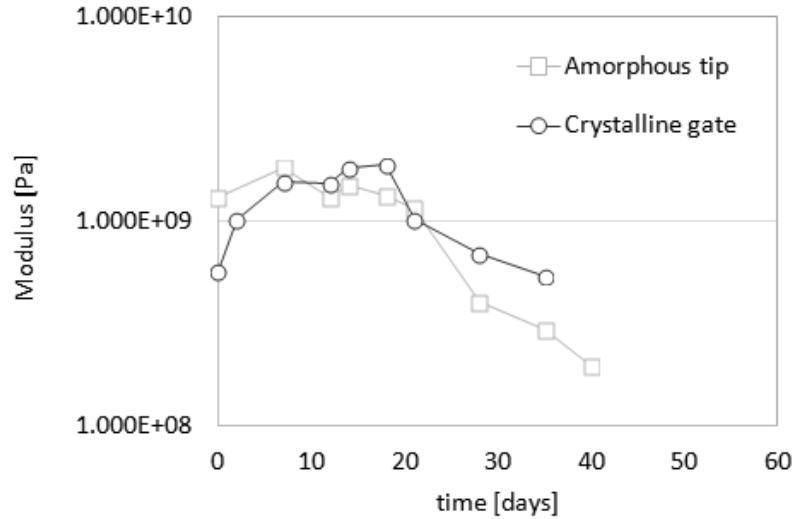


**Figure 73.** Evolution of modulus during hydrolysis of micro-injected biphasic PLA sample (amorphous gate, crystalline tip)

As the hydrolysis progresses, we can notice from Figure 73 a decrease in the modulus of the sample. Up to 21 days we can observe no differences between the moduli of the two different morphologies. At later times, the modulus of the crystalline phase is a little bit higher than for the amorphous phase.

The mechanical tests carried out on the two types of biphasic PLA samples confirm the same results.

#### *Images of hydrolyzed samples*

Figure 74 shows photos of the samples of micro-injected biphasic PLA (amorphous gate, crystalline tip) hydrolyzed for different lengths of time.

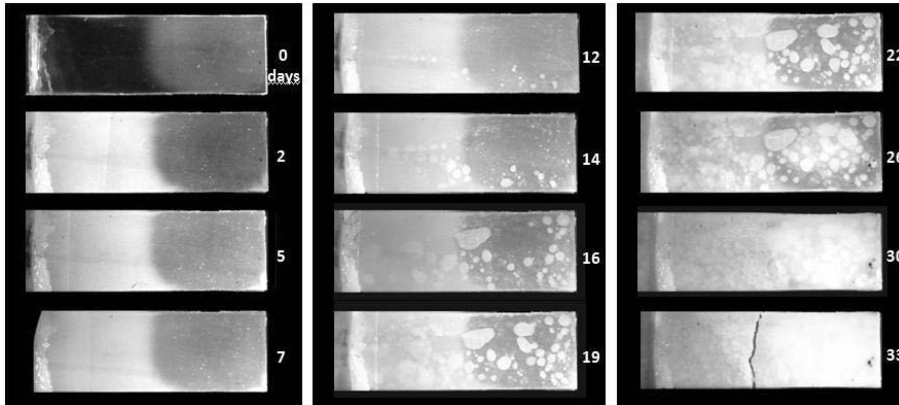


**Figure 74.** Images of hydrolyzed samples of micro-injected biphasic PLA sample (amorphous gate, crystalline tip)

We can see how the crystalline zone of the sample remains unchanged for up to 12 days. The amorphous zone, instead, has already changed after the second day: it turns from transparent to opaque. This could be due to the micro-fractures that are left by the water moving away from the sample during the drying phase. Obviously the crystalline zone has a lower water permeability at least for the first 25 days of hydrolysis. From 30 days on we can observe no differences between the two different morphologies.

These hydrolysis tests confirm that crystalline regions present a (slightly) better resistance to hydrolysis: the obtained biphasic samples present a selective degradation rate.

#### **4.1.2. Hydrolysis tests, experimental results: micro-injected biphasic PLA and PLA + LDH samples**

In the previous paragraph the actual presence of a selective degradation rate within the biphasic sample was verified. In this paragraph, the filler selected in the previous chapter will be employed as the filler of micro-injected biphasic PLA.

Two different samples were analysed:

- 4032D (amorphous gate; crystalline tip)
- 4032D + 3% LDH-succinic acid (PLA + LDH amorphous gate; PLA + LDH crystalline tip).

## Chapter 4

Below are reported the experimental results of the hydrolysis process in the solid state of micro-injected biphasic PLA and PLA + LDH samples at 58°C under the conditions mentioned in Chapter 2.

From the analyses carried out, we can observe not only a difference in the degradation rate due to the hydrolysis process in the two parts of the loaded sample, but can note the protective effect against the hydrolysis due to the presence of LDH in both phases.

### Calorimetric analysis (DSC)

Figure 75 shows the evolution of the degree of crystallinity ( $X_c$ ) as a function of hydrolysis time: for all the samples,  $X_c$  increases as the hydrolysis proceeds.

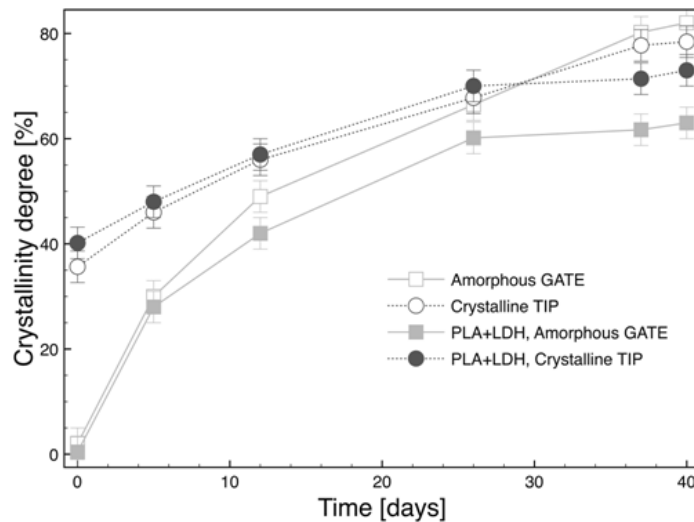


**Figure 75.** Evolution of degree of crystallinity during hydrolysis of micro-injected biphasic PLA and PLA + LDH samples (amorphous gate, crystalline tip)

In Figure 75 we can see the same things as in Figure 68:  $X_c$  of the crystalline phase increases more slowly than the  $X_c$  of the amorphous phase as the hydrolysis proceeds. This can be observed for both samples, loaded and pure PLA. The values of  $X_c$  for the sample with LDH are lower than those of the pure PLA sample, especially from 12 days on. The presence of LDH protects the sample from hydrolysis in both morphologies.

## Gel Permeation Chromatography (GPC)

Figure 76 shows the evolution of the weight average molecular weight ( $M_w$ ) during the hydrolysis of the micro-injected biphasic PLA and PLA + LDH samples.

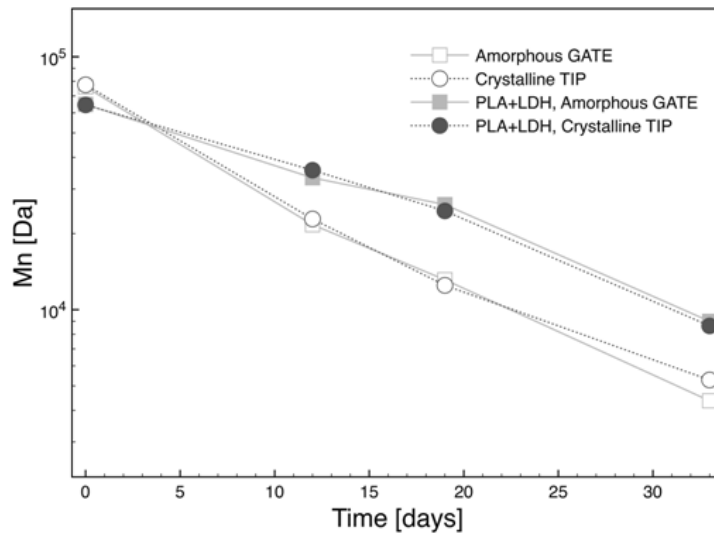


**Figure 76.** Evolution of number average molecular weight ( $M_n$ ) during hydrolysis of micro-injected biphasic PLA and PLA + LDH samples (amorphous gate, crystalline tip)

As we have observed before, the molecular weights decrease for both zones of the two samples.

From Figure 76 we can notice no differences in the  $M_n$  of the two different morphologies of the unhydrolyzed PLA and PLA + LDH samples: this confirms that no degradation occurred in the crystallization step.

We can observe no differences in the evolution of  $M_n$  as the hydrolysis proceeds between the two different morphologies of both samples. The values of  $M_n$  of the PLA + LDH sample are higher than those for the PLA. The  $M_n$  of PLA+ LDH decreases more slowly than that for PLA as the hydrolysis proceeds.

## Chapter 4

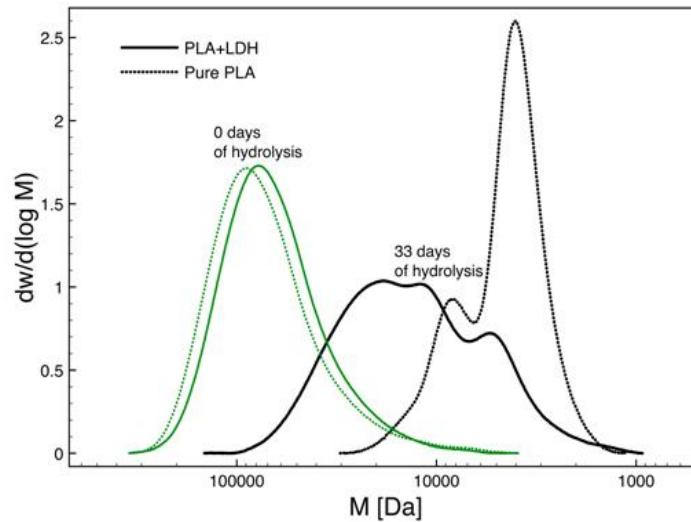


**Figure 77.** Evolution of molecular weight distribution during hydrolysis of micro-injected biphasic PLA and PLA + LDH samples (crystalline tip)

From Figure 77 it is possible to note how the molecular weight distribution curves of the two samples for the crystalline zones move towards lower molecular weights as the hydrolysis proceeds. As we observed in the previous paragraph, their shape changes over time: they become bimodal although they were previously unimodal.

We can observe no difference in the distribution curves of the two unhydrolyzed samples. After 33 days of hydrolysis, the distribution curve of crystalline PLA is shifted to lower  $M_n$  than the PLA+LDH one. After 33 days of hydrolysis, PLA has a bimodal distribution more pronounced than that for PLA+LDH: this indicates a stronger degradation.

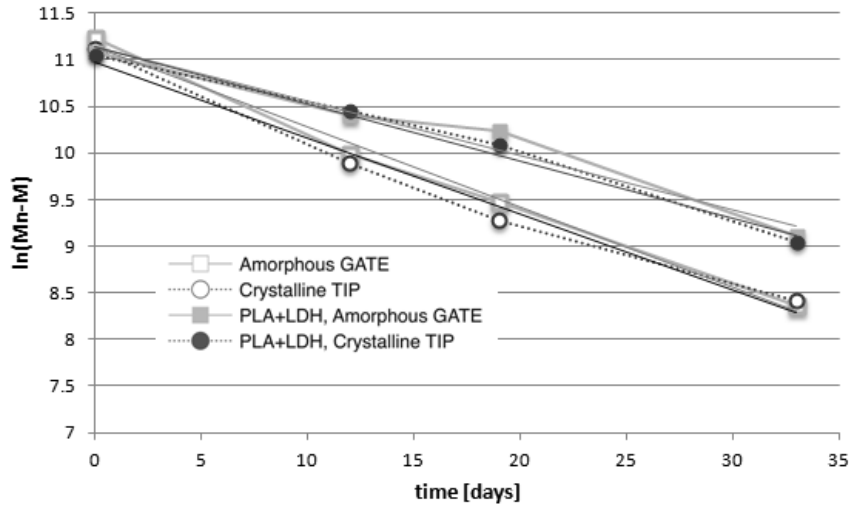


**Figure 78.** Evolution of  $\ln(Mn-M)$  during hydrolysis of micro-injected biphasic PLA and PLA + LDH samples (amorphous gate, crystalline tip)

The data of the two samples for both morphologies in the figure above have an approximately linear trend (the coefficients of determination reported in Table 4 are quite close to 1): the slope of the lines represents the value of the kinetic constant. Since the kinetic constant of hydrolysis depends on the pH of the medium in which the process takes place, the fact that the data shown in Figure 78 have a linear trend as a function of the duration of the hydrolysis means that the pH within the sample can be considered constant, just as found in the hydrolysis of the samples obtained by compression molding. Table 4 shows all the values of  $k'$  and the coefficients of determination.

**Table 9.** Kinetic constant of hydrolysis of micro-injected biphasic PLA and PLA + LDH samples (amorphous gate, crystalline tip)

	$k'$ [days <sup>-1</sup> ]	$R^2$
PLA amorphous	0.0861	0.9929
PLA crystalline	0.0816	0.9826
PLA + LDH amorphous	0.0583	0.971
PLA + LDH crystalline	0.0611	0.9863

There is no difference in the values of  $k'$  for the two morphologies of the two different samples. The values of  $k'$  of PLA + LDH are lower than those for PLA: samples loaded with LDH are more resistant to hydrolysis than are the pure PLA samples.

## Chapter 4

GPC analysis confirms the DSC results: the presence of LDH protects the sample from hydrolysis in both morphologies.

### Mechanical tests

Mechanical tests were performed on the hydrolyzed micro-injected biphasic PLA and PLA+LDH samples (amorphous gate, crystalline tip).

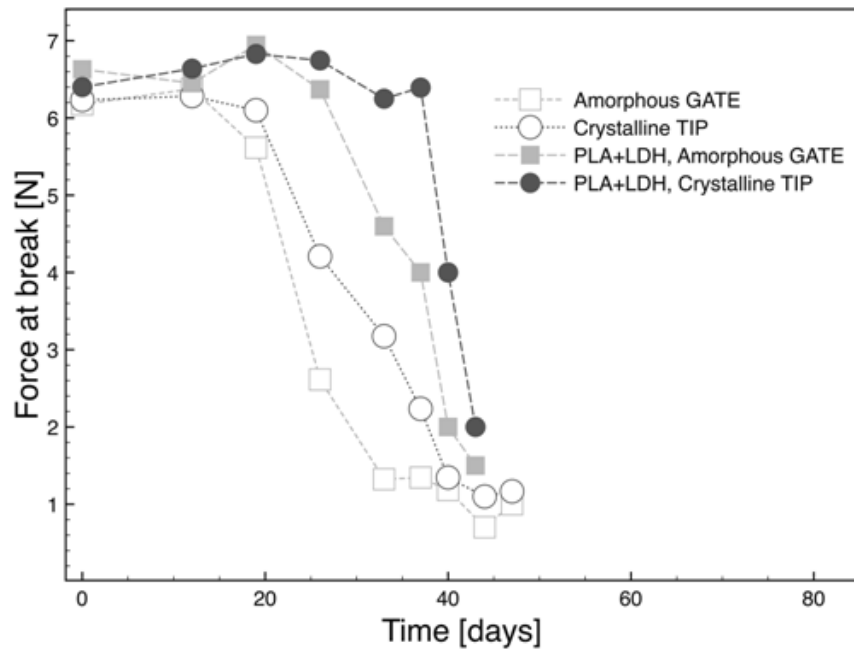


**Figure 79.** Evolution of force at break during hydrolysis of micro-injected biphasic PLA and PLA + LDH sample (amorphous gate, crystalline tip)

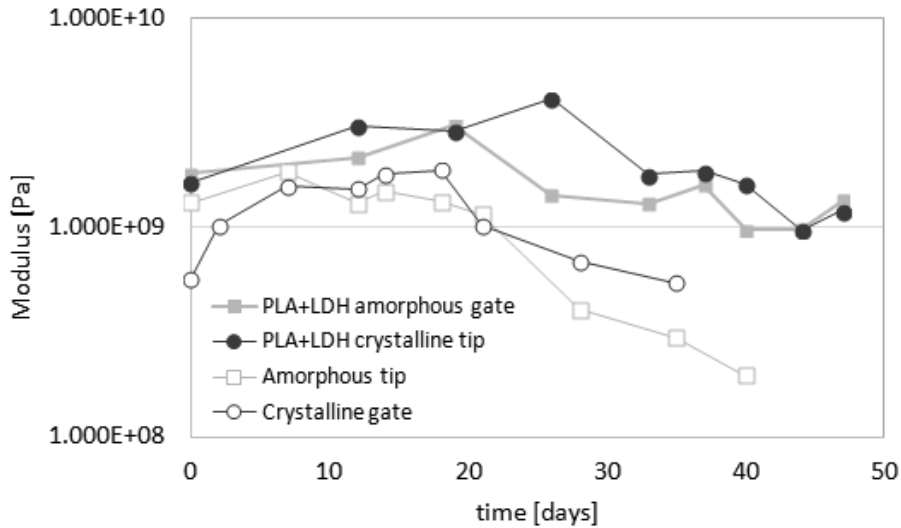


**Figure 80.** Evolution of modulus during hydrolysis of micro-injected biphasic PLA and PLA + LDH sample (amorphous gate, crystalline tip)

From Figure 79 we can see that the force at break of the loaded samples are higher than the PLA ones as the hydrolysis proceeds. In particular, for the amorphous zone, the break moves from 19 days for PLA to 26 days for PLA + LDH; for the crystalline zone, the break moves from 19 days for PLA to 33 days for PLA + LDH.

From Figure 80 we can see that the values of the modulus of PLA + LDH are higher than those for PLA, in both morphologies.

As the hydrolysis progresses, the modulus of the sample decreases. Up to 19 days we can observe no differences between the moduli of the two different morphologies of the two different samples. At later times, the modulus of the crystalline zone is higher than that of the amorphous zone, for both samples.

Chapter 4

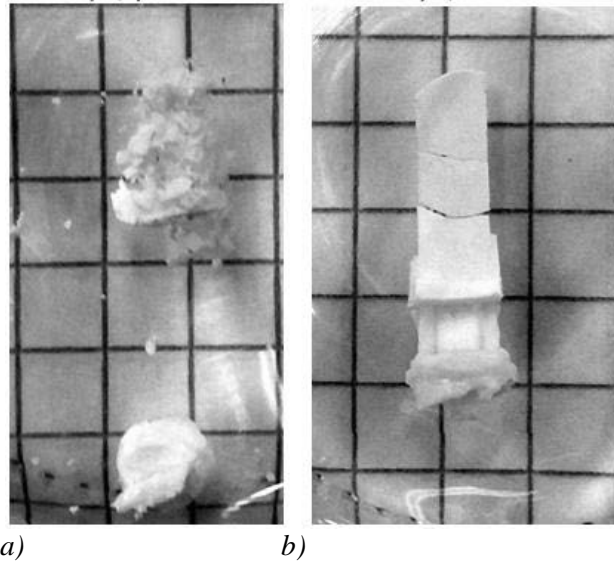


**Figure 81.** Images of hydrolyzed samples of micro-injected biphasic PLA and PLA + LDH samples at 50 days (amorphous gate, crystalline tip; a) PLA; b) PLA + LDH

From Figure 81 the protective effect of LDH added to PLA as filler is evident. After 50 days, no difference can be observed between the two morphologies, for either sample.

# Conclusions

The aim of this work has been obtaining bionanocomposites, by using the injection micro-molding technique, with a degradation rate which can be modulated in time.

As a biodegradable and biocompatible polymeric matrix, PLA (4032D and 4060D) was chosen; as fillers, LDH (with  $\text{NO}_3^-$  or  $\text{CO}_3^{2-}$  as interlayer anions), organic acids (succinic, fumaric and ascorbic acids), and LDHs intercalated with organic acids were selected. Eco-friendly and biocompatible additives were adopted to modulate the degradation rate of the PLA.

This experimental work can be divided into two steps:

1. The selection of materials;
2. The production and characterization of samples obtained by micro-injection molding using the materials selected in the previous step.

## First Step

Several mixtures of PLA and LDH (pure and intercalated with organic acid) have been obtained by an extrusion process. From all extruded materials, films were then obtained by compression molding. These films were then subjected to hydrolysis tests.

The hydrolysis process, as a function of the residence time of the samples in distilled water, was observed through monitoring:

- The temporal evolution of the weight of the samples;
- The evolution of the degree of crystallinity of the samples by means of the differential scanning calorimetry technique (DSC);
- The evolution of the glass transition temperature by means of the differential scanning calorimetry technique (DSC);
- The evolution of the molecular weights by means of gel permeation chromatography (GPC);
- Changes in mechanical properties.

## *Weight of samples*

Using LDH- $\text{NO}_3$  as filler makes PLA more resistant to hydrolysis for up to 45 days: for loaded PLA, the point of 10% weight loss is shifted from about 35 to about 40 days. After 45 days, there is no significant difference between the pure PLA and the PLA + 3% (LDH- $\text{NO}_3$ ).

## Conclusions

The experimental results show that there is an increase in the time needed to degrade to a given point for samples loaded with LDH-organic acid (in particular LDH-succinic acid) and a decrease in this time for samples loaded with organic acid alone.

Adding 3% of LDH-organic acid can protect PLA from the hydrolysis process, in particular LDH-succ and LDH-fum. LDH-succ has the best protective effect: to reach the same weight loss as for the pure PLA, the PLA to which has been added 3% (LDH-succ) needs a significantly longer time: the point of 10% weight loss is shifted from about 35 to about 50 days.

### *Degree of crystallinity and glass transition temperature*

As the hydrolysis proceeds, an increase in the degree of crystallinity is observed. The degree of crystallinity can increase for two reasons: a decrease in the amount of the amorphous phase present in the sample (erosion by hydrolysis) or a crystallization of molecules, which from the amorphous phase become part of the crystalline phase.

We also note that the degree of crystallinity, in some of the samples analysed, tends to decrease: this is a sign of a very advanced hydrolysis. It is in fact known that hydrolysis occurs initially above all in the amorphous area of the polymer, but at a certain point there is also a hydrolysis of the remaining crystalline part, thus causing a decrease in the degree of crystallinity.

As said before,  $X_c$  increases for all the samples. There are however some differences between the samples: up to 40 days 4032D + 3% (LDH-CO<sub>3</sub>) reaches a  $X_c$  higher than pure 4032D and 4032D + 3%(LDH-NO<sub>3</sub>); probably this indicates that this material is more severely hydrolyzed than the other. The lowest value of  $X_c$  is that for 4032D + 3% (LDH-NO<sub>3</sub>): LDH-NO<sub>3</sub> is the selected LDH able to make PLA more resistant to the hydrolysis process.

The value of  $X_c$  of pure PLA increases quickly, compared to that for PLA + LDH-organic acids, while  $X_c$  of 4032 + 3% LDH-organic filler increases but remains at lower values, especially 4032 + 3% LDH-succ: at the end of hydrolysis, the  $X_c$  of 4032 + 3% LDH-succ is about 10% lower than that of pure PLA.

Regarding the glass transition temperature, this is linked to the degree of crystallinity.  $T_g$  and  $T_m$  decrease for all the samples with the progression of the hydrolysis: their values remain higher for 4032D + 3% (LDH-NO<sub>3</sub>) with respect to pure PLA and 4032D + 3% (LDH-CO<sub>3</sub>) ( $T_g$  is higher by about 6°C). The same differences are observed for the PLA + 3% LDH-organic filler: all loaded samples show a higher  $T_g$  at the end of hydrolysis tests, in particular 4032 + 3%LDH-succ.

### ***Molecular weights***

The average molecular weights of the analysed samples decrease with the progress of the hydrolysis process.

The values of  $M_n$  and  $M_w$  are higher for 4032D + 3% (LDH-NO<sub>3</sub>) than for pure PLA: therefore, the presence of LDH-NO<sub>3</sub> as filler really protects PLA from hydrolysis. All samples with 3% LDH-organic acids as fillers kept higher molecular weight with respect to neat PLA with increasing time of hydrolysis, in particular 4032 + 3% LDH-succ, which has the lowest kinetic constant of the hydrolysis process.

### ***Mechanical tests***

The strength at break decreases as the hydrolysis progresses. After 21 days, the samples begin to break at decreasing mechanical stresses as the hydrolysis proceeds. For 4032D + 3% LDH-organic acid, the force at break is higher than that of neat PLA, in particular for 4032 + 3% LDH-succ. This mechanical analysis confirms what we observed in the other analyses: adding 3% LDH-organic acid protects PLA from hydrolysis, in particular when using LDH-succinic acid.

Using organic acids alone as fillers, all the analyses carried out show an acceleration of the hydrolytic process.

The same analyses have been performed using 4060D as polymeric matrix. 4060D hydrolyzes faster than 4032D. As observed for 4032D, also in the case of 4060D the presence of LDH-organic acids as fillers protects the sample from the action of hydrolysis, especially by using 3% LDH-succinic acid.

All the analyses performed confirmed that the sample that is most resistant to hydrolysis is 4032D + 3% LDH-succinic acid.

## **Second Step**

From pure 4032D and from 4032D + 3% LDH-succinic acid, both extruded, biphasic samples were obtained (half amorphous and the other half crystalline) by micro-injection molding. A new dynamic mold temperature control system for rapid heating and cooling of the mold was used. These biphasic samples were then subjected to hydrolysis tests.

The hydrolysis process was monitored by carrying monitoring:

- The evolution of the degree of crystallinity of the samples by means of the differential scanning calorimetry technique (DSC);
- The evolution of the molecular weights by means of gel permeation chromatography (GPC);
- Changes in mechanical behaviour.

## Conclusions

### ***Degree of crystallinity***

For all the sample, for both morphologies,  $X_c$  increases as the hydrolysis proceeds. The value of  $X_c$  of the crystalline phase, for 4032D and 4032D loaded, increases more slowly than the  $X_c$  of the amorphous phase as the hydrolysis proceeds: this probably indicates a slower degradation of the crystalline zone than of the amorphous zone. The values of  $X_c$  for the samples with LDH are lower than those of the pure PLA sample, especially from 12 days on. The presence of LDH protects the sample from hydrolysis in both morphologies.

### ***Molecular weights***

The molecular weights decrease for both zones of the two samples. We could observe no differences in the evolution of  $M_n$  as the hydrolysis proceeds in the two different morphologies of both samples. The values of  $M_n$  of the PLA + LDH sample are higher than for PLA. The value of  $M_n$  of PLA + LDH decreases slower than that for PLA as the hydrolysis proceeds.

The values of the kinetic constant of the hydrolysis of PLA + LDH are lower than for PLA: samples loaded with LDH are more resistant to hydrolysis than are the pure PLA samples.

The GPC analysis confirms the results of the DSC: the presence of LDH protects the sample from hydrolysis in both morphologies. No difference in  $k'$  between the two morphologies of the two different samples could be observed.

### ***Mechanical tests***

Up to 14 days, for pure PLA, where the force is near 6.5 N, there is no fracture in either phase. After 18 days, the amorphous zone begins to break at decreasing mechanical stresses as the hydrolysis proceeds. A break in the crystalline phase can be observed after 21 days. For the crystalline phase, the values of the force at break are a little bit higher than for the amorphous phase.

The force at break of loaded samples is higher than for PLA samples as the hydrolysis proceeds. In particular, for the amorphous zone the break moves from 19 days for PLA to 26 days for PLA + LDH; for the crystalline zone, the break moves from 19 days for PLA to 33 days for PLA + LDH.

Also in the micro-injected samples, the experimental results show that there is an increase in the time needed to degrade to a given point for the loaded samples compared to pure PLA, both for the crystal phase and for the amorphous one. Crystalline regions present a (slightly) better resistance to hydrolysis.

## Conclusions

Summing up, at the end of this experimental work, we can conclude that:

- Eco-friendly and bio-compatible additives can be adopted to modulate the degradation rate of PLA;
- The fillers can be melt-mixed with PLA;
- Using 3% (LDH-organic acid), succinic acid in particular, as filler makes PLA more resistant to the hydrolysis process in the solid state;
- PLA was successfully micromolded in a 200  $\mu\text{m}$  thick cavity by adopting a fast mold surface temperature control, obtaining biphasic samples;
- Hydrolysis tests confirmed that crystalline regions present a (slightly) better resistance to hydrolysis: the obtained biphasic samples present a selective degradation rate;
- By adding 3% (LDH-succinic acid) filler, a significant delay in degradation could be reached also in the micromolded samples.

All the characterizations concur well in demonstrating the efficiency of LDH filler in content as low as 3% wt. in delaying the hydrolytic degradation of PLA. Among the studied samples, the LDH-succ filler appears as a promising candidate to significantly delay the breakdown of PLA. It is our belief that such a combination of a food additive and a benign inorganic vessel may open new routes in designing PLA composites for targeted applications, which can range from durable ones, such as, for instance, automotive parts or equipment housing, to biological contact such as implants needing a given degradation rate or agricultural materials.



# Bibliography

- European Bioplastics. Bioplastics packaging – Combining performance with sustainability - Materials and market development in the packaging segment. Fact sheet, European Bioplastics, Berlin, Germany, 2014c. Available at: [http://en.european-bioplastics.org/wp-content/uploads/2011/04/fs/Packaging\\_eng.pdf](http://en.european-bioplastics.org/wp-content/uploads/2011/04/fs/Packaging_eng.pdf) Last accessed January 1, 2016.
- ARIAS, V., HOGLUND, A., ODELIUS, K. & ALBERTSSON, A. C. 2014. Tuning the Degradation Profiles of Poly(L-lactide)-Based Materials through Miscibility. *Biomacromolecules*, 15, 391-402.
- AURAS, R. 2010. *Poly(lactic acid) : synthesis, structures, properties, processing, and applications/ edited by Rafael Auras ... [et al.]*, Hoboken, N.J., Wiley.
- BALAGUER, M. P., ALIAGA, C., FITO, C. & HORTAL, M. 2016. Compostability assessment of nano-reinforced poly(lactic acid) films. *Waste Management*, 48, 143-155.
- BAYER, I. S. 2017. Thermomechanical Properties of Polylactic Acid-Graphene Composites: A State-of-the-Art Review for Biomedical Applications. *Materials*, 10.
- BELBELLA, A., VAUTHIER, C., FESSI, H., DEVISSAGUET, J. P. & PUISIEUX, F. 1996. In vitro degradation of nanospheres from poly(D,L-lactides) of different molecular weights and polydispersities. *International Journal of Pharmaceutics*, 129, 95-102.
- BENALI, S., AOUADI, S., DECHIEF, A.-L., MURARIU, M. & DUBOIS, P. 2015. Key factors for tuning hydrolytic degradation of polylactide/zinc oxide nanocomposites. *Nanocomposites*, 1, 51-61.
- DE JONG, S., ARIAS, E., RIJKERS, D., VAN NOSTRUM, C., KETTENES-VAN DEN BOSCH, J. & HENNINK, W. 2001. New insights into the hydrolytic degradation of poly (lactic acid): participation of the alcohol terminus. *Polymer*, 42, 2795-2802.
- DE SANTIS, F. & PANTANI, R. 2015. Melt compounding of poly (Lactic Acid) and talc: assessment of material behavior during processing and resulting crystallization. *Journal of Polymer Research*, 22, 1-9.
- DE SANTIS, F. & PANTANI, R. 2016. Development of a rapid surface temperature variation system and application to micro-injection molding. *Journal of Materials Processing Technology*, 237, 1-11.

## Bibliography

- EILI, M., SHAMELI, K., IBRAHIM, N. A. & YUNUS, W. M. Z. W. 2012. Degradability Enhancement of Poly(Lactic Acid) by Stearate-Zn<sub>3</sub>Al LDH Nanolayers. *International Journal of Molecular Sciences*, 13, 7938-7951.
- FISCHER, E. W., STERZEL, H. J. & WEGNER, G. 1973. Investigation of the structure of solution grown crystals of lactide copolymers by means of chemical reactions. *Kolloid-Zeitschrift und Zeitschrift für Polymere*, 251, 980-990.
- GARLOTTA, D. 2001. A literature review of poly(lactic acid). *Journal of Polymers and the Environment*, 9, 63-84.
- GLEADALL, A., PAN, J., KRUFIT, M.-A. & KELLOMÄKI, M. 2014. Degradation mechanisms of bioresorbable polyesters. Part 1. Effects of random scission, end scission and autocatalysis. *Acta Biomaterialia*, 10, 2223-2232.
- GORRASI, G. & PANTANI, R. 2013a. Effect of PLA grades and morphologies on hydrolytic degradation at composting temperature: Assessment of structural modification and kinetic parameters. *Polymer Degradation and Stability*, 98, 1006-1014.
- GORRASI, G. & PANTANI, R. 2013b. Effect of polylactic acid grades and morphologies on hydrolytic degradation at composting temperature: Assessment of structural modification and kinetic parameters. *Polym. Degrad. Stab.*, 98, 1006-1014.
- GORRASI, G., SORRENTINO, A. & PANTANI, R. 2015. Modulation of Biodegradation Rate of Poly(lactic acid) by Silver Nanoparticles. *Journal of Polymers and the Environment*, 23, 316-320.
- HA, J. U. & XANTHOS, M. 2010. Novel modifiers for layered double hydroxides and their effects on the properties of polylactic acid composites. *Applied Clay Science*, 47, 303-310.
- HARRIS, A. M. & LEE, E. C. 2010. Heat and Humidity Performance of Injection Molded PLA for Durable Applications. *Journal of Applied Polymer Science*, 115, 1380-1389.
- HARRIS, A. M. & LEE, E. C. 2013. Durability of polylactide-based polymer blends for injection-molded applications. *Journal of Applied Polymer Science*, 128, 2136-2144.
- HENTON, D., GRÜBER, P., LUNT & RANDALL, J. 2005. Polylactic acid technology. *Natural Fibers, Biopolymers, and Biocomposites*. Taylor & Francis, Boca Raton, FL, pp. 527-577.
- HERNÁNDEZ, J. S. P. 2014. Estudio de propiedades y compatibilidad de mezclas polipropileno (PP), ácido poliláctico (PLA) y nanopartículas de óxido de silicio (SiO<sub>2</sub>), mediante extrusión y

## Bibliography

- mezclado físico. available at <http://tesis.ipn.mx:8080/xmlui/handle/123456789/13308>.
- HGLUND, A., ODELIUS, K. & ALBERTSSON, A. C. 2012. Crucial Differences in the Hydrolytic Degradation between Industrial Polylactide and Laboratory-Scale Poly (L-lactide). *ACS Applied Materials & Interfaces*, 4, 2788--2793.
- HOCKING, P. J., TIMMINS, M. R., SCHERER, T. M., FULLER, R. C., LENZ, R. W. & MARCHESSAULT, R. H. 1995. Enzymatic Degradability of Poly(Beta-Hydroxybutyrate) as a Function of Tacticity. *Journal of Macromolecular Science-Pure and Applied Chemistry*, A32, 889-894.
- ITAVAARA, M., KARJOMAA, S. & SELIN, J. F. 2002. Biodegradation of polylactide in aerobic and anaerobic thermophilic conditions. *Chemosphere*, 46, 879-885.
- JIMENEZ, A., PELTZER, M. A. & RUSECKAITE, R. A. 2015. Poly(lactic acid) Science and Technology Processing, Properties, Additives and Applications Preface. *Poly(Lactic Acid) Science and Technology: Processing, Properties, Additives and Applications*, V-X.
- LI, S. M., GARREAU, H. & VERT, M. 1990. Structure Property Relationships in the Case of the Degradation of Massive Aliphatic Poly-(Alpha-Hydroxy Acids) in Aqueous-Media .1. Poly(DI-Lactic Acid). *Journal of Materials Science-Materials in Medicine*, 1, 123-130.
- LOSTOCCO & HUANG 1998. The hydrolysis of poly(lactic acid) poly(hexamethylene succinate) blends. *Polymer Degradation And Stability*, 61, 225-230.
- METTERS, A. T., BOWMAN, C. N. & ANSETH, K. S. 2000. A statistical kinetic model for the bulk degradation of PLA-b-PEG-b-PLA hydrogel networks. *Journal of Physical Chemistry B*, 104, 7043-7049.
- NALAWADE, P., AWARE, B., KADAM, V. J. & HIRLEKAR, R. S. 2009. Layered double hydroxides: A review. *Journal of Scientific & Industrial Research*, 68, 267-272.
- NOTTA-CUVIER, D., ODENT, J., DELILLE, R., MURARIU, M., LAURO, F., RAQUEZ, J. M., BENNANI, B. & DUBOIS, P. 2014. Tailoring polylactide (PLA) properties for automotive applications: Effect of addition of designed additives on main mechanical properties. *Polymer Testing*, 36, 1-9.
- OYARZABAL, A., MUGICA, A., MULLER, A. J. & ZUBITUR, M. 2016. Hydrolytic degradation of nanocomposites based on poly(l-lactic acid) and layered double hydroxides modified with a model drug. *Journal of Applied Polymer Science*, 133.

## Bibliography

- PANTANI, R., DE SANTIS, F., SORRENTINO, A., DE MAIO, F. & TITOMANLIO, G. 2010. Crystallization kinetics of virgin and processed poly(lactic acid). *Polymer Degradation And Stability*, 95, 1148-1159.
- PANTANI, R. & SORRENTINO, A. 2013. Influence of crystallinity on the biodegradation rate of injection-moulded poly(lactic acid) samples in controlled composting conditions. *Polymer Degradation and Stability*, 98, 1089-1096.
- PANTANI, R. & TURNG, L.-S. 2015. Manufacturing of advanced biodegradable polymeric components. *Journal Of Applied Polymer Science*, 132, n/a-n/a.
- PARTINI, M., ARGENIO, O., COCCORULLO, I. & PANTANI, R. 2009. Degradation kinetics and rheology of biodegradable polymers. *Journal of Thermal Analysis and Calorimetry*, 98, 645-653.
- PIEMONTE, V. & GIRONI, F. 2013. Lactic Acid Production by Hydrolysis of Poly(Lactic Acid) in Aqueous Solutions: An Experimental and Kinetic Study. *Journal of Polymers and the Environment*, 21, 275-279.
- SHIH, C. 1995. A graphical method for the determination of the mode of hydrolysis of biodegradable polymers. *Pharmaceutical research*, 12, 2036-2040.
- SIPARSKY, G. L., VOORHEES, K. J. & MIAO, F. D. 1998. Hydrolysis of polylactic acid (PLA) and polycaprolactone (PCL) in aqueous acetonitrile solutions: Autocatalysis. *Journal of Environmental Polymer Degradation*, 6, 31-41.
- SISTI, L., TOTARO, G., FIORINI, M., CELLI, A., COELHO, C., HENNOUS, M., VERNEY, V. & LEROUX, F. 2013. Poly(butylene succinate)/layered double hydroxide bionanocomposites: Relationships between chemical structure of LDH anion, delamination strategy, and final properties. *Journal of Applied Polymer Science*, 130, 1931-1940.
- SOROUDI, A. & JAKUBOWICZ, I. 2013. Recycling of bioplastics, their blends and biocomposites: A review. *European Polymer Journal*, 49, 2839-2858.
- SPERANZA, V., DE MEO, A. & PANTANI, R. 2014. Thermal and hydrolytic degradation kinetics of PLA in the molten state. *Polymer Degradation and Stability*, 100, 37-41.
- STLOUKAL, P., KALEDOVA, A., MATTAUSCH, H., LASKE, S., HOLZER, C. & KOUTNY, M. 2015. The influence of a hydrolysis-inhibiting additive on the degradation and biodegradation of PLA and its nanocomposites. *Polymer Testing*, 41, 124-132.

## Bibliography

- SUN, *Physical Chemistry of Macromolecules: Basic Principles and Issues*, 2nd edition, Wiley Hoboken, NJ, USA, 2004, p. 60
- TOKIWA, Y. & CALABIA, B. P. 2006. Biodegradability and biodegradation of poly(lactide). *Applied Microbiology and Biotechnology*, 72, 244-251.
- VERT, M., LI, S. & GARREAU, H. 1991. More About the Degradation of La/Ga-Derived Matrices in Aqueous-Media. *Journal of Controlled Release*, 16, 15-26.
- ZHOU, Q. & XANTHOS, M. 2008. Nanoclay and crystallinity effects on the hydrolytic degradation of polylactides. *Polymer Degradation and Stability*, 93, 1450-1459.



# Appendix

In this section DSC thermograms of all analyzed samples are reported.

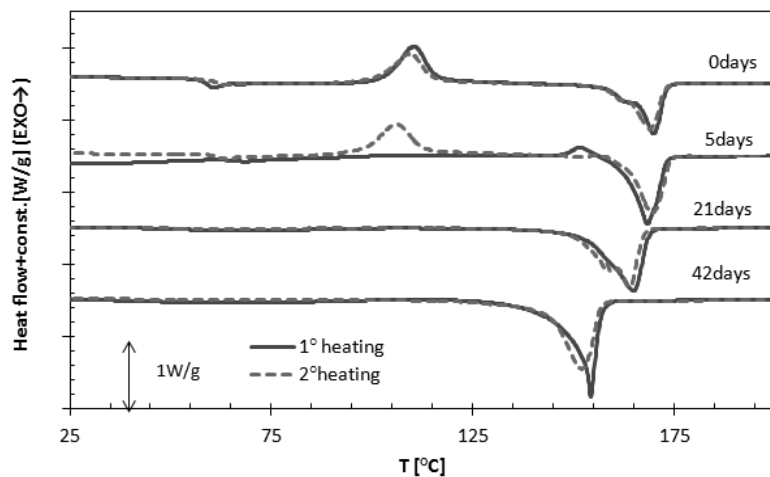


**Figure A1:** DSC thermograms of 4032D at selected times of hydrolysis.

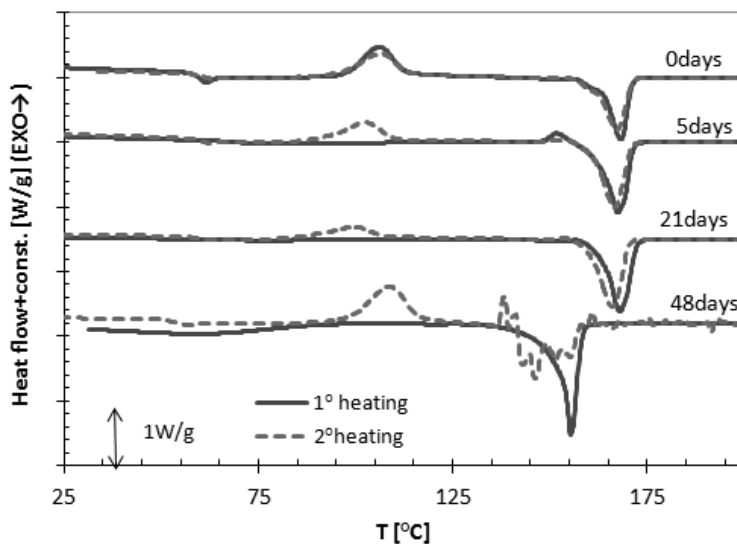


**Figure A2:** DSC thermograms of 4032D+(3%LDH-NO<sub>3</sub>) at selected times of hydrolysis.

Appendix

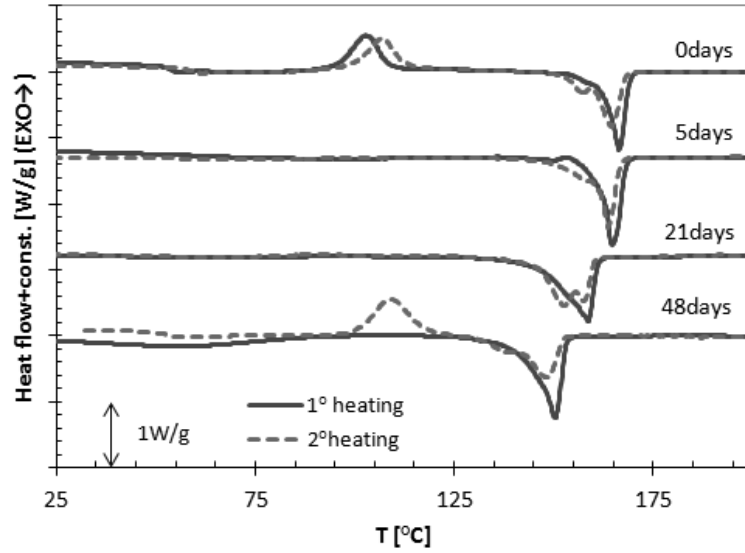


**Figure A3:** DSC thermograms of 4032D+(3%LDH-CO<sub>3</sub>) at selected times of hydrolysis

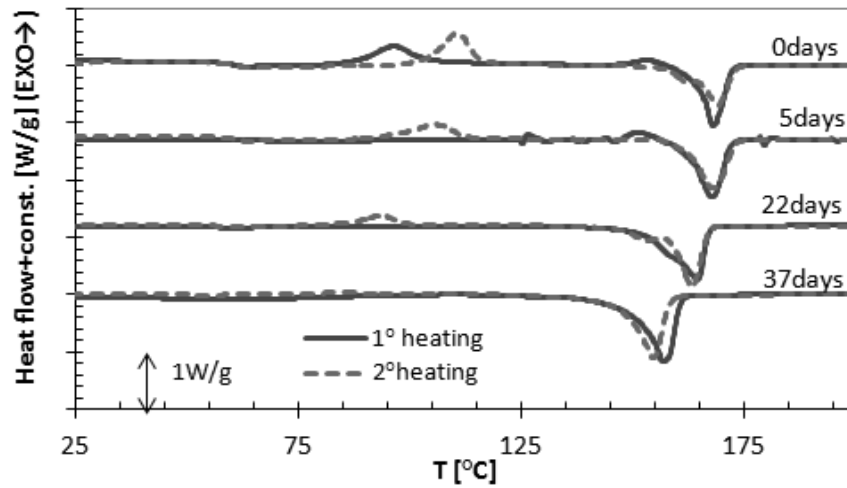


**Figure A4:** DSC thermograms of 4032D+(1%LDH-succ) at selected times of hydrolysis

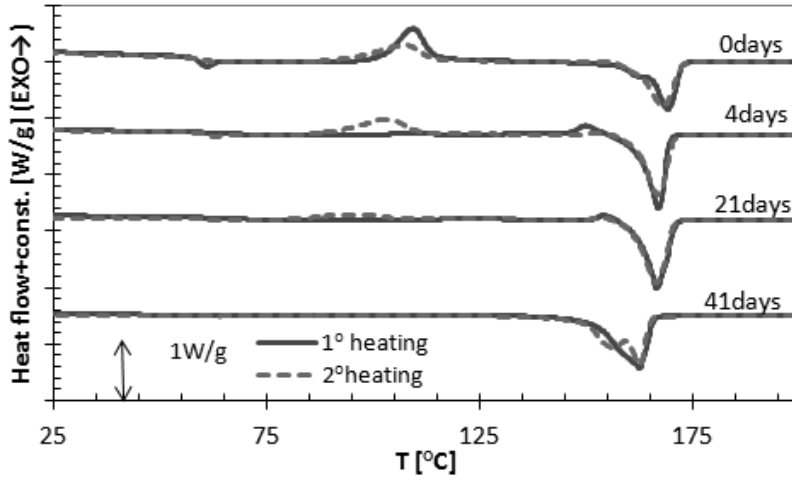


**Figure A5:** DSC thermograms of 4032D+(3%LDH-succ) at selected times of hydrolysis

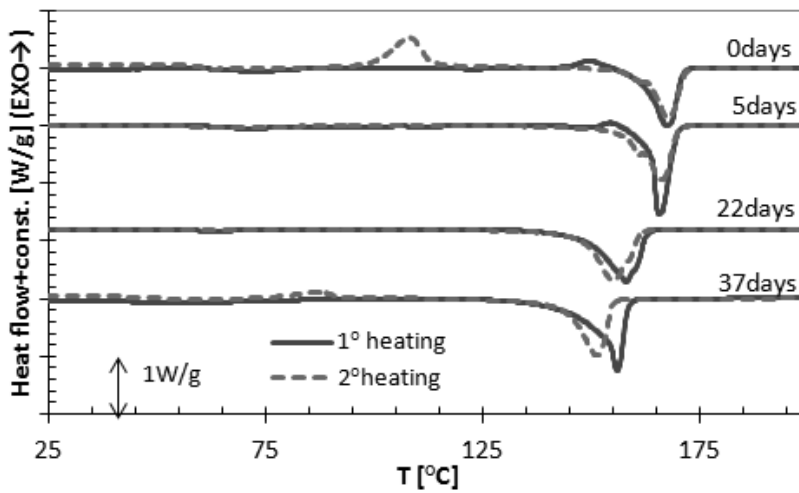


**Figure A6:** DSC thermograms of 4032D+(5%LDH-succ) at selected times of hydrolysis

Appendix

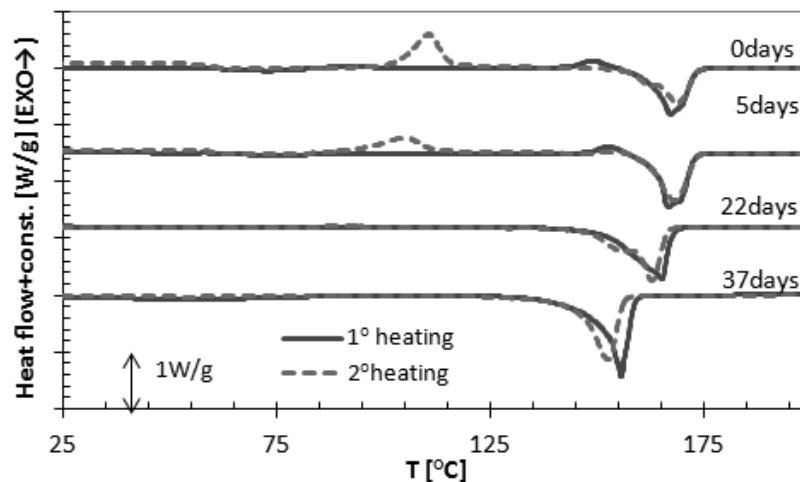


**Figure A7:** DSC thermograms of 4032D+(1%LDH-fum) at selected times of hydrolysis

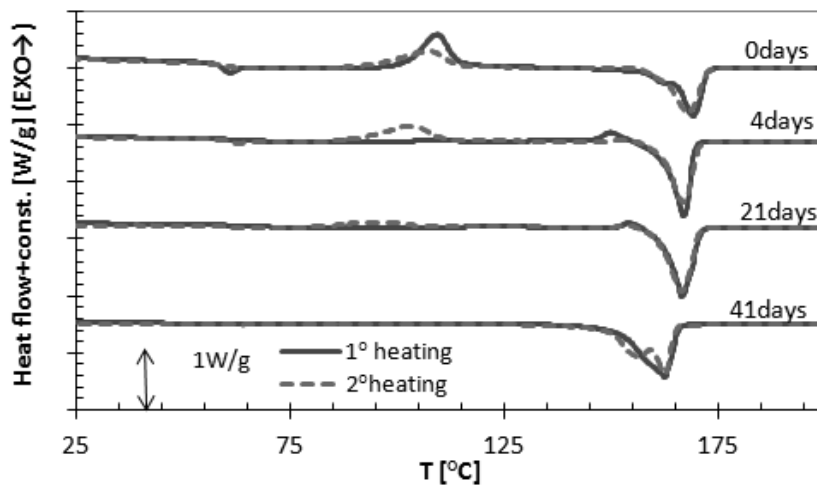


**Figure A8:** DSC thermograms of 4032D+(3%LDH-fum) at selected times of hydrolysis

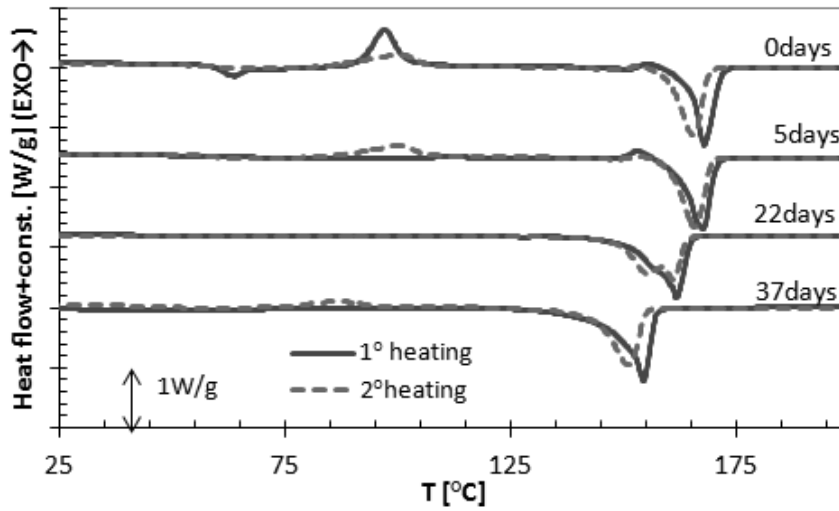


**Figure A9:** DSC thermograms of 4032D+(5%LDH-fum) at selected times of hydrolysis

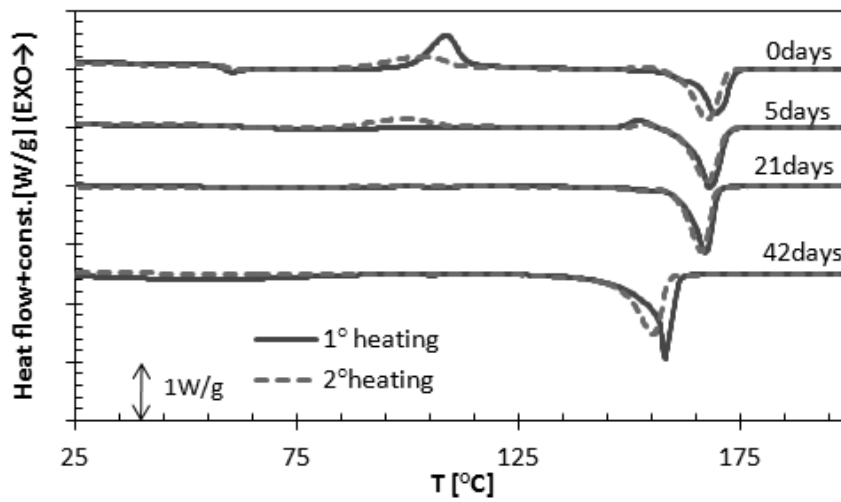


**Figure A10:** DSC thermograms of 4032D+(3%LDH-asc) at selected times of hydrolysis

Appendix

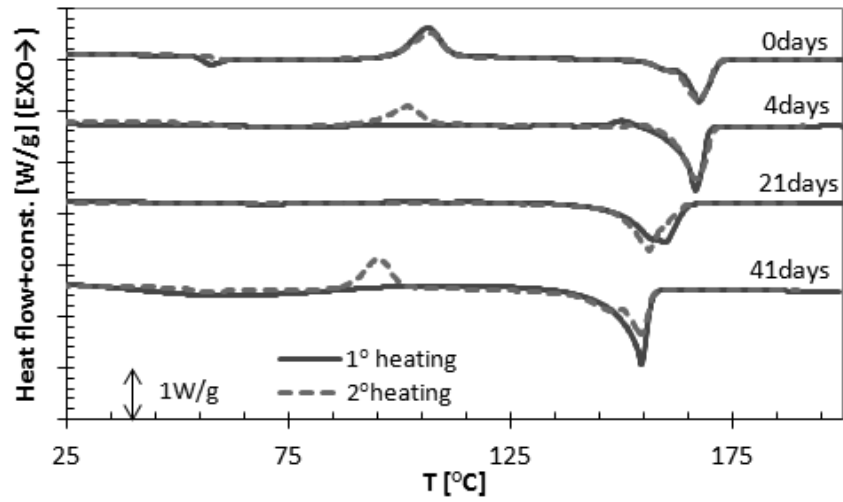


**Figure A11:** DSC thermograms of 4032D+(1% succ) at selected times of hydrolysis

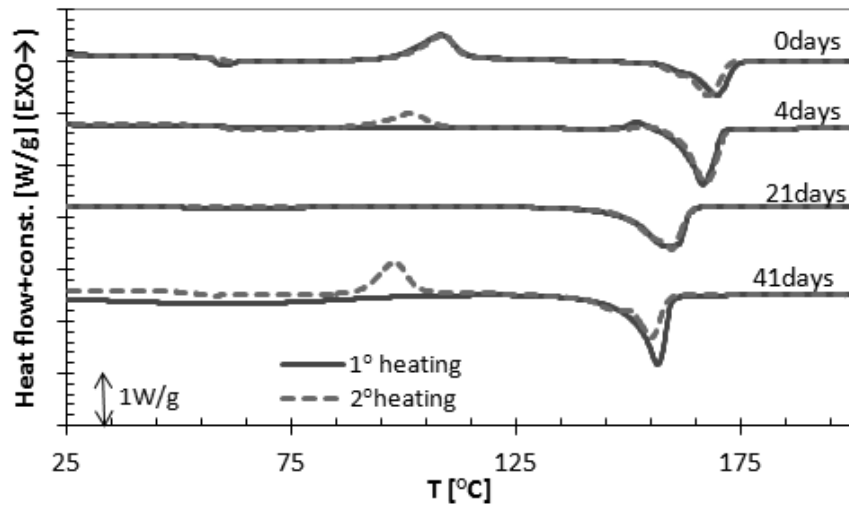


**Figure A12:** DSC thermograms of 4032D+(1% fum) at selected times of hydrolysis

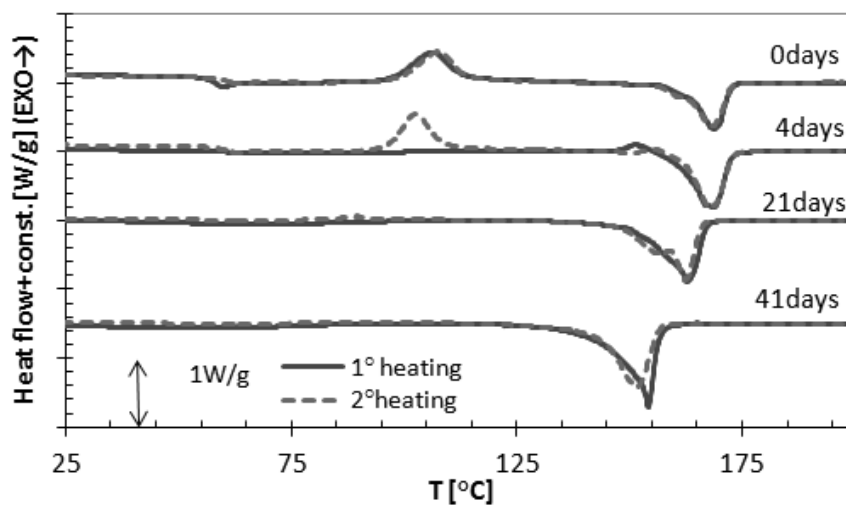


**Figure A13:** DSC thermograms of 4032D+(1%asc) at selected times of hydrolysis

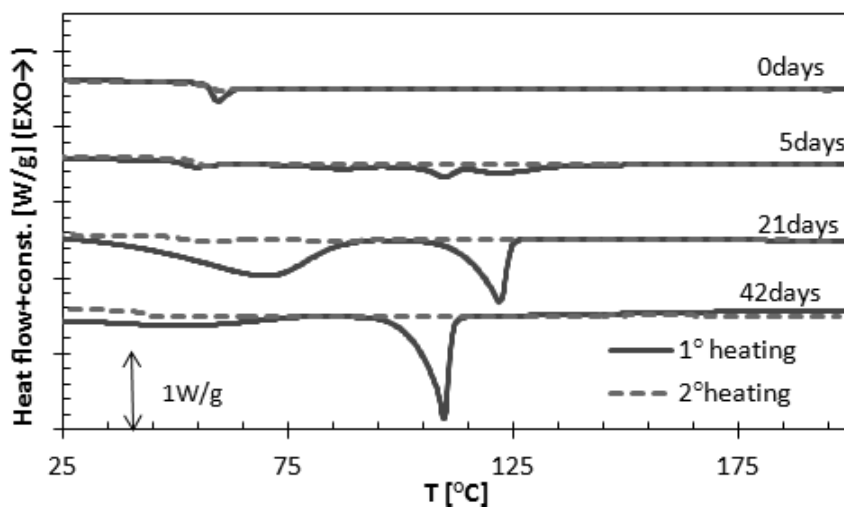


**Figure A14:** DSC thermograms of 4060D at selected times of hydrolysis

Appendix

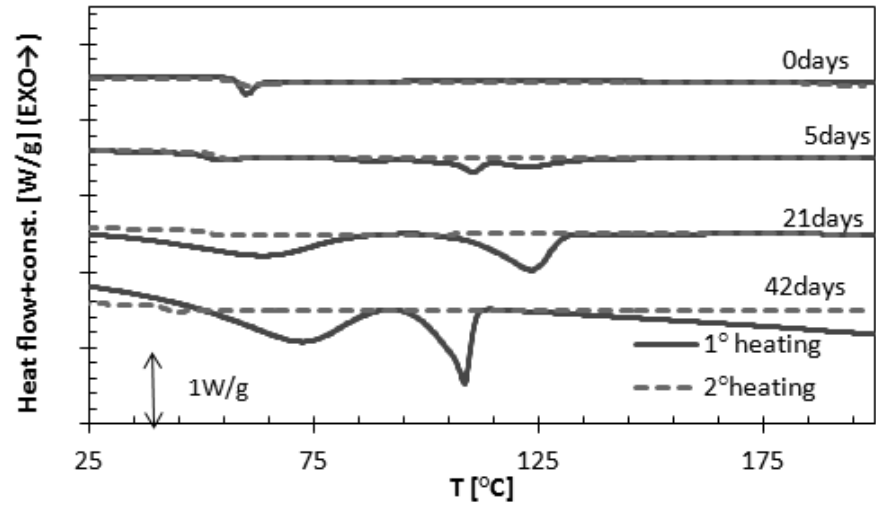


**Figure A15:** DSC thermograms of 4060D+(3%LDH-succ) at selected times of hydrolysis

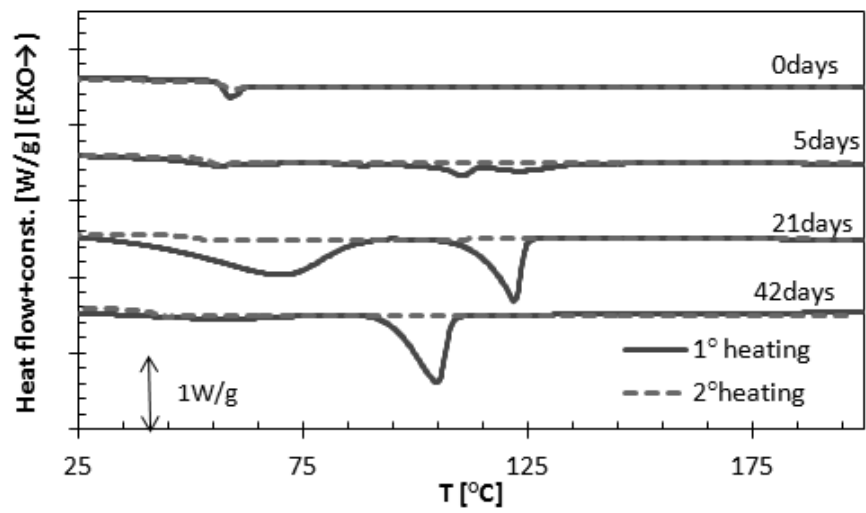


**Figure A16:** DSC thermograms of 4060D+(3%LDH-asc) at selected times of hydrolysis